COST Action TU1208

Action TU1208

Short-Term Scientific Missions: Year 3

Editors:
L. Pajewski & M. Marciniak

January 2018
www.GPRadar.eu

COST ACTION TU1208

CIVIL ENGINEERING APPLICATIONS OF GROUND PENETRATING RADAR

Short-Term Scientific Missions: Year 3

Editors:
Lara Pajewski & Marian Marciniak

PREFACE

SHORT-TERM SCIENTIFIC MISSIONS: YEAR 3

COST ACTION TU1208

"CIVIL ENGINEERING APPLICATIONS OF GROUND PENETRATING RADAR"

Short-Term Scientific Missions (STSMs) are among the best networking tools of COST (European COoperation in Science and Technology) Actions. They are aimed at supporting individual mobility of European researchers, in a flexible and bottom-up approach - a concept of particular interest to young scientists. STMSs significantly strengthen scientific networks and foster integration and collaboration - this is important to make Europe more competitive and put European scientists at the forefront of worldwide technological innovation.

In the framework of COST Action TU1208, we have noticed that STSMs are especially fruitful: in most cases, significant results are achieved by the involved scientists in a limited period of time and almost all exchange visits result in the publication of joint papers. We have also witnessed that collaborations started in the framework of STSMs tend to be very strong; we think that they will last for a very long time, well beyond the end of the mission and probably for the entire scientific carrier of the involved scientists.

In a STSM, a scientist from a COST Country or from an approved Institution in a Near Neighbour Country (NNC) has the opportunity to visit an institution or laboratory in a COST Country

participating in the Action, or an approved NNC institution, or else an approved International Partner Country (IPC) institution.

A STSM shall specifically contribute to the scientific objectives of the Action offering the grant, at the same time allowing the visiting scientist to learn new techniques or gain access to specific instruments and/or methods not available in the home institution.

STSM proposals are submitted by using the online application form, available at https://e-services.cost.eu/stsm. When a COST Action receives a proposal, the Management Committee (MC) performs the evaluation. The MC of Action TU1208 formally delegated the evaluation of STSM applications to the Action Chair and STSM Manager. The selection is based on the scientific scope of the STSM, which must be in line with the Action objectives (as already mentioned), and on the applicant curriculum vitae. Geographical issues and gender balance are taken into consideration, as well. A STSM applicant must be engaged in a research programme as a postgraduate student or postdoctoral fellow, or be employed by or officially affiliated to an institution or legal entity. The institution of the applicant and the host institution can be public or private, both from academia and industry.

Standard STSMs may have a minimum duration of 5 days and a maximum duration of 90 days. They have to be carried out in their entirety within a single grant period and within the Action's lifetime. Early-Career Investigators (ECIs) may extend the duration of the STSM beyond the 90 days in well-justified cases (the maximum allowed duration is 180 days).

The participation of ECIs in STSMs is strongly encouraged. For COST, the definition of ECI is based on the time that elapses between the date of the PhD (or equivalent experience) and the date of involvement in a COST Action. If this time span is less than eight years, a person fits the definition; periods of career's leave have to be added to the mentioned time span. Supporting ECIs to develop independent careers and to establish their first research group under their own responsibility is a strategic priority for COST.

A STSM Grant is a fixed financial contribution up to 2.500,00 EUR or 3.500,00 EUR for missions carried out by ECIs and longer than 90 days. The granted amount is based on the budget requested by the applicant and on the evaluation of the application by the MC. The aim of the grant is to support the costs associated with the exchange visit. It does not necessarily cover all expenses and has to be intended as a contribution to the travel and subsistence costs of the scientist performing the mission.

After performing the STSM, the Grantee has 30 calendar days from the end date of the mission in question to submit a scientific report to the Action Chair and STSM Manager, along with a letter prepared by the host scientist where he/she confirms the successful execution of the mission. The payment of the STSM Grant is subject to the approval of the submitted scientific report by the Action Chair and STSM Manager (note that, if one or both of them are involved in the STSM, then the Vice-Chair evaluates the report).

During Grant Period 3 of COST Action TU1208, twelve STSMs were funded and fruitfully carried out. This book is a collection of

scientific reports prepared by the scientists who performed the missions, in cooperation with the host scientists.

We are deeply grateful to COST for funding and supporting COST Action TU1208 "Civil Engineering Applications of Ground Penetrating Radar" and the research activities presented in this volume. We thank TU1208 GPR Association for funding the publication of this volume.

Lara Pajewski, Chair of COST Action TU1208
Marian Marciniak, STSM Manager of COST Action TU1208

STSM 1

NON-DESTRUCTIVE TESTS FOR RAILWAY EVALUATION: DETECTION OF FOULING AND JOINT INTERPRETATION OF GPR DATA AND TRACK GEOMETRIC PARAMETERS

Visiting Scientist: Mercedes Solla, University Of Vigo, Vigo, Spain (merchisolla@uvigo.es)

Host Scientist: Simona Fontul, National Laboratory for Civil Engineering (LNEC), Lisbon, Portugal (simona@lnec.pt)

STSM Dates: 1 June – 30 June 2015

1. PURPOSE OF THE STSM

Railways, as all transport infrastructures, have to behave properly during their life cycle. A regular maintenance policy has to be established, to guarantee high safety standards. Moreover, costs and traffic interruptions have to be limited.

Nowadays, track monitoring mainly consists in measuring parameters related to the track layout and rail wearing. Such monitoring procedures do not allow understanding the real causes of railway deficiency, which may be due to the presence of ballast pockets, fouled ballast, poor drainage, subgrade settlements or transitions problems. A more in-depth analysis of the conditions of both the railway platform and substructure is crucial to reduce maintenance costs and increase operational safety levels.

Non-destructive testing techniques can be effectively employed for railway assessment. The main purpose of this Short Term Scientific Mission (STSM) was to study how Ground Penetrating Radar (GPR) can be used to inspect railways. In particular, the assessment tasks addressed in the STSM research work are: detection of track defects at infrastructure level (Task 1), measurement of layer thickness (Task 2), and evaluation of fouling level of ballast (Task 3).

5

2. DESCRIPTION OF THE WORK CARRIED OUT DURING THE STSM AND MAIN RESULTS

This STSM report was selected for open-access publication on the first issue of the first volume of the new journal *Ground Penetrating Radar* (www.GPRadar.eu/journal). The interested Readers are therefore kindly invited to download the paper [1], which describes what we did during this STSM. Some results achieved during the mission were published in the book Ref. [2].

We consider of special importance the following STSM activities:

- subgrade inspection by combining different methods (GPR, FWD, LFWD) (Task 1),

- comparison of different GPR antennas (ground- and air-coupled) and development of data acquisition procedures for different pavement structures (Task 2)

- analysis of ballast condition with the aid of modelling (Task 3).

3. FUTURE COLLABORATION WITH THE HOST INSTITUTION

Let us mention that the STSM has been useful not only for the visiting and host scientists but also for the PhD Student Vânia Marecos, Member of COST Action TU1208 from LNEC. Almost three years ago, Vânia has enrolled in an international PhD programme: the Interuniversity Doctoral Program in Geotechnologies applied to Construction, Energy and Industry (GeoCEI), involving both the University of Vigo and the University of Salamanca. Vânia's thesis, entitled "Optimization of Ground Penetrating Radar testing at traffic speed for structural monitoring of pavements," is jointly supervised by Dr Mercedes Solla and Dr Simona Fontul. Vânia participated in the STSM activities and this was certainly very important for her.

Overall, the STSM has strengthened the cooperation between the involved scientists, who will surely continue to collaborate.

ACKNOWLEDGEMENT

REFERENCES

[1] M. Solla and S. Fontul, "Non-destructive tests for railway evaluation: detection of fouling and joint interpretation of GPR data and track geometric parameters," Ground Penetrating Radar, Vol.1(1), pp. 75-103, January 2018.

[2] Non-destructive techniques for the evaluation of structures and infrastructure, Editors: B. Riveiro and M. Solla. Publishing House: CRCPress/Balkema – Taylor & Francis Group. April 2016. Book Series: "Structures and infrastructures;" e-book ISBN: 978-1-315-68515-1; hardcover book ISBN: 978-1-138-02810-4; DOI: 10.1201/b19024-1.

.

STSM 2

USE OF GPR AND STANDARD GEOPHYSICAL METHODS TO EXPLORE THE SUBSURFACE

Visiting Scientist: Raffaele Persico, Institute for Archaeological and Monumental Heritage IBAM-CNR (r.persico@ibam.cnr.it)

Host Scientist: Sebastiano D'Amico, University of Malta, Msida, Malta (sebdamico@gmail.com)

STSM Dates: 14 July – 24 July 2015

1. PURPOSE OF THE STSM

This STSM aimed at performing Ground Penetrating Radar (GPR) and passive seismic measurements in interesting sites in Malta.

The used radar system was a prototypal stepped-frequency reconfigurable GPR. The original system was recently implemented by IBAM-CNR together with the University of Florence and IDS Ingegneria dei Sistemi, within the Italian research project AITECH (www.aitechnet.com/ibam.html). During a previous STSM, carried out in 2014, the prototype was brought to Norway and compared with stepped-frequency commercial systems manufactured by 3d-radar. Based on the results collected during that mission, the prototype was improved. The mission in Malta represented an opportunity to test on real scenarios the improved version of the prototype.

Moreover, it is worth mentioning that, during this STSM, GPR measurements were performed for the first time in Malta.

2. DESCRIPTION OF THE WORK CARRIED OUT DURING THE STSM AND MAIN RESULTS

This STSM report was selected for open-access publication on the first issue of the first volume of the new journal *Ground Penetrating Radar* (www.GPRadar.eu/journal). The interested Readers are

8

therefore kindly invited to download the paper [1], which describes in detail what we did during this STSM.

3. FUTURE COLLABORATION WITH THE HOST INSTITUTION

After the STSM, we cooperated at the organization of a TU1208 Training School held in Malta in January 2016.

We hope to have future occasions to perform integrated prospecting, possibly also inserting additional geophysical techniques beyond GPR and passive seismic. We recently presented a proposal to a bilateral call explicitly directed to Italian-Maltese collaborations.

ACKNOWLEDGEMENT

REFERENCES

[1] R. Persico and S. D'Amico, "Use of Ground Penetrating Radar and standard geophysical methods to explore the subsurface," Ground Penetrating Radar, Vol.1(1), pp. 1-39, January 2018.

STSM 3

GPR INSPECTIONS IN TUNNELS FOR EFFECTIVE CONSTRUCTION AND MAINTENANCE OF TRANSPORT INFRASTRUCTURES

Visiting Scientist: Luca Bianchini Ciampoli, Roma Tre University, Rome, Italy (luca.bianchiniciampoli@uniroma3.it)

Host Scientist: Amir Alani, University of West London, London, United Kingdom (amir.alani@uwl.ac.uk)

STSM Dates: 08 September – 12 December 2015

1. PURPOSE OF THE STSM

The original purpose of the STSM concerned the application of ground-penetrating radar (GPR) in tunnels. In particular, the main goal was to start up and bring forward as much as possible the development of a guideline for GPR inspection of tunnels.

During the research stay I had the opportunity to deal also with two additional topics:

- GPR detection of utilities (I compared the performance of different GPR devices and studied processing methodologies).
- The use of non-destructive techniques for the evaluation of the health of living valuable trees.

2. DESCRIPTION OF THE WORK CARRIED OUT DURING THE STSM

2.1 GPR APPLICATIONS ON TUNNELS: EUROPEAN GUIDELINES

2.1.1. Introduction

A significant open issue concerning the reliability of geophysical methods and in particular of ground penetrating radar (GPR), both in research and professional context, is a general lack of international standards. This is a major problem to be solved, in order to gain scientific strictness for the GPR practices, and to

easily extend results reported in a country, to the international community. Producing international guidelines can represent an important step forward, in this sense. In the memorandum of understanding of the COST Action TU1208 is clearly stated that one of the main general aims of the Action is the "development of innovative protocols and guidelines which will be published in a handbook and constitute a basis for European Standards, for an effective GPR application in CE tasks; safety, economic and financial criteria will be integrated within the protocols".

Of course this is not a simple task to be accomplished. Firstly, survey procedures are highly dependent on the objective of the survey itself. Due the aim of the geophysical test, the GPR system, the antenna configuration, and even the processing procedures may change. Besides, these procedures are also influenced by the environmental conditions in which the tests are performed. This affects several aspects, spanning from hardware to software, but including, for instance, also safety measures. Due to these reasons, one of the main goal of COST Action TU1208 was just the development several guidelines related to the main application of GPR in the field of Civil Engineering. In the context of this STSM, I had the opportunity to face the problem of planning the development of a guidelines handbook for carrying out GPR surveys in tunnels. The work done during this STSMrepresents a starting point for the development of the guidelines, and provides a logical structure to the document to be filled by future studies.

2.1.2. State of the Art

To produce a handbook of guidelines for GPR surveys in tunnel environment represents a challenging task due to several reasons that later on will be deepened. Within them, one of the most significant is the lack of literature references specific to the use of GPR in tunnel monitoring, in terms of guidelines. There are only a few scientific works concerning the GPR application, with different purposes, in tunnel environment. In this field, GPR has shown to be a useful tool for detecting the presence of a natural tunnel

[Stevens et al., 1995; Takahashi and Sato, 2006; Monte et al., 2010], and for assessing the structural stability of the tunnel in the construction phase [Qu et al., 2006; Li et al., 2008] and during its service life-time of the tunnel [Caldarelli et al., 2003; Abraham and Derobert, 2003]. More in detail, as far as the stability of the already-realized tunnel is concerned, one of the main topic faced by the scientific community is the characterization of the tunnel lining [Silvast and Wiljanen 2008; Lalagüe and Hoff 2010; Zhang et al. 2010; Xiang et al. 2013; Alani and Banks 2014]. An overview about the use of GPR for Tunnel diagnostic is given by Stryk et al. [2015]. This publication, included in a wider work concerning the GPR application in the field of civil engineering [Benedetto and Pajewski, 2015], represents one of the main references for the purposes of developing guidelines for tunnels. Despite, as said, references of national or international standards are lacking, it is possible to retrieve some documents concerning the standardization of the use of GPR for different scopes. In particular, the American Society for Testing and Materials (ASTM) produced several international documents containing instructions and advices for testing, by using GPR, the subsurface in general [ASTM D6432, 2011], the asphalt-covered bridge decks [ASTM D6087, 2008], and for assessing the thicknesses of road pavement layers [ASTM D4748, 2010]. These documents are remarkably rigorous, hold significant standardization effectiveness and represented a good starting point for developing the structure of the guidelines during the TTSM. Nevertheless, the most helpful document was the draft of the guidelines developed in the context of the COST Action TU1208, concerning the investigation of flexible pavements by using GPR.

REFERENCES

Abraham, O., Dérobert, X.; Non-destructive testing of fired tunnel walls: The Mont-Blanc Tunnel case study; NDT and E International Volume 36, Issue 6, September 2003, Pages 411-418 (2003)

Alani, A.M., Banks, K.: Applications of Ground Penetrating Radar in Medway Tunnel-Inspection of Structural Joints. In: 15th International

Conference on Ground Penetrating Radar (GPR), Brussels, Belgium (2014)

ASTM D4748-10.: Standard Test Method for Determining the Thickness of Bound Pavement Layers Using Short-Pulse Radar (2010)

ASTM D6087-08.: Standard Test Method for Evaluating Asphalt-Covered Concrete Bridge Decks Using Ground Penetrating Radar (2008)

ASTM D6432-11.: Standard Guide for Using the Surface Ground Penetrating Radar Method for Subsurface Investigation (2011)

Benedetto, A., Pajewski L.; Civil Engineering Application of Ground Penetrating Radar; Ed. Springer (2015)

Cardarelli, E., Marrone, C., Orlando, L.; Evaluation of tunnel stability using integrated geophysical methods; Journal of Applied Geophysics; Volume 52, Issue 2-3, February 2003, Pages 93-102 (2003)

Lalagüe, A., Hoff, I.: Determination of space behind pre-cast concrete elements in tunnels using GPR. In: 13th International Conference on Ground Penetrating Radar (GPR), pp. 1–5. Lecce, Italy (2010)

Li, S., Xue, Y., Zhang, Q., Li, S., Li, L., Sun, K., Ge, Y., Su, M., Zhong, S.,Li, X.; Key technology study on comprehensive prediction and early-warning of geological hazards during tunnel construction in high-risk karst areas; Yanshilixue Yu Gongcheng Xuebao/Chinese Journal of Rock Mechanics and Engineering; Volume 27, Issue 7, July 2008, Pages 1297-1307 (2008)

Monte, L.L., Erricolo, D., Soldovieri, F., Wicks, M.C.; Radio frequency tomography for tunnel detection; IEEE Transactions on Geoscience and Remote Sensing; Volume 48, Issue 3 PART 1, 2010, Article number 2029341, Pages 1128-1137 (2010)

Qu, H., Liu, Z., Zhu, H.; Technique of synthetic geologic prediction ahead in tunnel informational construction; Yanshilixue Yu Gongcheng Xuebao/Chinese Journal of Rock Mechanics and Engineering; Volume 25, Issue 6, June 2006, Pages 1246-1251 (2006)

Silvast, M., Wiljanen, B.: ONKALO EDZ—Measurements using ground penetrating radar (GPR) method, working report, Posiva Oy, p 66 (2008)

Stevens, K.M., Lodha, G.S., Holloway, A.L., Soonawala, N.M.; The application of ground penetrating radar for mapping fractures in plutonic rocks within the Whiteshell Research Area, Pinawa, Manitoba, Canada; Journal of Applied Geophysics, Volume 33, Issue 1-3, Pages 125-141. (1995)

Takahashi, K., Sato, M.; Parametric inversion technique for location of cylindrical Structures by cross-hole measurements; IEEE Transactions on Geoscience and Remote Sensing; Volume 44, Issue 11, November 2006, Article number 1717729, Pages 3348-3355 (2006)

Xiang, L., Zhou, H., et al.: GPR evaluation of the Damaoshan highway tunnel: A case study. NDT and E Int. 59, 68–76 (2013)

Zhang, F., Xie, X., et al.: Application of ground penetrating radar in grouting evaluation for shield tunnel construction. Tunn. Undergr. Space Technol. 25(2), 99–107 (2010)

2.2. A Study case: underground utilities detection through GPR

2.2.1. Introduction

During the three months of STSM at the University of West London, I had the opportunity to collaborate to the organization of the Training School "Ground Penetrating Radar for road pavement assessment and detection of buried utilities" held by the COST Action TU12808 at the University of West London (October 12-14 2015). Besides the standard classes, the Training School scheduled two practical training, which took place during the first and the second day.

Thanks to the collaboration of Utsi Electronics, who provided the GPR equipment, it was possible to put into practice the theoretical classes just heard. In the first day, the trainees had chance to conduct electromagnetic tests, with several GPR devices, over a flexible pavements located internally to the University. Trainees were free to direct the GPR surveys where they preferred. After the data were collected, trainees had the opportunity to face a processing phase, by using the PC's furnished by the hosting university. Data were uploaded and then basic processing procedures were applied. In the second day, the practical training was held in a car parking of the University. A previous check of the design drawings of the parking showed that in that area were

buried several utilities pipes. With the aim of detecting such utilities, trainees were sorted in three groups.

Each ground employed a different GPR system to survey a particular area within the parking. This time the survey protocol was more rigorous and trainees were invited to draw on the surface a grid to follow when collecting the data. After the data collection, a rough processing phase was performed in the PC lab. The gathered data were really useful for giving to the trainees the idea of the potentialities of GPR in detecting buried utilities, but represented a cue for a research work as well. Indeed, besides the presence of design drawings of the area, which is not a so common condition, we found in availability of data collected through several GPR configuration, meaning many different centre frequencies of inspection. We decided, then, to gather all the data and to work on a comparison between different radar system and different processing techniques, with the aim of defining the best configuration of hardware-software for detecting and imaging the buried utilities.

2.2.2. The experimental framework

The experimental experience consisted in defining three grids onto the paved surface of the parking locating within the Saint Mary's Building of the University of West London, London – see Figure 1. Since maintenance works occupied part of the parking, the three grids were distributed in the remaining space. It proved hard to retrieve the data coming from one of the three GPR systems, so this work, at the moment, is focused on two configurations out of the whole three Figure 2. The two grids, namely 1 and 2, covered paved areas of 4 × 10 m and 6 × 7 m, respectively. Due to limited time resources, the spatial resolution of the grid was set as 1 m. With such a poorly dense sampling, it is thus expected a low imaging effectiveness. Nevertheless, it is worth expecting a good detection performance of the subsurface utilities network. By observing Figure 2, it is possible to verify intersections between the selected grids and the existing utilities as reported in the map. In particular, grid 1 overlaps the direction of a drainage pipe (dashed blue line),

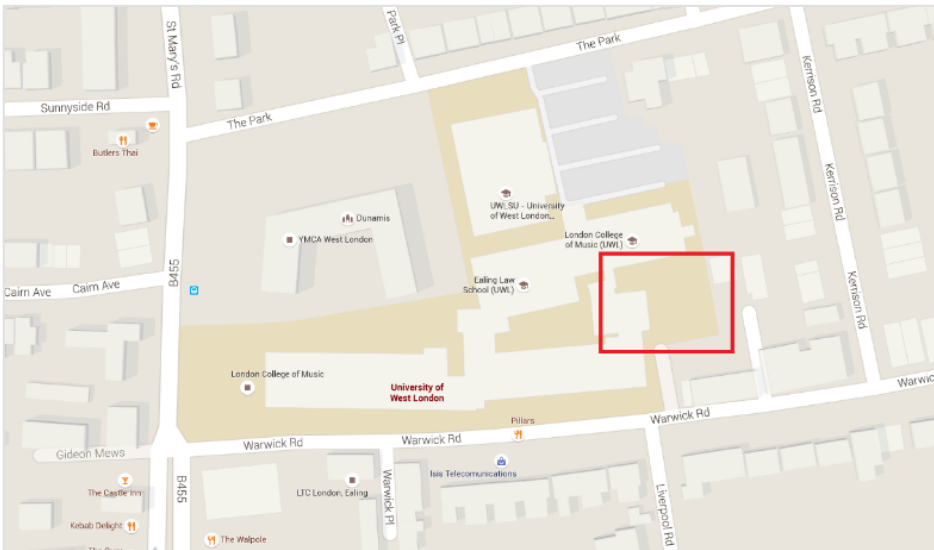while grid 2 intercepts a big-sized retention tank located at an unknown depth (cyan rectangle).

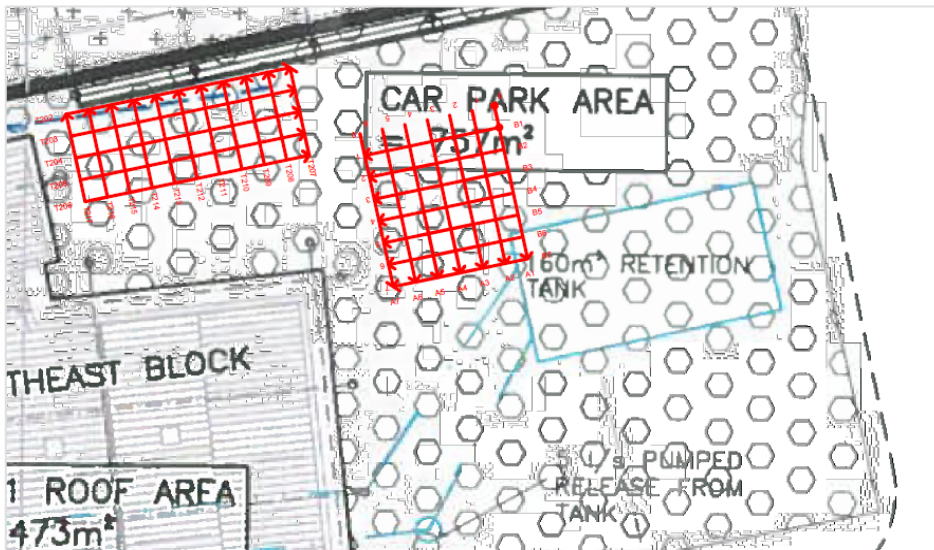
Fig. 1 – Location of the survey site

Fig. 2 – Design drawing of the parking with the two survey grids

More design drawings were available for the check of existing underground utilities. In Figure 3 is shown another drawing reporting the same tank of Figure 2, even if in a slightly different position (blue rectangle), and a network of Light Voltage (LV) cables (blue double-lines), running just below the grid 2.
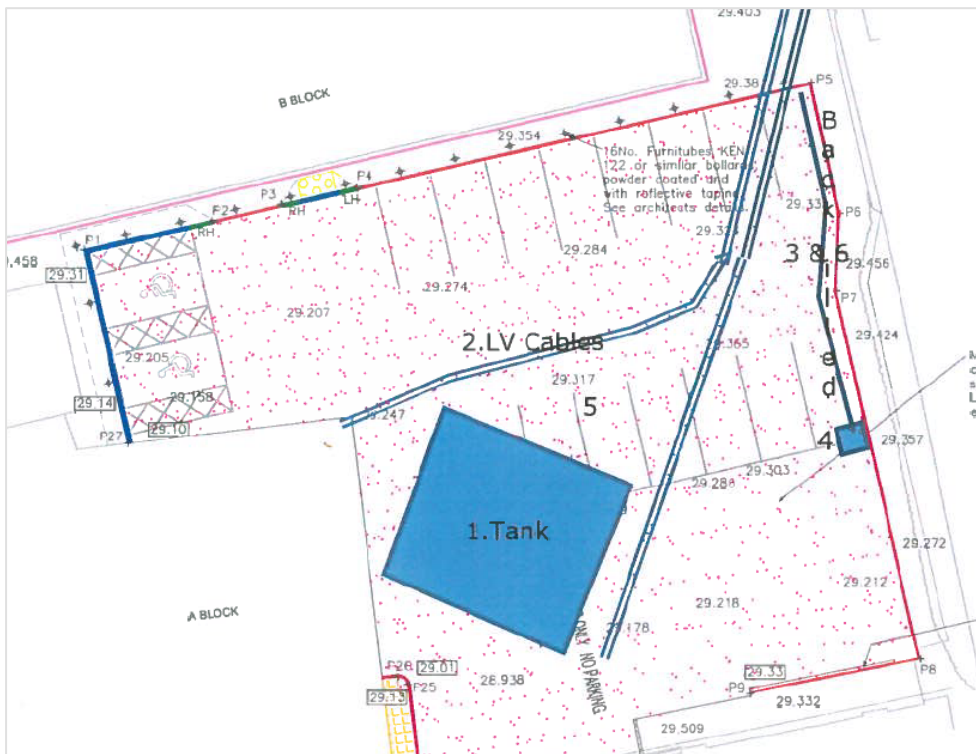

Fig. 3 – Second design drawing of the parking

Another important step of the experimental phase is the visual inspection of the survey site. Indeed, it was possible to retrieve information about the presence of underground utilities by checking whether the paved surface was subjected to excavations subsequent to the construction of the parking. By looking at an aerial view of the parking Figure 4 it is possible to match the information coming from the second design drawing Figure 3 and

confirming the presence of a LV cable network, recognizable from the concrete-paved paths. Another important insights that is possible to retrieve by a visual inspection of the survey site is the contingent presence of three different types of pavement: always referring to Figure 4, is it possible to recognize

i) a brick-paved area, dedicated to disable parking, in the top-left corner,

ii) the original flexible pavement located in the central part of the parking and interested by the excavation for the LV cable installation and

iii) a rigid concrete pavement probably realized on the occasion of the retention tank realization, in the bottom-right part of the picture.

Fig. 3 – Aerial picture of the parking with visible LV cables paths

2.2.3. The GPR equipment

The GPR systems were furnished by Utsi Electronics Ltd. In particular three devices were employed:

1. A Data Logger ground-coupled pulsed system, equipped with a 400 MHz centre frequency shielded antenna and mounted on a cart Figure 5, used for grid 2.
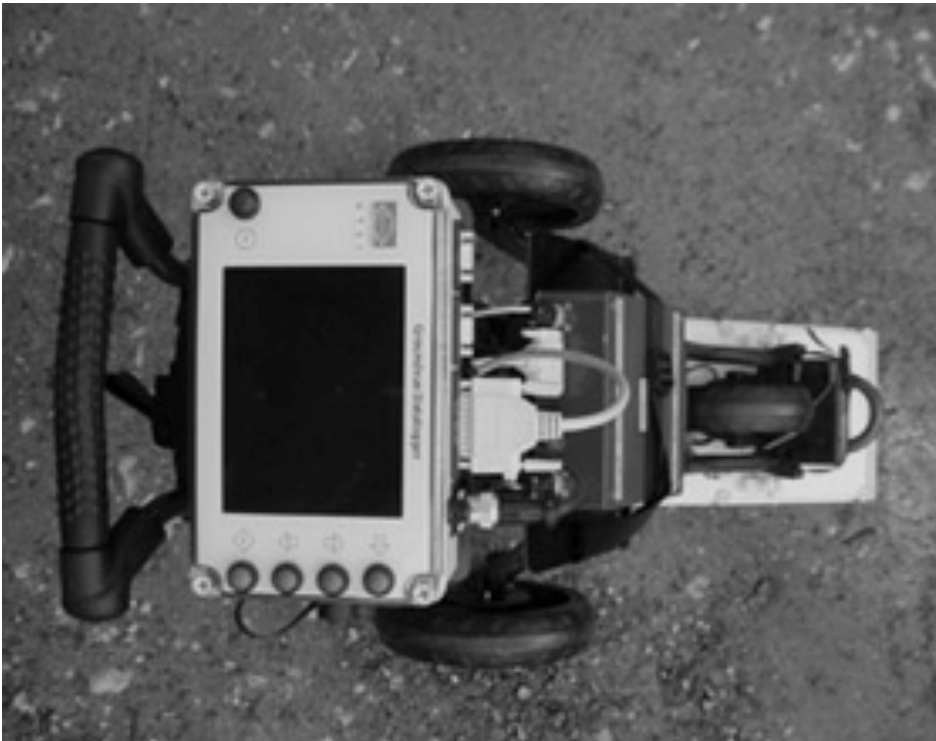

Fig. 5 – Data Logger by Utsi Electronics

2. A GroundVue 3_1 ground coupled pulsed 3-channels system, operating at three different centre-frequencies, of 250 MHz, 500 MHz, 1 GHz Figure 6, and employed for grid 1.

Fig. 6 – GroundVue 3_1 by Utsi Electronics

3. A GroundVue 3_8 ground coupled pulsed 8-channels system, operating in parallel at high frequency (4 GHz) Figure 7, employed for grid 3.

2.2.4. Data Processing

The next step is represented by the processing phase. In the research plan the processing has to be carried out by adopting three methods:

- Commercial Software (Reflex, IDS GRED, RADAN, …)
- Free-source Software (GprMax, MatGpr, …)
- Mathematical Computer Software (Matlab, Python, …)

At the state of the art, data were processed by using Matlab 2010. One first issue encountered in processing the data is the need for flipping the traces collected along the grid lines in order to uniform the direction of scan. This procedure was necessary since, to avoid wastes of time, half the scans were performed in one direction, and the other half were performed in the way back. For resolving this issue, a relevant code was implemented in Matlab.
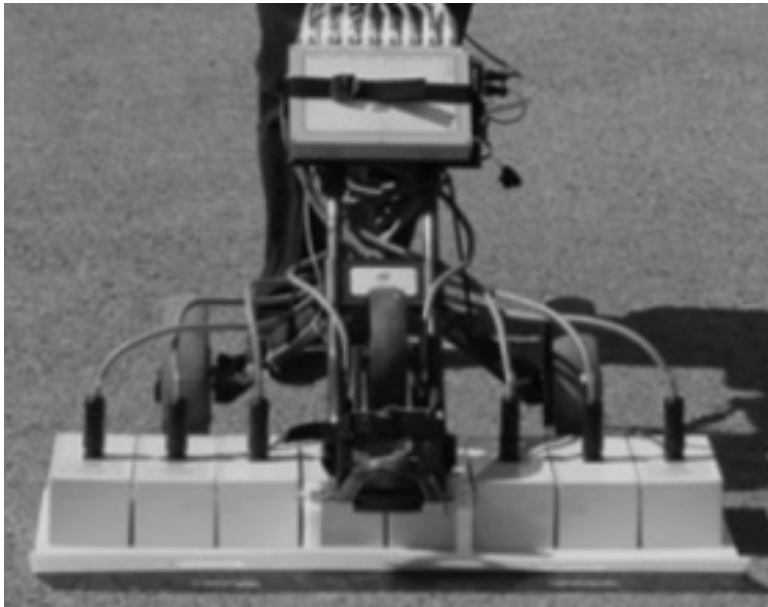

Fig. 7 – GroundVue 3_8 by Utsi Electronics

Subsequently, data were subjected to time-zero correction procedures. In this way, the thin layer of air between the source of the antenna and the paved surface is deleted from the signal. This step is mandatory for a quicker and correct time-depth conversion. Then, a Zero-offset removal was applied to each trace.

This processing step is performed by subtracting from each sample of the processed trace, the mean of the amplitude of the single trace. In this way, every radar sweep is centred on zero, and

is so ready for further steps, as gain or migration procedures. Moreover, a background removal was applied to each radar scan, in order to better highlight the underground dishomogeneities, which could represent a buried utility. It is worthwhile reminding that, since the background removal works substracting from each sample the value of the average amplitude, calculated at the same reflection time on the whole radar scan, one of the results of this procedures is to remove all the continuous horizontal layers. The Figure 8 shows a radar trace from the data collected by the Data Logger (400 MHz centre frequency) before Figure 8 (a) and after Figure 8(b). It is clearly visible that due to subtraction of the average, in spatial terms, all the constant horizontal reflections (caused by noise, in this case) have been removed.
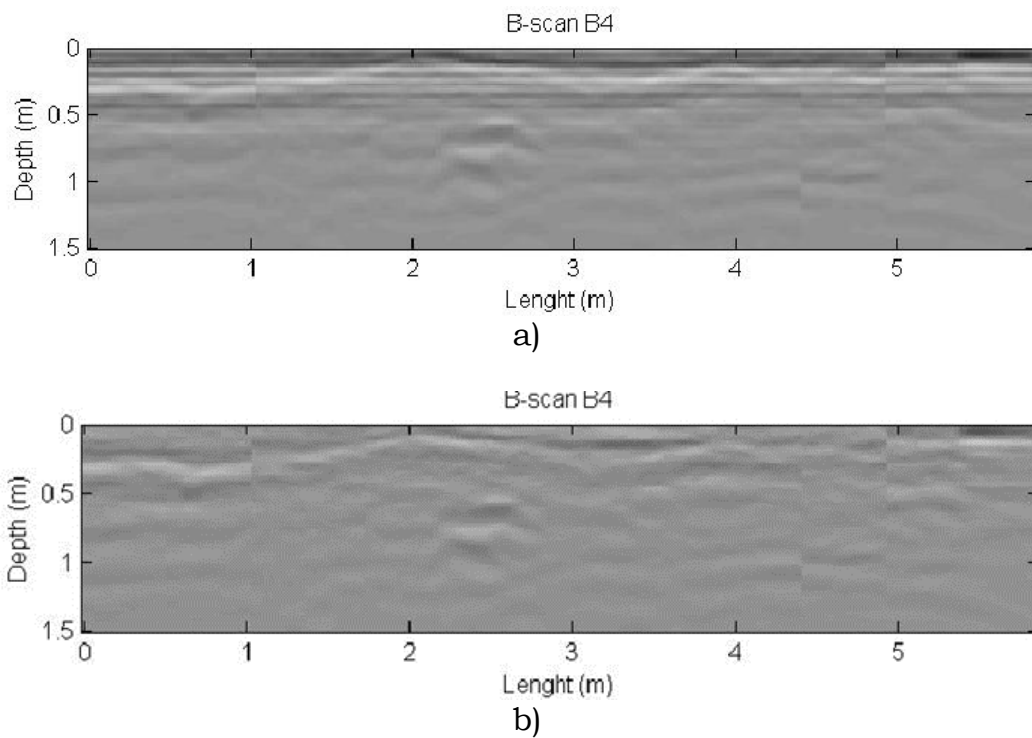

a)

b)

Fig. 8 – B-scan of a GPR survey (a) before and (b) after background removal

It was definitely easier, after the background removal, to recognize the layers of the pavement and the presence of a discontinuity in the reflection localized at around 2.5 m, probably due to a buried pipe.

Next steps in the data processing will include bandpass filters applied in the frequency domain, in order sensibly increase the signal-to-noise ratio, and the migration procedure, in order to collapse hyperbolic reflection to a point and then to infer more information about the precise depth of the target and its size.

2.3. NON-DESTRUCTIVE HEALTH MONITORING OF STANDING TREES

2.3.1. Introduction

During the three-month period spent at the University of West London, in the context of a starting research project involving several scientific parts and taking place within the Q-Garden, in London, I had the chance to face the topic of the health monitoring of standing trees through non-destructive technologies. As the study was at its very first steps, I dealt with a bibliographic research concerning the state of the art about this particular subject.

2.3.2. The State of the Art

The term Non-Destructive Evaluations (NDE) is generally referred to any process addressed to the determination of physical or mechanical properties of an object, that does not involve any disturb or modification of the assessed target. The techniques through which the NDE are carried out and that lead to the provision of the desired information (qualitative or quantitative, depending on the case) are generally named Non-Destructive Test (NDT) techniques. [Ross and Pellerin, 1991; Bodig, 1995]. Since trees have begun to be felled and used as material for human purposes, primary amongst them the production of load-bearing structural elements such as beams or pillars, a first sort of NDE was performed. The nature of this first evaluation was based on the

visual recognition of external symptoms of inner biological decays or defects.

This kind of assessment was aimed at the selection of the best timbers for the different purposes and at the avoidance of both time and resources wastes related to the felling of already decayed trunks. The first scientific examples of NDE date back to the early twentieth century, and exploited the theory of elasticity and the new generation testing tools. Main goal of the researcher was the definition of the strength of wood, expressed in terms of elasticity modulus (E [MPa]), by applying static [Horig, 1935; Kollmann and Krech, 1960] and dynamic methods [Barducci and Pasqualini, 1948; Hearmon 1948; Jayne 1955; Fukada et al. 1956; James 1959]. What once was a purely qualitative method upgraded to a scientific inspection method, named Visual Tree Assessment (VTA) [Mattheck and Breloer, 1994]. The need for efficiency in wood industry led the research activity towards the development of always more reliable methods and simultaneously encouraged the employment of new methodologies. In such this framework first applications of ionizing radiations [Cown and Clement, 1983], ultrasounds [Beall, 1987], microwaves [Martin et al., 1987], electrical resistivity [Kumar and Gupta, 1993] and more methodologies for the assessment of quality of wood-based materials, are recorded. More recently, the research efforts in this field began to be addressed also towards different goals. As the sensibility for the natural environment has greatly increased in the last decades, management and control of the forestall heritage and floral system has become a high priority objective. Even though the wood of dying and decayed trees plays an important role, increasing structural and biological diversity of the forest, creating an habitat for wildlife, and providing depots for organic matter recycling agents [Parks and Shaw], it appears mandatory to face the issue represented by unknown pathogens, usually coming from abroad, due to trade processes or carried along by the wind. The occurring of the spreading of such pathogens, fostered by the wind especially in tall-stem trees, can lead to epidemic phenomena often causing the quick death of entire forests.

Two different approaches can be adopted to avoid such an eventuality. An active one, consisting in the avoidance of the contact between the pathogenic spores and the trees being protected. This can be achieved by performing bio-security measures at the borders of the interested country or region. Thus, the final goal of this approach is to actively hit the source of the problem, keeping the threat out of the borders. A second one, passive instead, consists in applying a policy of control and management of the forestall heritage, in order to identify the early stage symptoms of the disease. Once identified, it will be possible to eradicate the problem or, at least, limit the spreading below epidemical thresholds [UK Forestry]. Since this approach is based on the monitoring of living trees, often considerably aged and valuable, invasive methods of health assessment such as branches cutting off or incremental coring, are to be considered non suitable. Here lies the key-role played by NDE in this framework. Indeed, these evaluations not only allow assessing the trees without involving any damage to the tree itself, but also permit high-efficiency surveys with a large number of specimens monitored in a relatively short time, a competitive costs.

REFERENCES

I. Barducci, G. Pasqualini; Misura dell'attrito interno e delle costanti elastiche del legno, Zanichelli, 1948

F.C. Beall; Future applications of acoustic emission and acousto-ultrasonics. Proc of the 6th Symposium on Nondestructive Testing of Wood. Pullman (Washington, USA), pp. 369-376, 1987

J. Bodig, K. C. K. Cheung, T. P. Cunningham; Engineered wood construction: Structural properties for LRFD, Journal of Structural Engineering (US), 1995

D. J. Cown and B. C. Clement; A wood densitometer using direct scanning with x-rays; Wood Science Technology, 17(2): 91-99, 1983

E. Fukada, S. Yasuda, J. Kohara, H. Okamoto; Dynamic Young's modulus and piezoelectric constants of old timber; Bull Kubayasi Institute of Physics Research, 6, 104-107, 1956

R. F. S. Hearmon; Elasticity of wood and plywood, HM Stationary Office, London, 1948

H. Hurig; Anwendung der Elastizitatstheorie anisotroper Korper auf Messungen an Holz., Ing. Arch. 4: 570-576, 1935

B. A. Jayne; A nondestructive test of glue bond quality; Forest Products Joirnal, 5(5); 294-301; 1955

M. Kumar and R. C. Cupta; Electrical resistivity of Acacia and Eucalyptus wood chars; Journal of Materials Science, 28, 440-444, 1993

F. Kollmann and H. Krech; Dynamic measurement of damping capacity and elastic properties of wood, U.S. Dept. of Agriculture, Forest Service, 1960

P. Martin, R. Collet, P. Barthelemy, G. Roussy; Evaluation of wood characteristics: Internal scanning of the material by microwaves; Wood Science Technology, 21: 361-371, 1987

C. Mattheck and H. Breloer; The body language of Trees. A handbook for Failure Analyisis; HMSO, London, Uk, 1994

C. G. Parks and D. C. Shaw; Death and Decay: A Vital Part of Living Canopies; Northwest Science, 1996

R. J. Ross and R. F. Pellerin; Nondestructive Testing for assessing wood members in structures, a review; U.S. Dept. of Agriculture, Forest Service, 1991

3. DESCRIPTION OF THE MAIN RESULTS OBTAINED DURING THE STSM

3.1 GPR APPLICATIONS ON TUNNELS: EUROPEAN GUIDELINES

The guidelines, named "Guidelines for investigating Tunnels by using Ground Penetrating Radar, with particular regard to location of reinforcement in tunnel lining, thickness of tunnel lining, homogeneity of tunnel linings, structural detailing, moisture ingress detection" are structured as follows:

• Scope

In this brief section is given a depiction of the objective of these guidelines. As mentioned, the main task is to uniform towards a higher quality level, the standard and the reliability of the GPR procedures. The target of the guidelines includes the survey equipment, the field procedures and the interpretation methods.

- Reference Documents

This section stands for a bibliography of all the documents used as reference for developing the guidelines. The documents are sorted in COST Action TU1208 publications, COST Action TU1208 co-edited publications, and other documents.

- Terminology

For a greater readability of the guidelines, this section includes all the scientific terms used throughout the document, sorted in General Terms, Terms Specific to Ground Penetrating Radar, and Terms specific to Tunnel Engineering.

- Apparatus

This section will describe the radar devices possibly employed for tunnel inspections. First the most used GPR systems, i.e. pulsed radar and Stepped Frequency Continuous Wave (SFCW) radar, and the most common antennas (ground-coupled and air-coupled) are described. Then, a sub-section is dedicated to the description of the supplementary survey techniques, which can hold a key-role in such a complex environment as tunnels.

- Preliminary Activities

Herein are listed all the operation that must be done before the GPR surveys, in order to avoid time wastes and interpretation faults. A first step is represented by a reconnaissance survey, i.e. a visual inspection of the tunnel for identifying every possible issue that could be encountered during the survey and that, if not taken into account, could slow down or make impossible the testing. In this sense, possible challenges, obstacles, accessibility to the tunnel, and so on, are features that must be checked. A second mandatory step, prior to the surveys, is the compiling of information about the structure. For a quicker and correct interpretation of the data, and for an indication about where to collect the radar data, it is important to have knowledge of the tested environment as complete as possible. Before starting the surveys, then, it is crucial to gather the more information about the

surveyed structure, like design drawings, construction materials, quality of built, historical issues, previous works, etc. Another important preliminary activity is a clear meeting with the client. In this occasion, it is crucial to set the objectives of the survey and to clarify to the client what is deliverable by carrying out a GPR survey. This will avoid disappointments over the results of the survey. Once fixed the objectives, it is important to proceed with a detailed planning for survey. In this section are listed the activities that the surveying team has to perform prior to the survey, in order to not incur in delays during the tests, or in the collection of low-interpretable data. In this sense, it is important to check the required facilities and infrastructures, to choose the proper antenna system so that the resolution gained is coherent with the size of the targets, to train the operator if it appears necessary and to check the availability of equipment in time (e.g., the batteries). Concerning the operations on-site, it is important to have a clear idea of the conditions in which the operators will be performing the test, and of what will be the methodologies employed. With this purpose, it is useful to produce two reports, before the surveying phase. The first one will be named "method statement" and will include the precise description of how the data will be practically collected. The second, namely "risk assessment of the whole operation", is a very important document, including all the safety measures that must be taken into account to avoid as far as possible, accidents on-field. Moreover, in this phase of preliminary activities, the GPR system needs to be calibrated, and the survey paths have to be set. In particular, here it is mandatory to think about the geo-referencing of the collected data. Often, the GPS does not work in tunnel environment. This fact forces to adopt different measures to have properly referenced data, which is a fundamental condition for proceeding to a correct interpretation of radar data.

- Methodologies

This section deals with the explanation of how the set objectives are going to be achieved. Of course this is a matter that changes, inevitably, from case to case depending upon the requirements of the projects. Nevertheless, herein will be listed the most common

methodologies suitable for tunnel inspection through GPR. The section includes the Hardware and the Software components, the approach to the survey and the possible solutions to the georeferencing issue, the possible supplementary equipment, as scissor lift or spatial vehicle, and the data processing and interpretation processes.

- Applications

Here are listed the main application of GPR in the tunnel engineering. This section is the core of the guidelines, and includes the real operative indications for the companies or research teams that are planning a new GPR survey. For every application was considered a sub-section dedicated to the general methodology to be applied. Moreover, insights concerning the data collection, the data processing and the interpretation of data will be given. Even though new break-through from the research community will surely enlarge the field of applicability of GPR in the inspection of tunnels, at the moment, the main applications of this tool are: location of reinforcement in tunnel lining; the evaluation of the thickness of the tunnel lining; the analysis of the homogeneity of the tunnel lining; the structural detailing; the moisture ingress detection.

3.2 A STUDY CASE: UNDERGROUND UTILITIES DETECTION THROUGH GPR

By looking at the B-Scans and through a tomographic approach (C-Scan visualization), it was possible to reach a first step of interpretation of the data. Here is reported a preliminary analysis of the grid 1. In Figure 9 is reported the visual inspection of the area interested by the survey, delimited by the white dashed line. It is clearly visible the change of pavement between the bricks and the asphalt, and the utilities network, in blue dashed lines. Besides, a small manhole is identified and signed with a red rectangle.

At high frequency (1GHz) is easily possible to verify the change of pavement Figure 10, located at around 7 m. After this

distance, indeed, it is possible to identify different layers typical of a flexible pavement. By observing the same longitudinal scan collected at low frequency (250 MHz), the information is still recognizable, even at a lower resolution Figure 11.
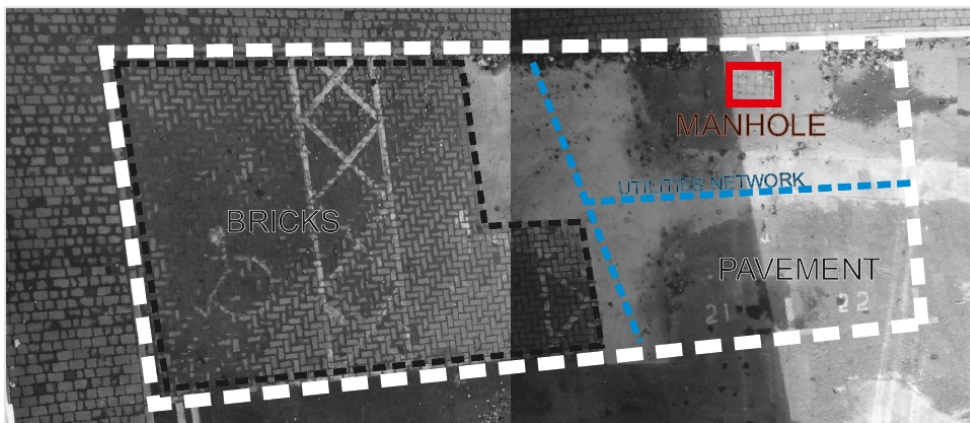

Fig. 9 – Visual inspection of grid 1

Furthermore, in this case is possible to detect, it is possible to detect multiple reflections coming from objects located at around 2.5m, 5.5m and 7.5m distance and at a depth ranging from 0.4m to 0.8m, which can possibly be originated by buried pipes, as the visual inspection partially seems to suggest (blue dashed line in Figure 8. Same targets were evidently located at a too high depth for the penetration of the electromagnetic wave with a 1 GHz of frequency, given the nature of the materials passed through.

The tomographic approach seems to confirm the presence of a buried utility pipes as well. If C-scan at 75 cm of depth is considered, the information coming from the 250 MHz data found confirm in three oblique red lines, indicating areas of high amplitude value Figure 12. This is a first example of how choosing a survey frequency despite another one can radically affect the quality of the information it is possible to retrieve from the survey itself.
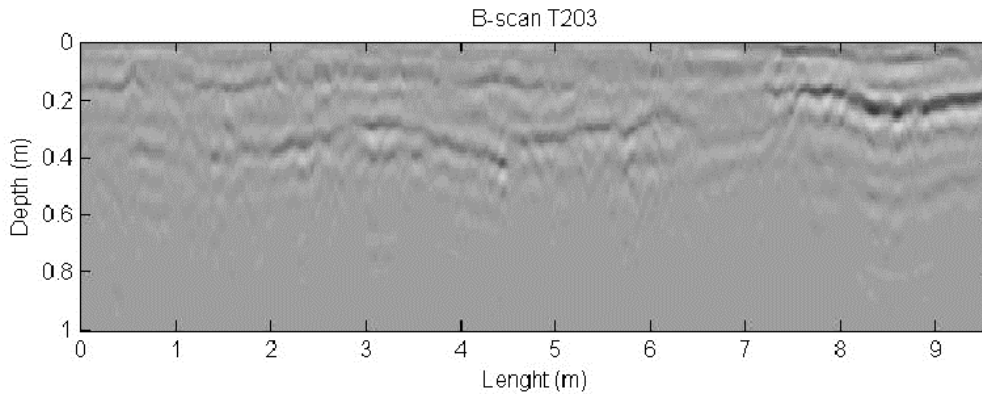
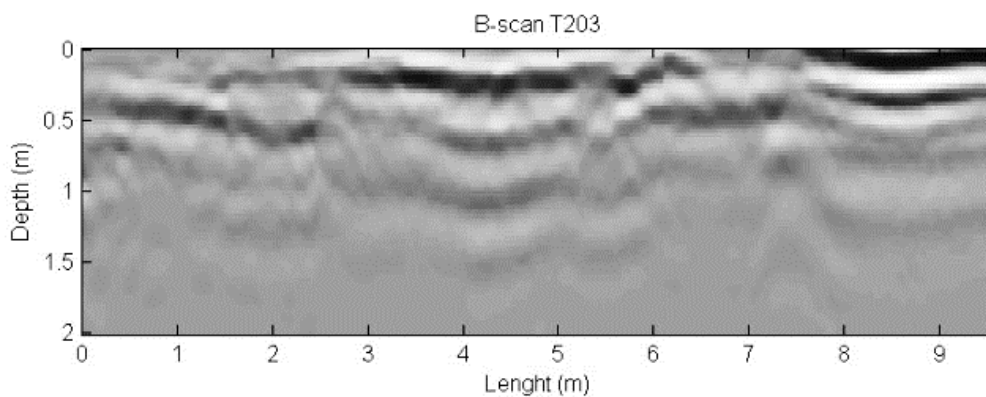**Fig. 10 –** Longitudinal 1GHz scan of grid 1.

Fig. 11 – Longitudinal 250 MHz scan of grid 1

3.3. NON-DESTRUCTIVE HEALTH MONITORING OF STANDING TREES

The information gathered in this period are meant to be included in a wider review about the topic. The main goal of this review will be the identification of the gap of knowledge in this field of research. Subsequently, an experimental project in order to plan the surveys on the trees in the Q – Garden has to be developed with care. The achieved results will then be useful for future publication, possibly within the framework of transversal activities of COST Action TU1208.

4. FUTURE COLLABORATION WITH THE HOST INSTITUTION

As the University of West London will be provided of GPR facilities, new research experiences will be surely settled. Moreover, when the Q-Garden Project will join in an active phase, the collaboration between Roma Tre University and University of West London will be re-established in order to joint different competences and to achieve better results.

5. FORESEEN PUBLICATIONS/ARTICLES RESULTING FROM THE STSM

The paper "Buried utilities detection with GPR: a comparison between employed central frequencies and processing procedures" was presented at the 16th International Conference of Ground Penetrating Radar (GPR 2016), The Hong Kong Polytechnic University, 13-16 June 2016. Moreover, the review concerning the health monitoring of standing trees through non-destructive techniques will be submitted to a journal, once completed.

ACKNOWLEDGEMENT

STSM 4

PROCESSING ALGORITHMS TO ASSESS WATERFRONT LOCATION IN BUILDING MATERIALS BY USING GPR

Visiting Scientist: Isabel Rodríguez Abad, Universitat Politècnica de València, Valencia, Spain (isrodab@upvnet.upv.es)

Host Scientist: Jean-Paul Balayssac, INSA Toulouse-Univeriste Paul Sabatier, Touluose, France (jean-paul.balayssac@insa-toulouse.fr)

STSM Dates: 06 November – 22 November 2015

1. PURPOSE OF THE STSM

The durability of concrete structures and other building materials, such as timber, depends mainly on the ease whereby water and any aggressive chemical agents dissolved therein can penetrate. Therefore, measuring water penetrability in building materials is crucial mostly when structures are in service. In this context, non-destructive techniques play an important role. In particular, the electromagnetic waves emitted by Ground-penetrating radar (GPR) are very sensitive to the water content of the medium through which they propagate.

This fact provides an interesting opportunity to analyse if the GPR technique allows the assessment of water penetrability in building materials with enough accuracy. In line with this, after having conducted several laboratory experiments and relevant analysis studying the capability of GPR to assess water penetrability in hardened concrete, it is necessary to develop specific processing algorithms to understand how the water penetrates and how the wave parameters will be affected in different building materials. Water content has a decisive influence on the dielectric properties of building materials. Therefore, changes in wave parameters will occur as a result of the advance of the waterfront and might provide reliable information, both

qualitative and quantitative, about where the waterfront is located. In particular, the application of GPR in the building materials area is providing very promising and interesting results, which highlight the strong relation between wave propagation parameters (velocity and energy level) and water content.

During this STSM, research activities focused on the analysis of the capability of the GPR technique for evaluating water penetration into building materials (concrete and timber), through the assessment of the waterfront advance.

2. DESCRIPTION OF THE WORK CARRIED OUT DURING THE STSM

For this purpose two different experimental programs were designed and conducted:

- Concrete samples were manufactured (water/cement = 0.65), which after curing (90 days) and oven drying were immersed in water for a certain time.
- 4 batches of pines timber samples (Ruso, Mobila, Pinaster and Insignis) were put under study. The four types of timber were chosen among the most commercialized in Spain used for building structural purposes, so as the dimensions of the samples.

In both experimental programs, the samples were immersed in water 3 cm for a certain time: see Figure 1a.

After that GPR measurements were performed at specific time intervals, removing the samples from water to conduct the GPR acquisition. A 2.0 GHz centre frequency antenna manufactured by GSSI was used to carry out the measurements: see Figure 2. A metallic reflector was placed at the bottom of all samples.

Regarding the concrete sample measurements, the antenna was placed over the same side of the sample that was immersed into water, since previous successful studies have been conducted placing the antenna in the dry side. But in the case of timber samples, the acquisition was performed placing the antenna in both sizes, over the immersed side and subsequently over the dry

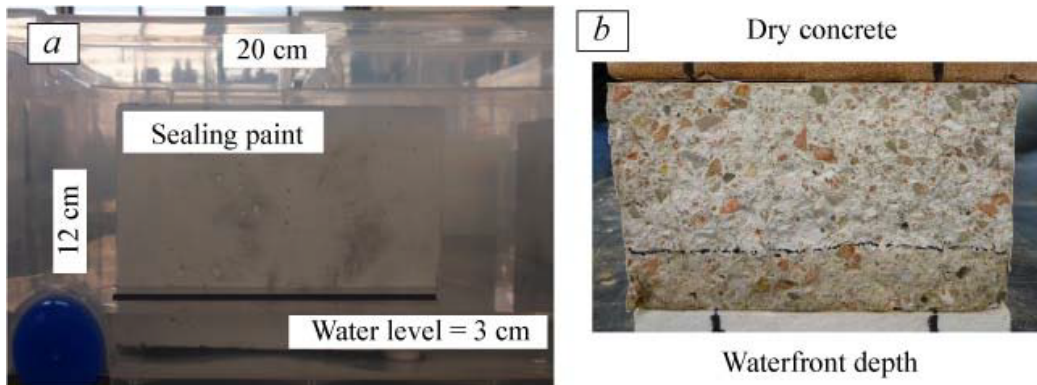side of the samples, since it was the first attempt to detect waterfront location.

Fig.1 – (a) Concrete samples immersed into water; (b) Waterfront marked in the sample after breaking the samples in two pieces.
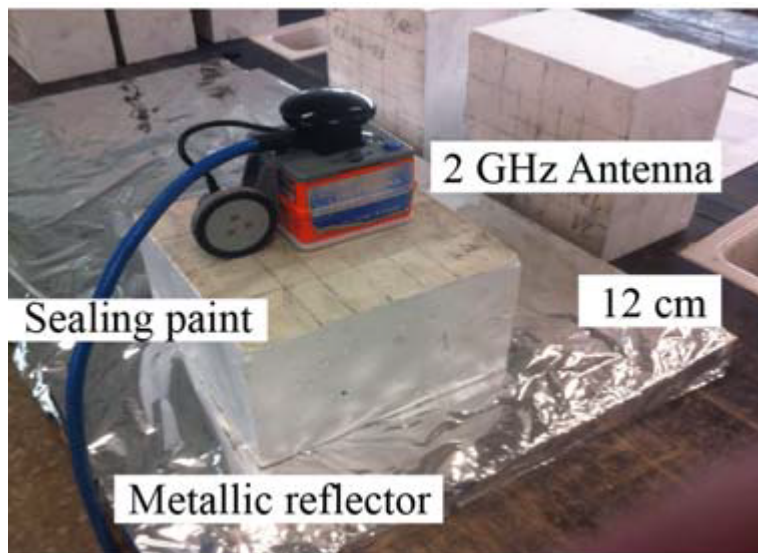

Fig. 2 – Static GPR acquisition.

Another difference in the two experimental programs was that in the case of the concrete samples the waterfront advance was possible to be estimated by breaking the sample, right after the GPR measurements: see Figure 1b. Therefore, all GPR parameters will be compared with the waterfront location estimated by visual inspection. Nevertheless, it was not possible to break the timber samples after acquiring the GPR measurements; therefore the GPR parameters will be compared with the absorption coefficient.

3. DESCRIPTION OF THE MAIN RESULTS OBTAINED DURING THE STSM

3.1. CONCRETE EXPERIMENT

Waterfront evolution:
Firstly, water content coefficient (CA) was calculated – see Table I.

$$C_A(\%) = \frac{M_{im} - M_d}{M_d} * 100 \qquad [1]$$

where *Md* is the dry mass of the sample and *Mim* is the mass after the immersion into water. Secondly, after breaking the sample, the waterfront depth was measured in both sides of the broken sample – see Figure 1b. The final waterfront depth (*Wf*) value employed to correlate with the GPR data was the average of the front line marked by visual inspection in both sides – see Table I.

3.1.1 EFFECT OF WATER CONTENT ON DIRECT AND REFLECTED WAVE SIGNALS

Previously to perform any measurements in the radargrams, it was necessary to understand the received signals. They were composed by two parts: the direct wave, considering this one as the overlap between the air wave and the direct wave itself, and the reflected wave at the bottom of the samples: see Figure 3. Both of them are composed by 3 peaks, respectively.

To calculate the propagation velocities, it is necessary to measure the arrival times in the radargrams. But, the received direct wave is an overlap that occurs between the air wave and the direct wave itself. Therefore, it was very complex to determine

which the maximum representative of the direct wave arrival is. Regarding the reflected wave, due to the fact that the wave travelled inward the material and in its path suffered attenuation and the effect of the media, it was also very complex to determine the exact position of the reflected arrival time.

TABLE I – WATER CONTENT PARAMETERS

Sample	*tim* (min)	*Wf* (cm)	CA (%)	Sample	*tim* (min)	*Wf* (cm)	CA (%)
1	20	0,52	0,31	**13**	260	3,58	1,33
2	40	1,27	0,46	**14**	305	3,56	1,42
3	60	1,21	0,50	**15**	325	3,65	1,51
4	80	1,88	0,63	**16**	345	3,94	1,64
5	100	1,97	0,68	**17**	365	4,09	1,64
6	120	2,14	0,74	**18**	385	4,60	1,79
7	140	2,36	0,82	**19**	405	4,22	1,77
8	160	2,56	0,88	**20**	425	4,17	1,80
9	180	2,71	0,91	**21**	445	4,42	1,80
10	200	2,72	0,99	**22**	465	4,66	1,98
11	220	2,80	0,98	**23**	485	4,56	2,01
12	240	3,11	1,12	**24**	505	4,66	1,93

* **tim**: Immersion time

For all this reasons, the velocity was calculated with all the peaks combinations of the direct and reflected waves, in order to assess which one provided better agreement with the waterfront advance. For each sample and peak combination, the velocity was calculated with the following equation:

$$v = \frac{2d}{\Delta t_D^R} = \frac{\left(2\sqrt{h^2 + \frac{d_0^2}{2}}\right)}{\Delta t_D^R} \qquad [2]$$

Where d is the half of the path that the wave travelled, $d0$ was the distance between emitter and receiver (4 cm) and h the width of the sample (12 cm). Finally, the velocity difference when the sample was dry and wet was determined by equation 3 and Table II.

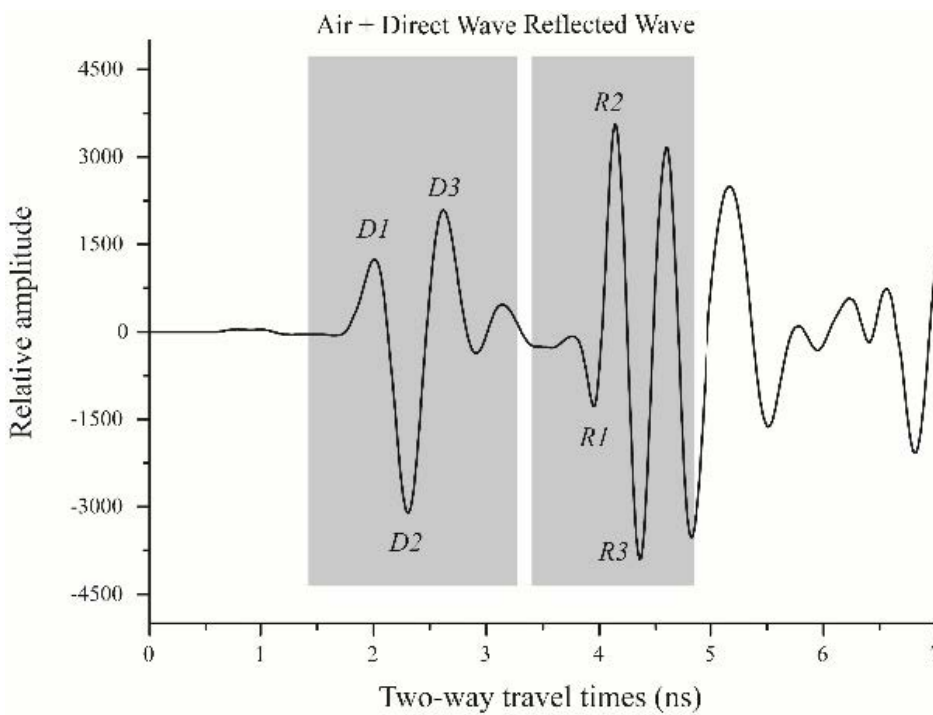$$\Delta v \left(\frac{cm}{ns}\right) = v_i - v_d \qquad [3]$$

Fig. 3 – Direct and reflected wave maximums when the simple was dry.

38

where vi is the wave velocity when the sample was immersed into water and vd was the velocity when the simple was dry. As it can be observed in Table II all velocity increments calculated from peak D1 were found to be negatives. This was the expected result, but in the velocity increments calculated from peaks D2 and D3, the first few samples (up to a immersion time of 80 minutes) presented positive increments. They cannot be really positives, because of the water content increase. The point is that an overlap is occurring between the air and direct wave with the waterfront reflection, resulting in an offset of the D2 and D3 peaks. In addition, the velocity increments were correlated with the waterfront depth, to check which peaks combination provided a better agreement between both parameters.

In Figure 4 (a), (b) and (c) the better results of these adjustments were depicted. The results show a good agreement between velocity increments and waterfront depth for all peaks combinations (R2 = 94 99%), except for the ones that were calculated with the peak D3. This result was expected, since D3 is the peak that is most affected by two signals: the direct wave and the reflection of the waterfront. Therefore, it cannot be used as representative of the waterfront evolution. Very interesting adjustments were found when using peak D2. As describe above this peak is also affected by the 3 signals, as D3, and also positive velocity increments were obtained. Nevertheless, it is very interesting to point out that even this mix of the 3 signals correlates quite well with the waterfront advance.

These results are of quite importance, because even if we are not able to locate the waterfront reflection or if it was overlapped with the direct wave signal, we might predict the waterfront position with high reliability. In particular, the peaks combination calculated with peak D1 to assess the velocity increments presented an excellent correlations, which best one is plotted in Figure 5 combination peak R1 D1.

TABLE II – VELOCITY INCREMENTS (CM/NS) CONSIDERING ALL PEAKS COMBINATIONS OF DIRECT AND REFLECTED WAVES

|	R1	R1	R1	R2	R2	R2	R3	R3	R3
1	0,06	0,25	0,47	0,08	0,15	0,29	0,12	0,04	0,11
2	0,44	0,41	0,86	0,42	0,25	0,53	0,39	0,12	0,29
3	0,42	0,23	1,07	0,41	0,09	0,67	0,31	0,10	0,54
4	0,69	0,62	2,00	0,62	0,56	1,36	0,59	0,56	0,82
5	0,74	0,79	2,23	0,62	0,65	1,75	0,50	0,51	1,32
6	0,72	0,64	1,18	0,62	0,55	0,97	0,51	0,45	0,74
7	0,74	0,70	1,36	0,65	0,61	1,11	0,61	0,58	0,97
8	0,86	0,82	1,50	0,77	0,74	1,27	0,68	0,65	1,05
9	0,95	0,92	1,50	0,83	0,78	1,21	0,73	0,70	1,03
10	0,96	0,95	1,38	0,85	0,83	1,16	0,74	0,72	0,96
11	0,92	0,90	1,32	0,82	0,80	1,13	0,73	0,71	0,96
12	1,10	1,03	1,28	0,96	0,90	1,08	0,86	0,82	0,96
13	1,28	1,25	1,15	1,15	1,12	1,05	0,94	0,89	0,80
14	1,31	1,43	1,42	1,15	1,23	1,21	0,84	0,83	0,72
15	1,39	1,46	1,35	1,21	1,26	1,15	0,98	0,98	0,85
16	1,53	1,69	1,71	1,39	1,52	1,55	1,06	1,11	1,04
17	1,52	1,70	1,74	1,32	1,44	1,44	1,02	1,06	0,97
18	1,66	1,96	2,39	1,50	1,74	2,07	1,05	1,14	1,24
19	1,57	1,78	1,89	1,39	1,55	1,62	1,08	1,15	1,11
20	1,61	1,80	2,10	1,44	1,59	1,82	1,07	1,11	1,17
21	1,64	1,85	2,19	1,44	1,60	1,85	1,05	1,09	1,14
22	1,72	1,96	2,29	1,54	1,73	1,98	1,09	1,15	1,18
23	1,67	1,90	2,18	1,48	1,66	1,87	1,09	1,15	1,17
24	1,66	1,85	2,34	1,49	1,65	2,03	1,09	1,13	1,28
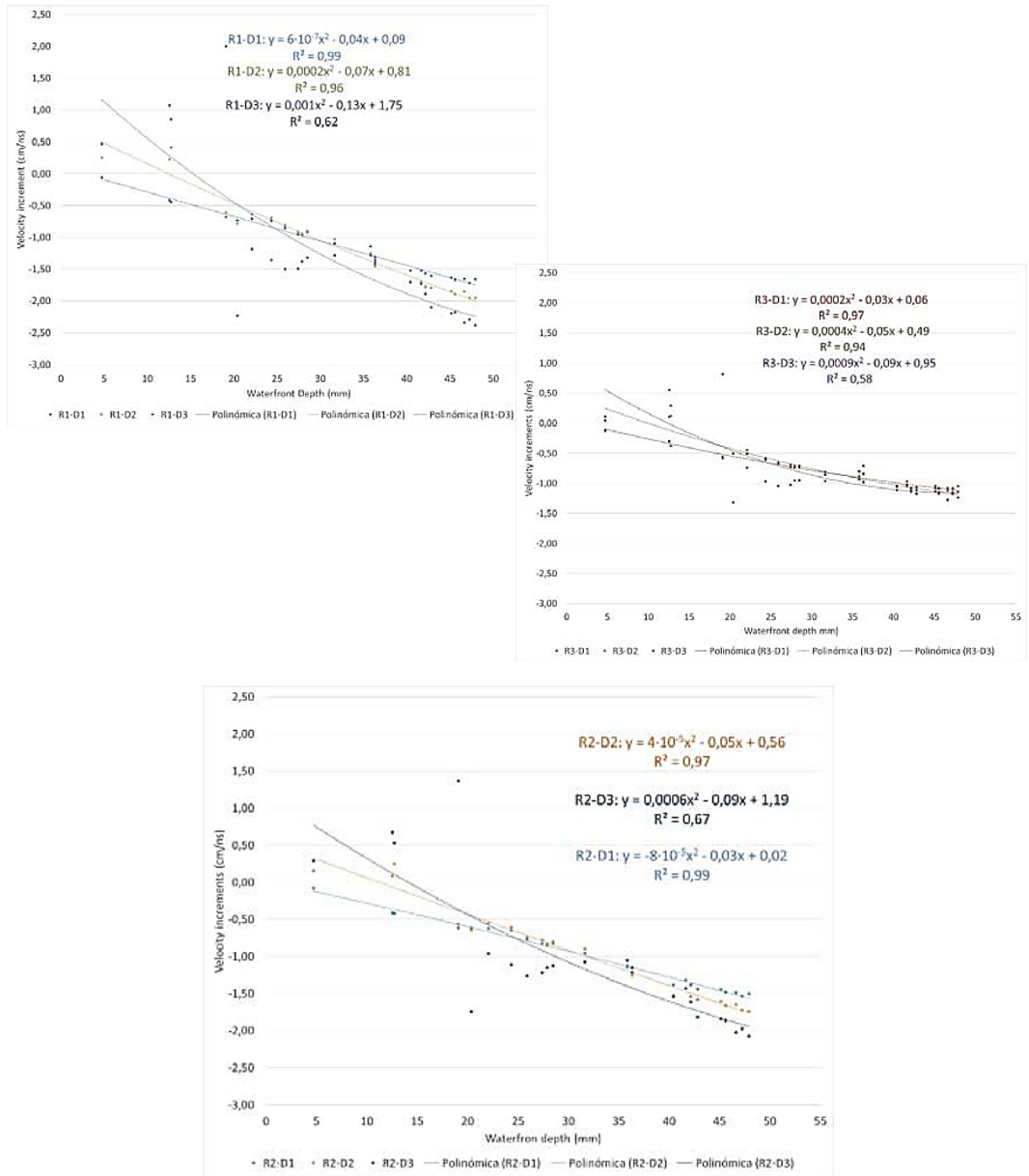
Fig. 4 – Waterfront depth adjustments versus velocity increments for all peaks combinations
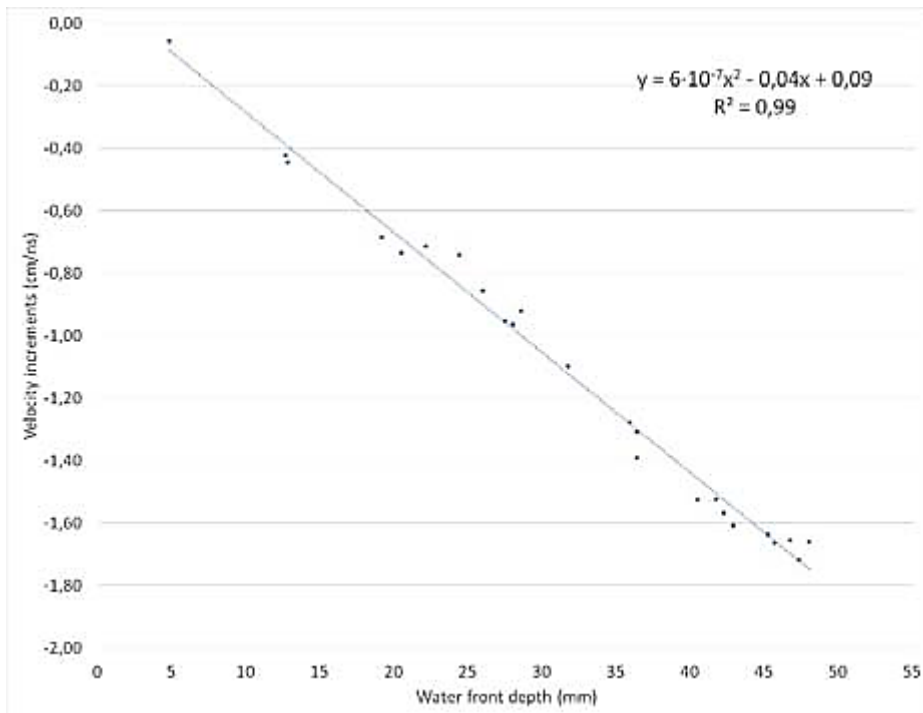
Fig. 5 – Velocity increments calculated with the peaks D1-R1 versus waterfront depth.

3. EFFECT OF WATERFRONT REFLECTION ON THE SIGNALS

The next step was to process the waterfront reflection. From sample 1 to sample 15 the waterfront reflection was overlapped with the direct wave - see Figure 6. Nevertheless, as the waterfront depth increased its signal become more easily identifiable (from sample 16 to sample 24). The waterfront reflection consisted on 3 maximums (F1, F2 and F3). But only when the waterfront reflection is separated from direct wave can be identified. Prior to any calculation of the waterfront location, it was necessary to check if the waterfront identification was correctly performed. With this aim the best correlation between the arrival times of the direct and reflected peaks and the waterfront peak was calculated.
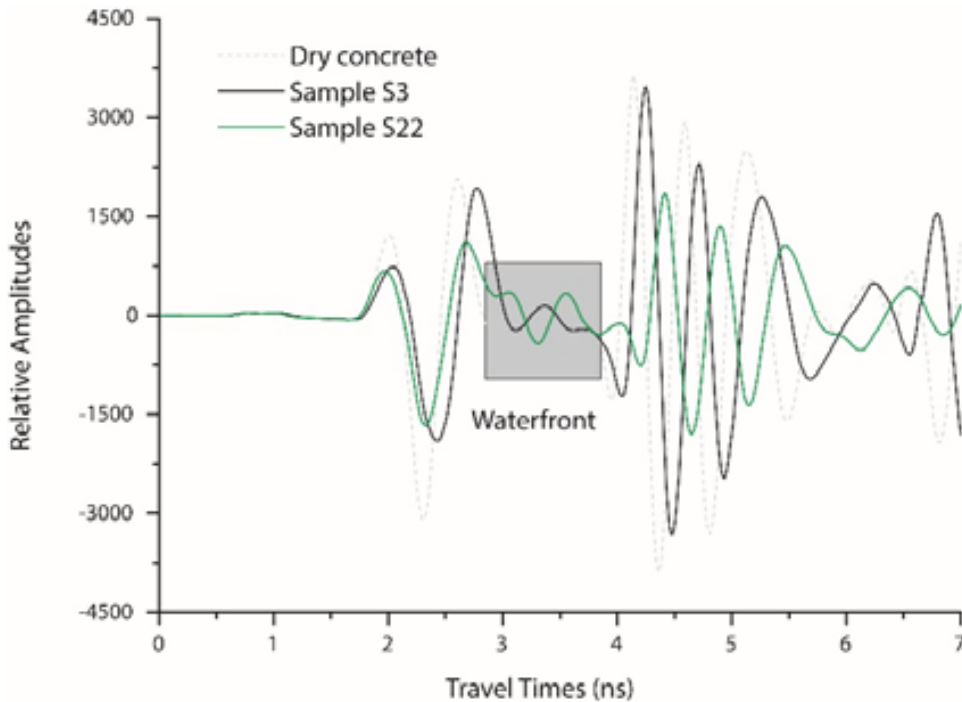
Fig. 6 – Waterfront reflection advance in the radar signals while water content increases.

As it can be observed in Figure 7 an excellent agreement was found between peak D2 of the direct wave and F3 of the waterfront reflection. Likewise, excellent results were found when relating peak R3 of the reflected wave and F3 of the waterfront. These results are of great importance, because that means that the GPR technique working with only one commercial antenna of 2 GHz central frequency has enough sensitivity to detect a waterfront that ranges from 0,52 mm to 4,66 cm. Even in the case that the waterfront reflection is overlapped with the direct wave, as it occurs, for the first 16 samples (345 minutes of immersion) the offset produced in the direct wave can be related with the waterfront arrival with high reliability.
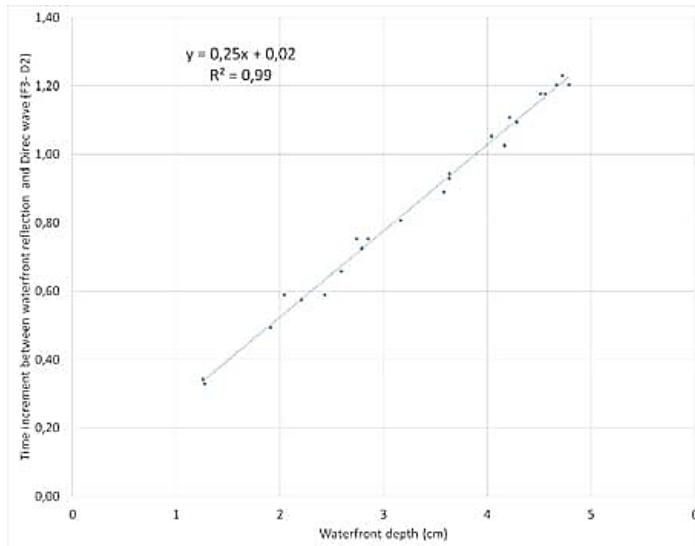
a)
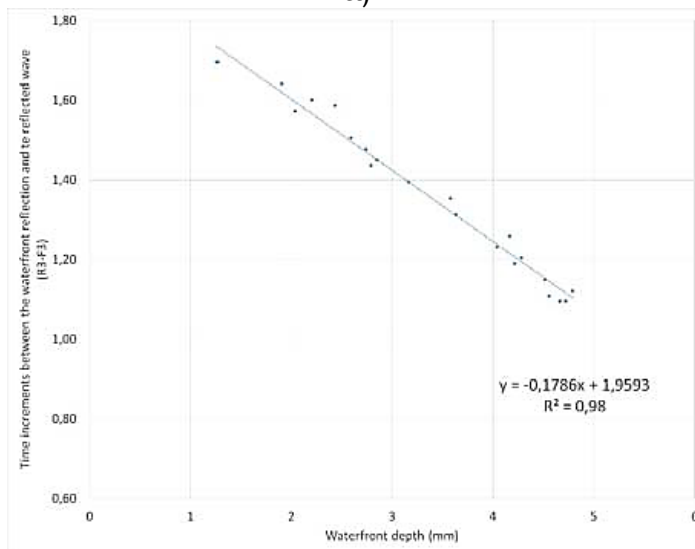
b)

Fig. 7 – (a) Adjustments of the time increment between the direct wave arrival and the waterfront reflection and the waterfront depth; (b) Adjustments of the time increment between the reflected wave arrival and the waterfront reflection and the waterfront depth.

44

3.2. TIMBER EXPERIMENT

3.2.1. WATER CONTENT EVOLUTION

Firstly, water content coefficient (*CA*) was calculated following equation 1, and the complete results are detailed in Table III.

TABLE III – WATER CONTENT EVOLUTION (%) FOR TIMBER SAMPLES

Immersion time (min)	sample Ruso	C_A	sample Mobila	C_A	sample Pinaster	C_A	sample Insigne	C_A
20	3	1,29	3	2,12	3	2,38	3	1,27
40	4	2,13	4	2,94	4	6,51	4	1,60
60	5	1,67	5	4,50	5	4,61	5	2,11
80	6	1,70	6	3,54	6	4,54	6	1,67
100	7	1,66	7	3,43	7	10,72	7	2,38
120	8	2,28	8	3,52	8	6,15	8	2,58
140	9	3,99	9	4,18	9	6,18	9	2,65
160	10	4,48	10	4,40	10	14,69	10	3,05
180	11	3,50	11	4,40	11	11,97	11	2,59

It is important to highlight that, although all samples remain the same time in water not all of them absorbed the same percentage of water. This is a first difference between concrete and timber samples, since not all timber species follow the same pattern in relation to water absorption, regardless of their density.

3.2.2. EFFECT OF WATER CONTENT ON DIRECT AND REFLECTED WAVE SIGNALS

After a first qualitative inspection of the radargrams, it was observed that the signals were not specially affected by the water absorption – see Figure 8, regardless where the antenna was placed (over the immersed or dry surface) and the analysed parameter (velocity and amplitudes).

Only in same cases the amplitude traces were found to be affected by water content. This will be later discussed. It was not observed a pattern of the signals alteration due to the density of the

samples or the quantity of water absorbed. In deed the best results were obtained with the Mobila samples, which total water content increment was found to be 2,38 %. On the contrary, the Pinaster samples had a total increment water content of 12,31%. Therefore, it was expected that the signals were more affected. Nevertheless, this was not the case, since the worst results were found for this timber specie.
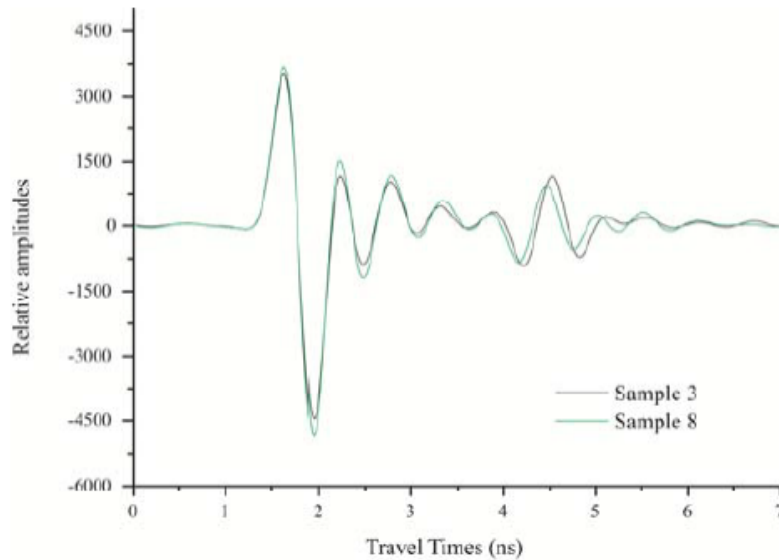

Fig. 8 – Typical traces registered in *Pinaster* samples when it was 20 and 120 minutes immersed into water.

3.2.3. ANALYSIS OF VELOCITY INCREMENTS AFTER IMMERSION

To confirm whether or not the velocities of the waves were affected by the water content increase, propagation velocities were calculated with equation 2. After that, the velocities increments between when the samples were dry and immersed in water were calculated following equation 3. In order to check if there was correlation between these increments and the water content increment different adjustments were conducted. The best results are summarized in Table IV.

TABLE IV – R2 (%) OF THE ADJUSTMENTS BETWEEN VELOCITY INCREMENTS AND C_A

Antenna position		Peaks combination to calculate velocities								
		R1-D1	R1-D2	R1-D3	R2-D1	R2-D2	R2-D3	R3-D1	R3-D2	R3-D3
Dry side	Ruso	x	x	x	x	x	x	82	60	62*
	Mobila	x	x	x	x	x	x	x	x	x
	Pinaster	67	66	87	x	x	x	x	x	x
	Insignis	75	x	x	x	x	x	x	x	x
Wet side	Ruso	x	x	x	x	x	x	x	x	60
	Mobila	x	66	x	x	x	x	x	x	x
	Pinaster	59	x	x	54	x	67	x	x	x
	Insignis	60	x	x	67	x	62*	x	x	x

*No physical meaning of the obtained fitting equation

The results showed, as it was firstly observed qualitatively, that the arrival times were slightly affected by the water content increment. In Table IV, it is indicated with *x* correlations that were lower than the 50%. There were not many differences in the results whether the antenna was placed on the immersed side of the samples or on the dry one. In the cases, that correlations higher than the 60 % were found, the resulting equation of the adjustment presented a reliable tendency.

In Figure 9, two examples of these agreements are depicted. Considering the non homogeneity of the timber samples, these results wouldn´t be very negative. But, the problem relayed on the few cases that these acceptable correlations were found. Therefore, it was not possible by means of this experiment to confirm that in timber samples, it was possible to detect the water content absorption; in particular using wave velocities increments.
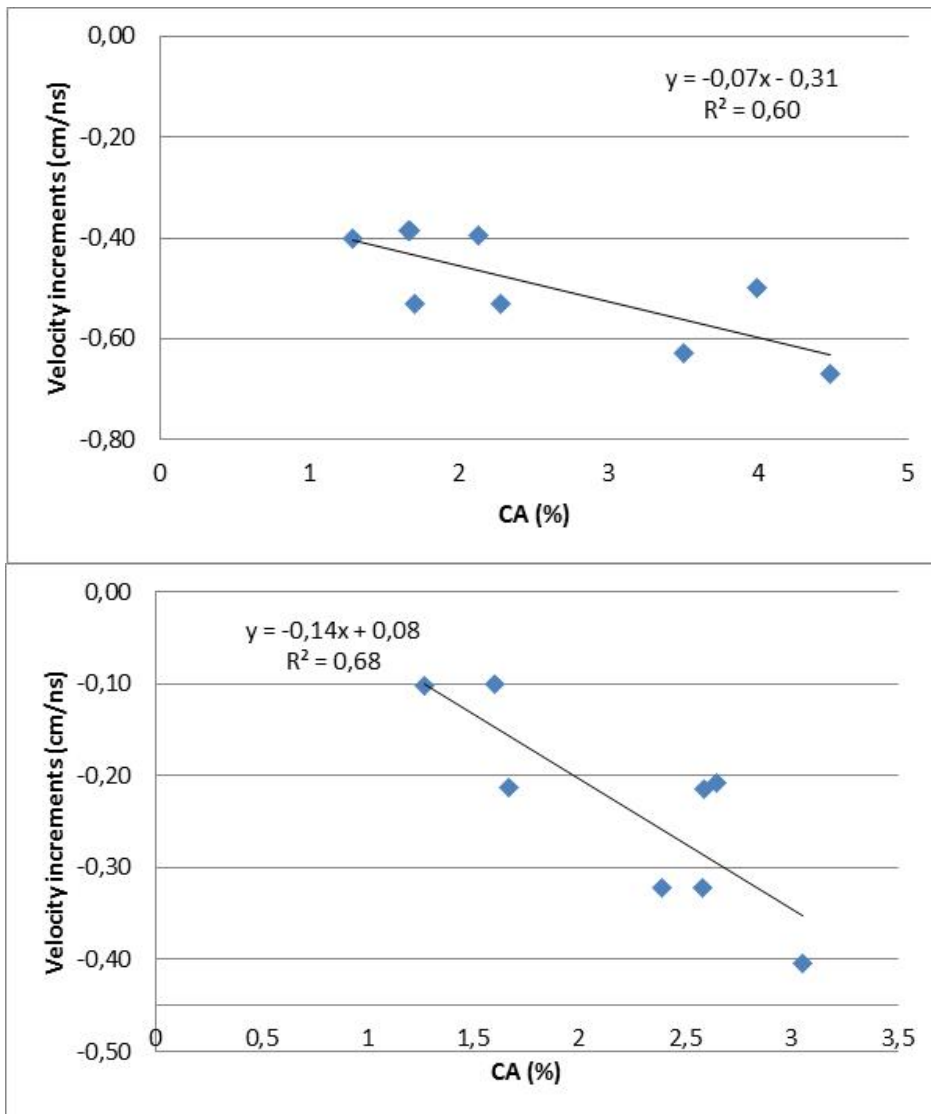
Fig. 9 – Best adjustment in: (a) Ruso samples between velocity increments and CA, when calculating the velocity with the peaks combination R3-D2 and the antenna placed on the dry side; (b) Insignis samples between velocity increments and CA, when calculating the velocity with the peaks combination R2-D1 and the antenna placed on the wet side.

ANALYSIS OF AMPLITUDE INCREMENTS AFTER IMMERSION

To conduct the analysis of the amplitudes increments due to the water absorption, they were calculated as follows:

$$\Delta A_r = A_i - A_d \qquad [4]$$

where A_i is the relative amplitude when samples were immersed into water and A_d was the velocity when samples were dry. As with velocity increments, correlations between amplitudes increments and water content were calculated. The best results are summarized in Table V.

TABLE V – R2 (%) THE ADJUSTMENTS BETWEEN AMPLITUDE INCREMENTS AND C_A

Antenna position		Analyzed peaks					
		D1	D2	D3	R1	R2	R3
Dry side	Ruso	x	x	x	x	55	x
	Mobila	x	x	x	x	x	x
	Pinaster	x	x	x	x	67	x
	Insignis	x	61*	x	x	x	x
Wet side	Ruso	x	x	x	70	72	72
	Mobila	x	50	62	90	85	86
	Pinaster	x	x	x	x	89	81
	Insignis	x	76	81	x	x	x

*No physical meaning of the obtained fitting equation

In this case, as it can be observed in Table V, only with R2 was found a reasonable correlation in two timber species when the antenna was placed on the dry side. Nevertheless, better results

were found when the antenna was placed on the wet side – see Figure 10. Peaks R2 and R3 showed a good agreement for 3 of the 4 species analyzed. These results would be of great interest, in case they were obtained for all species. Unfortunately, this was not the case. Therefore we are not in the position to confirm that this amplitude peaks variation provided reliable enough information about the water content variation in timber.

4. FUTURE COLLABORATION WITH THE HOST INSTITUTION

The STSM has been very productive and rewarding. To have the possibility to discuss the results with Professor Jean Paul Balayssac and Professor Gilles Klysz has been a great opportunity to learn more about GPR signals processing. As a result, future collaborations have been foreseen regarding, on one side, further processing of the data of concrete experiment; and on the other side, the possibility to design a new experiment for timber samples. Results of concrete experiment are very promising and we will continue collaborating, since further analyses might be conducted to achieve the last goal of the experiment: the assess in cm the location of the waterfront advance. In relation to the timber experiment, the results were not found as good as expected. We have been discussing about the requirements that a new experiment should meet, to improve the reliability of the results.

5. FORESEEN PUBLICATIONS/ARTICLES RESULTING FROM THE STSM

Results of concrete experiment are very successful and interesting. Further processing should be performed to achieve the final goal of the research, that is, to assess the waterfront location. When this last step will be completed, we will write a paper describing the achievements and submit it to a journal in the Construction Engineering area, In reference to the timber experiment, we are in a too preliminary step to consider publishing any of the results obtained so far. Previously, it is necessary to improve the experiment design.
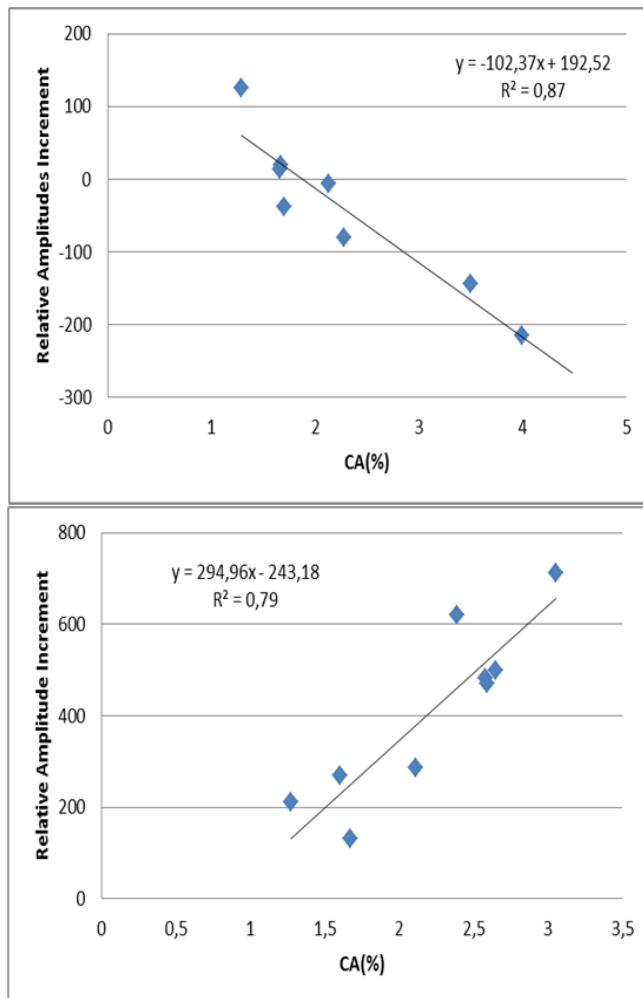
ACKNOWLEDGEMENT

Fig.10 – (a) Best adjustment in Mobila samples between amplitudes increments and CA, when analysing peak R1 and (b) in Insignis samples, analysing peak D3: the antenna was on the wet side of the sample.

STSM 5

Moisture evaluation of wood material using GPR

Visiting Scientist: Hamza Reci, Institute of Geosciences, Energy, Water and Environment (IGEWE), Polytechnic University (PUT), Tirana, Albania (h.reci@geo.edu.al)

Host Scientist: Mehdi Sbartai, I2M Laboratory Department of Environmental Civil Engineering (I2M-GCE), University of Bordeaux, Talence, France (zm.sbartai@i2m.u-bordeaux1.fr)

STSM Dates: 9 November -10 December 2015

1. Purpose of the STSM

The purpose of this STSM was to study the sensitivity of GPR electromagnetic waves to moisture variation in wood material in relation with the direction of fibers and polarization of Electromagnetic field. The relations between relative permittivity and moisture content and the amplitude attenuation with distance was a target study using the direct waves in Wide Angle Radar Reflection (WARR) configuration, where one antenna is moved while the other remains stable. The measurements of the travel-times with WARR method were recorded with different separations between Transmitter (T) and Receiver (R) antennas.

Comparison of results measured with reflected waves and direct waves was of main importance as from other works it is clear that they have different behaviour in relation with moisture variation, due to the different path of propagation. Several studies have been carried out by the I2M team, University of Bordeaux, using direct and reflected waves for the evaluation of water content on concrete materials and wood [1-3]. As related to the wood material there is one study carried out using the reflected waves on wood for different humidity and different wood samples, in all the direction

of polarization using GPR technique at 1.5 GHz ground coupled antenna [3].

The direct wave method was tested in one sample with humidity 12% and dimensions: 19 cm wide, 18 cm thickness and 60 cm longitude. The measurements were carried out in only one direction of propagation (electric field polarized perpendicular). The results show that the direct wave signal is measurable. In addition, the permittivity measured with the direct wave is lower than that measured with the reflected wave due to the fact that both waves have different propagation directions with respect to fibre. As a consequence this work continued with different moisture content in order to study the behaviour of direct waves as function of moisture. The interesting part of using the direct wave (the wave that propagates between the transmitter and receiver is that it doesn't need neither a reflector nor the thickness of the sample.

The comparison with reflected method of these results was one of the topics of this STMS in order to overcome the difficulties that come from the slowness of WARR method. Results taken from the measurements are compared with those from FO (reflected method) with one antenna (1.5 GHz or 2.6 GHz), realized from the previous studies from the I2M and already published [1-3]. The extraction of dielectric constant, velocities from direct waves (WARR) and reflection methods and comparison of the taken results was another goal of this STMS.

2. Description of the work carried out during the STSM

The GPR approach used during this work consisting in using both methods: direct wave measurements using the WARR method and reflected method, by transmitting a very short electromagnetic pulse into the material using ground coupled antenna with central frequency 1.5 GHz as a transmitter and as receiver another antenna. The measurements were carried out in one wood sample of type Epicea (Spruce), with dimensions: longitude 600 mm, width 190 mm and thickness 176 mm - see Figures 1A, 1B.

Air wave, E vector perpendicular

Direct wave, E vector perpendicular to fibers
Distance TxRx, 16-26cm

A)

Air wave, E vector parallel

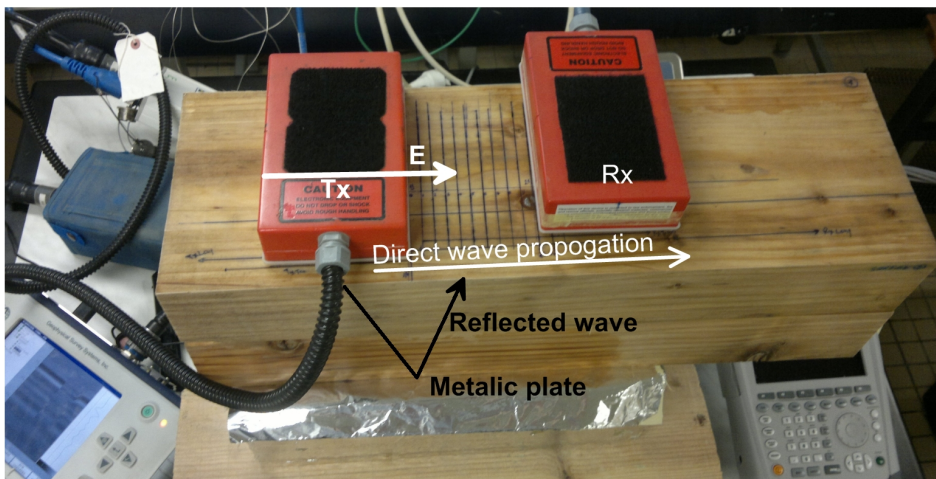Direct wave, E vector parallel to fibers
Distance TxRx, 11-21cm

B)

Fig.1 – Measurements with GPR in two directions with GSSI SIR 3000 equipment connected with two antennas of 1.5GHz. A) Measurements on air and on sample where the E field is perpendicular to the fibres. B) Measurements on air and on the sample where the E field is parallel to the fibres.
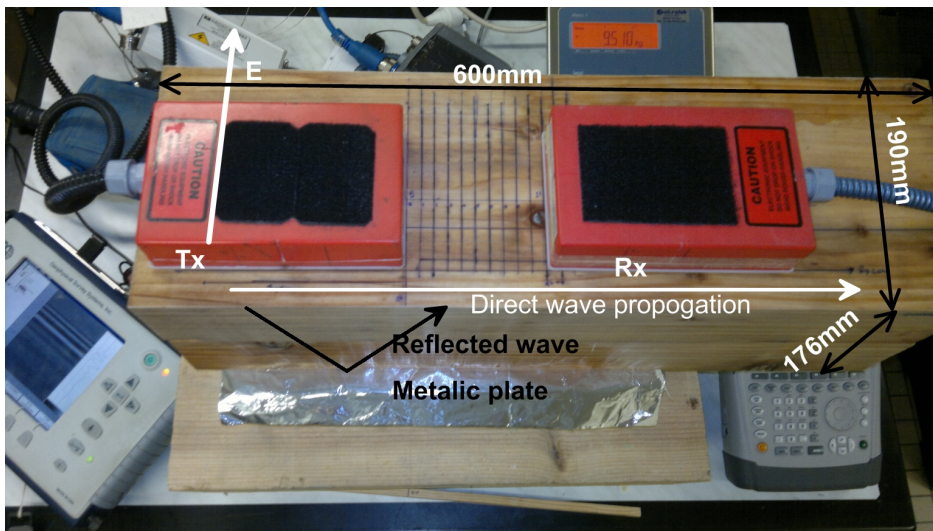
A)

B)

Fig.2 – Schematic principle of GPR measurements using ground coupled antennas using the direct wave WARR method. A) Electric field is perpendicular to the fibres. B) Electric field is parallel to the fibres.

The thickness of 176mm was realized putting two samples together with the same dimensions. The method used was WARR, in order to study the velocity of EM and evaluating the real permittivity in relation with humidity by mass water. The measurements started in humidity of 12%. After that, the wood sample was immersed into the water and during the monitoring of its humidity, measurements were carried out in two directions ((A) longitudinal direction where the electric field was polarized perpendicular, (B) transversal directions where E is polarized parallel – see Table I). Humidity by mass water (%) was calculated with the following expression:

$$Humidity\ (\%) = \left(\frac{W - W_0}{W_0}\right) 100 \qquad (1)$$

where, W_0, is the weight of the sample with 12% humidity, W the weight of the sample after immersing into the water. The weight of the samples was measured with a balance in grams.

TABLE I – HUMIDITY BY MASS WATER OF THE SAMPLES AND TOTAL (%)

Hours in water	Weight upper	Weight lower	Weight total (gr)	Humidity Upper (%)	Humidity Lower (%)	Humidity Total (%)
0	3443	3470	6913	12	12	12
4	3656	3718	7374	18.18646529	19.14697406	18.6685954
20	3852	3992	7844	23.87917514	27.04322767	25.4673803
40	3956	4132	8088	26.89979669	31.0778098	28.99696225
68	4068	4298	8366	30.15277374	35.86167147	33.01837118
134	4508	4665	9173	42.93232646	46.43804035	44.69202951
216	4807	5016	9823	51.61661342	56.55331412	54.09460437
357	5256	5400	10656	64.65756608	67.61959654	66.14436569

The Figure 3 shows the humidity by mass water for both samples (upper and lower) and the sample in total with respect to the time of immersion into the water. As seen from the graph, during the first 30 hours, the humidity increases sharply, then after that time there is an increase almost curvilinear with time.
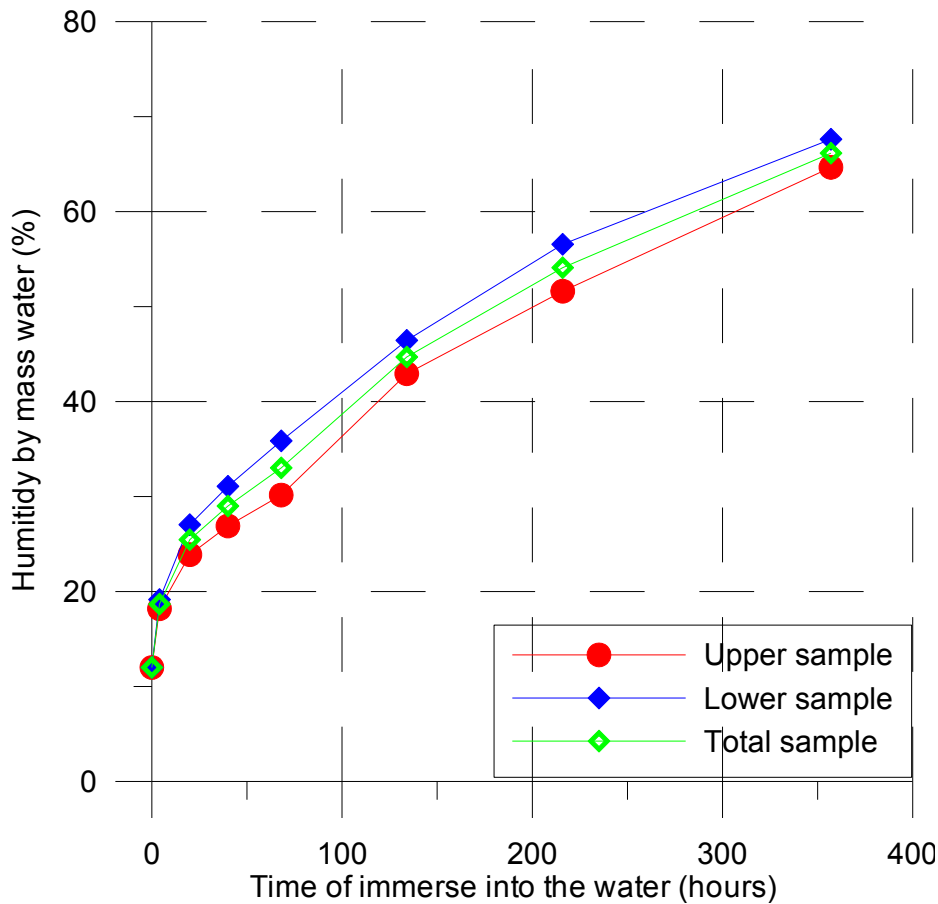
Fig. 3 – The dependence of humidity by mass water with the time of immerse into the water.

The measurements were realized for all the humidity presented on Table I. The scope of measuring like that was to study the variability of direct+ wave velocity when the electromagnetic field is polarized in two directions perpendicular and parallel to the wood fibers respectively. In order to have a distinction between reflected and direct waves, a metallic plate was set to the à bottom of the wood sample – see Figure 2. In this way, the abrupt changes in dielectric properties between metallic plate and the sample caused

the reflection of EM field where it was recorded and amplified by the receiving antenna.

3. DESCRIPTION OF THE MAIN RESULTS OBTAINED DURING THE STSM

Introduction

The electromagnetic wave propagates in air with the speed of light (0.3 m/ns). In the wood structure, which is a dielectric anisotropic material, the velocity of electromagnetic wave is reduced, since it is dependent on the relative dielectric permittivity, ε_r, the relative magnetic permeability, μ_r, and the electrical conductivity, σ [4-7]. The velocity of electromagnetic waves in a host material is given by:

$$v = \frac{c}{\sqrt{\varepsilon_r \mu_r + \frac{1+\sqrt{1+(\sigma/\omega\varepsilon)^2}}{2}}} \qquad (2)$$

where c, is the electromagnetic wave velocity in vacuum (0.3 m/ns), $\varepsilon = \varepsilon_r \varepsilon_0$ the dielectric permittivity, and ε_0 the dielectric permittivity in free space (8.854·10^{12}F/m), $\omega = 2\pi f$ the angular frequency, where f is frequency, and the expression $\sigma/\omega\varepsilon$ is the loss factor. In non-magnetic ($\mu_r = 1$) low-loss materials as wood, where $\sigma/\omega\varepsilon \approx 0$, the velocity of electromagnetic waves is reduced to the expression:

$$v = \frac{c}{\sqrt{\varepsilon_r}} \qquad (3)$$

The Equations 1 and 2 show that the velocity of electromagnetic waves propagating in the material is decreased compared to the velocity in the air. In low-loss (i.e. resistive) materials the maximum decrease is a factor of nine, which is the velocity of electromagnetic waves in fresh water (0.034 m/ns, [4]). Several processes lead to a reduction of the electromagnetic signal strength. Among the most important processes are attenuation, spherical spreading of the energy, reflection/transmission losses at interfaces and scattering of energy. Scattering is due to objects with a dimension similar to

the wavelength and is therefore most pronounced for higher frequencies.

Special attention should be drawn to the attenuation, which is a function of dielectric permittivity, ε, magnetic permeability, μ, and electrical conductivity, σ, as well as the frequency of the signal itself, $\omega = 2\pi f$. The attenuation coefficient isexpressed as:

$$a = \omega \sqrt{\varepsilon\mu \frac{\sqrt{1+(\frac{1}{\omega\varepsilon})^2}-1}{2}} \qquad (4)$$

In low-loss materials, where $\sigma/\omega\varepsilon \approx 0$, the attenuation coefficient is reduced to:

$$a = \frac{\sigma}{2}\sqrt{\frac{\mu}{\varepsilon}} \qquad (5)$$

The attenuation is proportional to the electrical conductivity, which leads to high attenuation in materials with high electrical conductivity. The propagation of electromagnetic waves is affected by the presence of moisture content, density and grain and also depends on the frequency of the emitted electromagnetic field [4-12]. For this reason, GPR is becoming increasingly successful to characterize moisture content of different building materials [7-12]. Regarding timber, there are studies that analyses the capability of GPR technique to assess the principal physical parameters such as dielectric anisotropy, moisture content, density, etc. Authors such as [1-5] have focused their research on the ability of the GPR direct wave for non-destructive testing of concrete structures with successful results. These results are of practical interest because sometimes it is difficult to detect the reflection in the opposite side of a sample, when applying the technique onsite.

4. GPR MEASUREMENTS DESCRIPTION

Dielectric relative permittivity was measured using direct wave recorded by GSSI SIR 3000 system connected to a couple of

1.5GHz ground-coupled antennas on the Epicea (Spruce) wood sample, monitoring the humidity as the sample was immersed into the water as described in section 2. For the direct wave method (WARR), the distances between transmitter and receiver were 16 to 26 cm and 11 to 21 cm for perpendicular and parallel polarization of E vector respectively. Whereas for the reflected waves, the distance between receiver and transmitter used were 16 and 11 cm respectively for perpendicular and parallel polarizations. The arrival times were taken with Radan Software and Matlab. For each measurement, the direct air wave and direct wave on the sample were recorded – see Figure 4, 5.

From the direct waves for each distance (16-26 cm) for the case where E field is polarized perpendicular and 11-21 cm for the case where E field is polarized in parallel direction is determined the velocity from direct waves from those picking arrivals (positive picks), as the slope of the linear regression of arrival time of direct wave versus the distance, as shown in Figure 6 for the case of 18.18% humidity.

For the determination of the velocities from the reflected waves an aluminium plate was placed on the bottom of the wood sample – see Figure 1, 2. The picks used for calculation of velocity with reflected method are the positive for the direct wave (+D) and the positive for the reflected wave (+R) as depicted in Figure 4 ,5, where the following expressions were used:

For the direct air wave in the point +D, the arrival time is:

$$t_{air} = t_0 + t_{air}^{real} = t_0 + \frac{d_{TR}}{V_0} \tag{6}$$

For the reflected wave on the wood in point, +R:

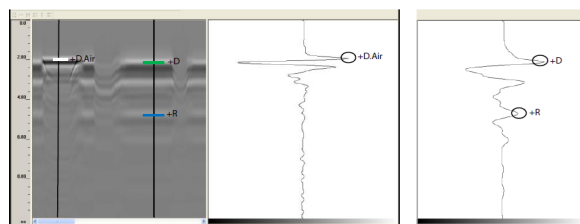$$t_r = t_0 + t_r^{real} = t_0 + \frac{d_R}{V} \tag{7}$$
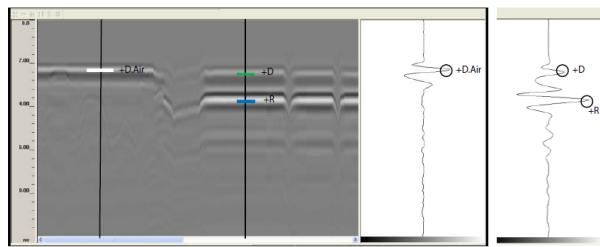
A) Direct air, direct wave and reflected wave, for 12% humidity. Electric field is polarized perpendicular to fibers
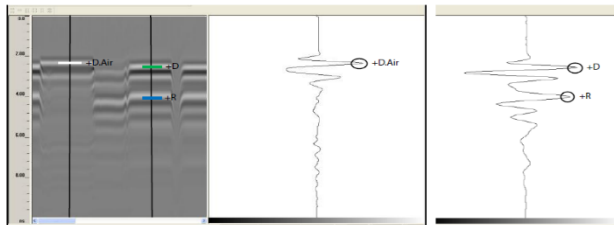
B) Direct air, direct sample and reflected wave for 22 % humidity. Electric field is polarized perpendicular to the fibers.
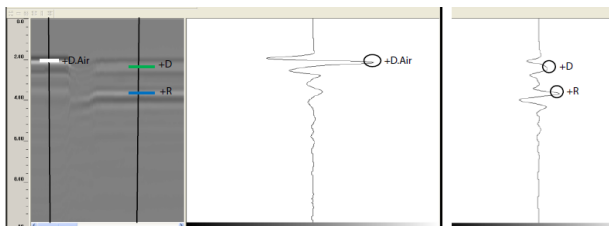
C) Direct air, direct sample and reflected wave for 12% humidity. Electric field is polarized parallel to fibers

D) Direct air, direct sample and reflected wave for 22% humidity. Electric field is polarized parallel to fibers.

Fig. 4 – The picking of positive picks of direct air wave, direct wave and reflected wave on the sample for perpendicular and parallel polarization of E field at 12% and 22% humidity.
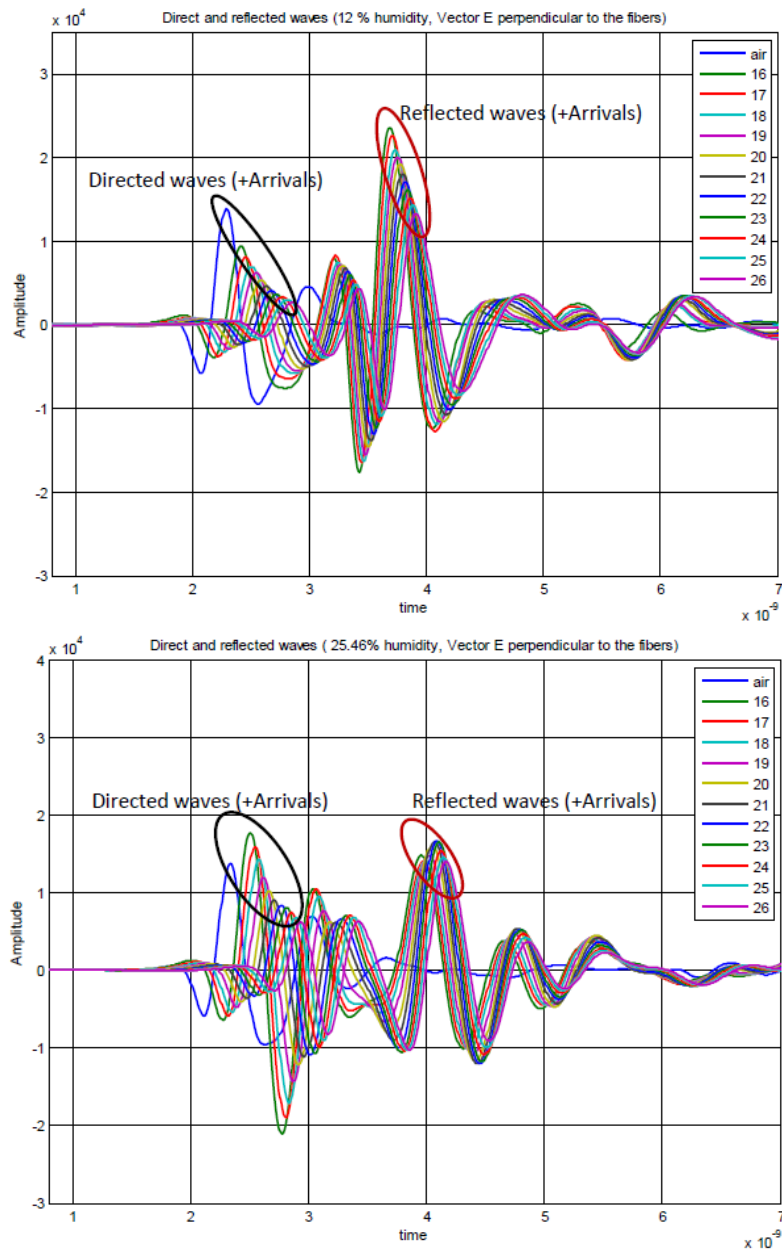
Fig. 5 – Direct air wave, direct and reflected wave on the sample for perpendicular and parallel polarization of E field at 12% and 25.46% humidity.
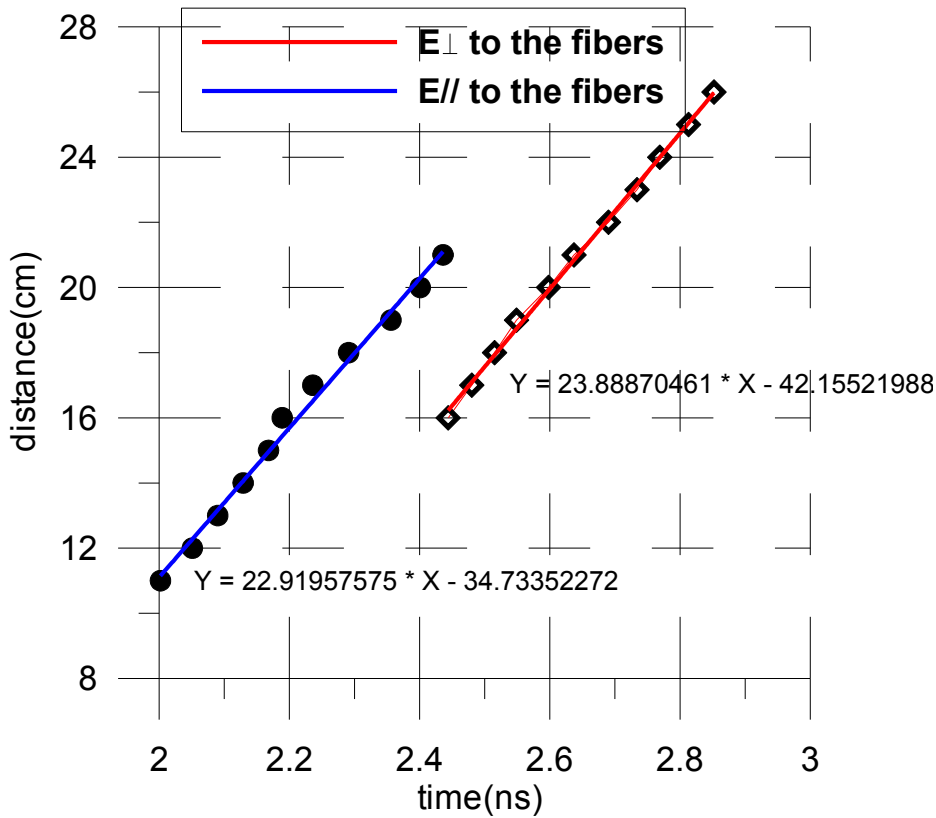
Fig. 6 – Determination of Velocities from direct waves, from the arrival times for two configurations (case of 18.18% humidity).

From the combination of equations 4 and 5 we get the velocity on the wood sample:

$$V = \frac{d_R}{\Delta t + \frac{d_{TR}}{V_0}} \tag{8}$$

Where: $\Delta t = t_r^{real} - t_{air}^{real}$, is the difference of arrival times between positive of the direct air wave and positive reflected wave – see Figure 4, 5. t_{air}^{real}, is the arrival time of the direct air wave (reference signal), t_{air}^{real}, is the arrival time of the reflected wave and, d_{TR}, is the propagation distance of the arrival time of direct air wave. This is

the distance between the Transmitter and Receiver. d_R, is the distance of the propagation of reflected wave, which is given by the equation:

$$d_R = 2\sqrt{(\frac{d_{TR}}{2})^2 + h^2} \tag{9}$$

Where h, is the distance between the surface of measurements and the bottom of the sample (thickness of the sample), The dielectric constant of the wood sample is calculated from the expression:

$$\varepsilon' = \left(\frac{V_0}{V}\right)^2 \tag{10}$$

where V_0 is the velocity of light (30cm/ns), V, is the velocity of the propagation on the wood. The dielectric constants were calculated using the expression 10. In Table II are presented the values of the real permittivity (dielectric constants) for different humidity for both polarizations (perpendicular and parallel to wood fibres), whereas in Figure 7, 9 the graphs of this variation. The dielectric constants for different humidity by mass water of reflected waves method were calculated for distances between Transmitter and Receiver 16 cm when the E field is polarized perpendicular, and 11 cm for the case where E field is polarized parallel to the fibres - see Figure 1, 2.

The values are presented on Table II, whereas the graphs are presented in Figure 8, 9.

As seen from the Figure 7, 9 and Table II, from the WARR method, there is small change of dielectric constants in both directions of polarization (the maximum value difference 0.35), and a linear increase of values with moisture. This happens due to the fact that propagation of EM field has the almost the same direction as in the case or radial polarization depicted from previous studies [1-3, 11-12]. As related with the reflected waves, Figure 8, 9, and Table II, the values of dielectric constant in relation with humidity change significantly with the direction of polarization of the vector

E, and those results are in agreement with previous works [3, 10-12]. There is a difference on the values of dielectric constant where the field is polarized perpendicular in comparison with values when the E field is parallel to fibres.

Table II – Dielectric constants in relation with humidity by mass water for direct and reflected waves.

Direct wave (WARR) method			Reflected wave method		
Humidity (%)	Vector E, perpendicular	Vector E, parallel	Humidity (%)	Vector E, perpendicular	Vector E, parallel
12	1.56	1.67	12	2.24	2.35
18.18	1.57	1.71	18.66	2.36	4.38
23.87	1.71	2	25.46	2.92	6.32
26.89	1.87	2.09	28.99	2.96	6.81
30.15	2.01	2.36	33.01	3.18	7.56
42.9	2.54	2.8	44.69	3.9	8.65
51.6	2.91		54.09	4.544	10.69
64.65	3.12		66.14	5.718	12.728

As seen from the above figures, we can say that the direct wave behaves completely different comparing with reflected waves. This is because the reflected wave has a path that is completely different from the direct waves. The direct waves propagate in the upper part of the sample and the effect of the polarization is small and it behaves like the radial polarization, because the direct wave propagates parallel to fibre for both polarizations.

Whereas the reflected wave propagate entire the wood thickness and the effect of anisotropy is significant. From the measurements we conclude that for the case where E field is perpendicular to fibres, the direct waves can be distinguished above 60% humidity but it is almost impossible to detect the arrival times of direct waves above 43% humidity in Figure 7, 9b, when the E field is parallel to the fibres, because the signal is lost and the picking of their amplitudes cannot be realized.
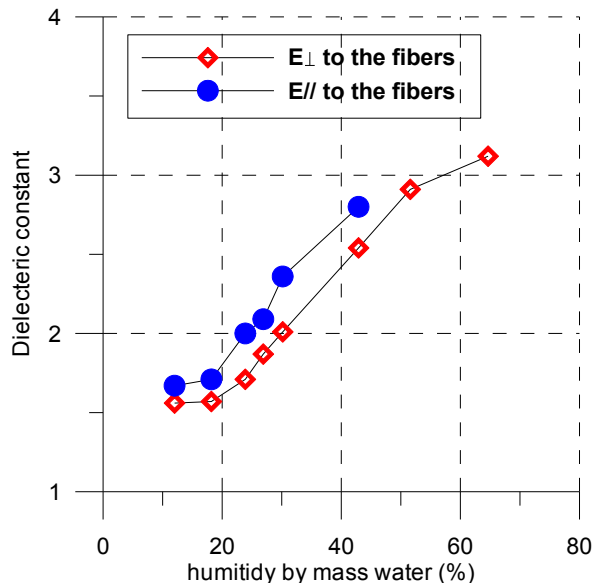
Fig. 7 – Variation of dielectric constants with humidity from the direct wave method (WARR) for perpendicular and parallel polarization of E field.
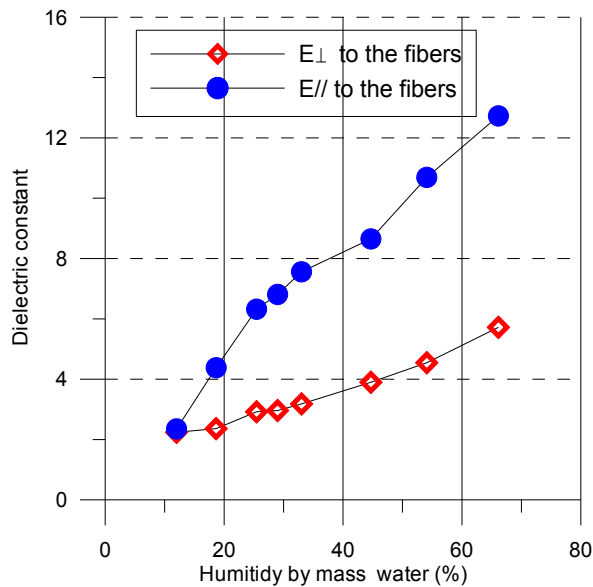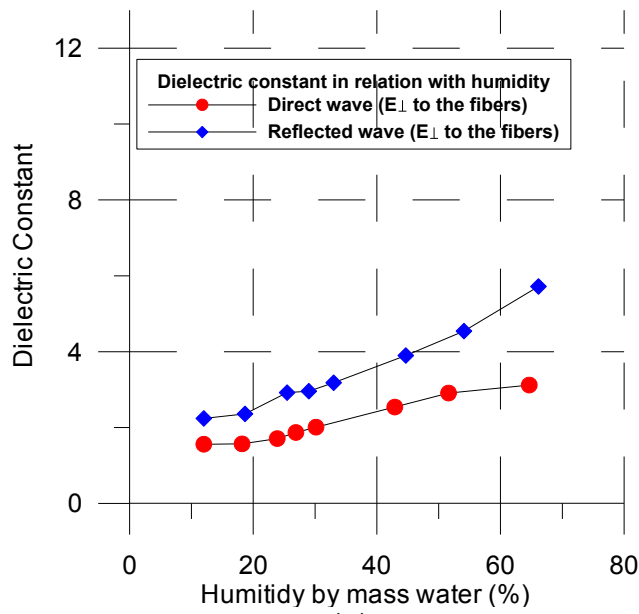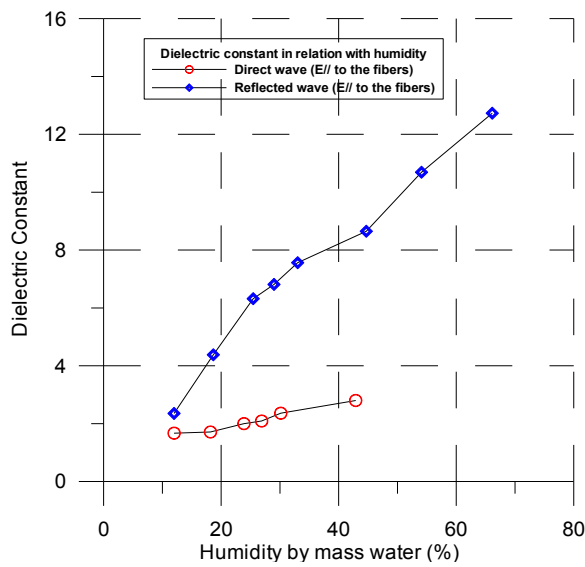

Fig. 8 – Variation of dielectric constants with humidity from the Reflected wave method for perpendicular and parallel polarization of E

field.

(a)

(b)

Fig. 9 – Variation of dielectric constants with humidity from the direct (WARR) and reflected wave methods, 9a) for perpendicular polarization

of E field and 9b) for parallel polarization of E field.

5. AMPLITUDE ANALYSIS

The amplitude attenuation with distance was another topic of this work. For every water mass humidity (%), the amplitude from the direct waves was normalized with the amplitude of direct air wave. In Figures 10 and 11 is presented the variability of the normalized amplitude of the direct wave with the distance and humidity.

As seen from Figure 10, the amplitude has an exponential attenuation with distance as depicted from previous works [1-3, 10-12]. With increasing humidity the normalized amplitude of the first distances is greater than one, for the perpendicular polarization, and this may be caused due to a superposition of direct wave with direct air wave in smaller distances [11, 12].
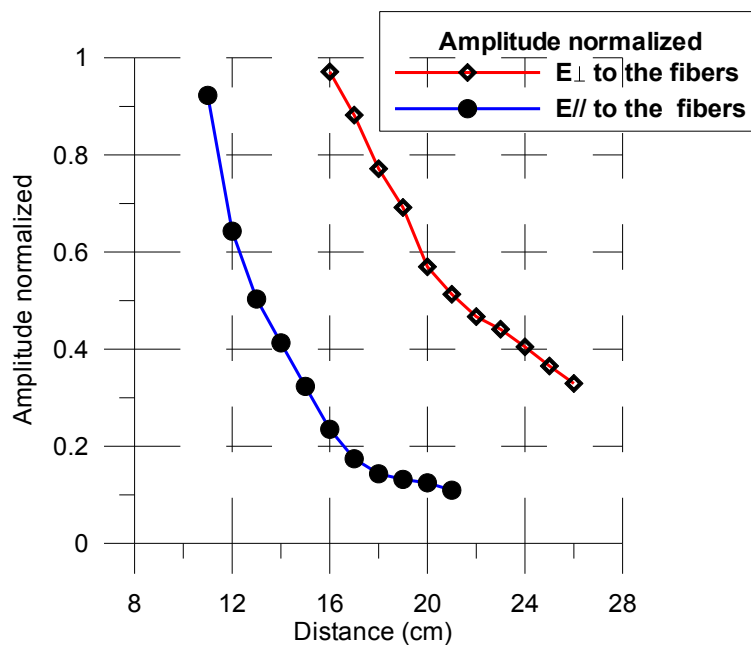
Fig. 10 – The attenuation of amplitude with distance for direct waves, for perpendicular and parallel polarization of E field (18.18% humidity).
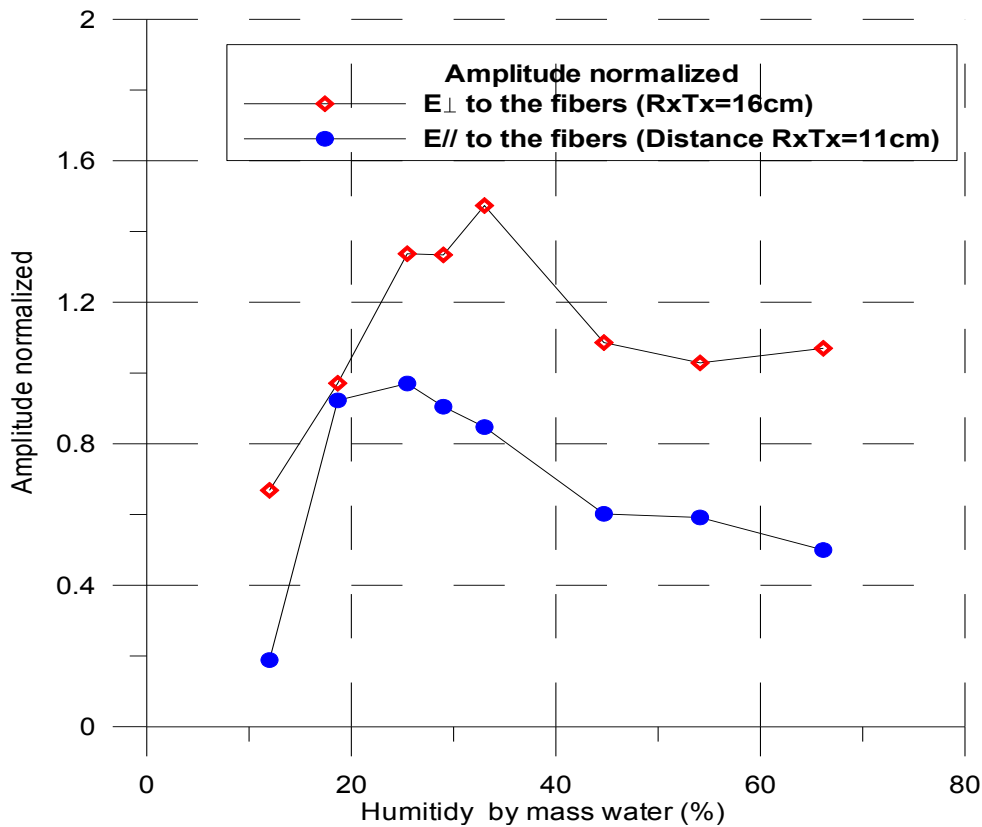
Fig. 12 – Normalized amplitude of direct wave with respect to humidity, for perpendicular and parallel polarization of E field.

With increasing humidity, the normalized amplitude increases and starts to decrease after 33% and 25% humidity, for perpendicular and parallel polarization respectively. This conclusion should be proved with other measurements on different kinds of wood (different densities), in order to have a clear picture of it.

Further analysis will be carried out on the existing data for the amplitudes of the reflected waves at distances between transmitter and receiver 16 cm and 11 cm for perpendicular and parallel polarization of E field respectively, in order to see their behaviour as a function of humidity.

6. CONCLUSIONS

From the above discussion we conclude that the main results of this work are as follows: The results taken from this work from the reflected waves, show that the effect of wood anisotropy is significant on the variation of relative permittivity with moisture content on wood sample and that is in good agreement with the previous results [1-3, 10-12]. As related the direct waves, a small change in the dielectric constants exists between transversal and parallel directions. The dielectric constant shows values that coincide with the case of radial polarization of the EM field.

This can be explained from the propagation path of direct waves. Since the EM field of direct waves, propagates in the upper part of the sample, the effect of polarization is almost the same in both directions as it is the case of radial polarization when the reflected method was used. As related to the amplitude attenuation, it can be seen that in the case where the E field is perpendicular to the fibres, the amplitudes of direct waves increase with humidity and their normalized values represent values greater than 1.

This can be explained by the fact that the direct air wave and direct wave in wood could be superimposed when the distances between receiver and transmitter are small. Such results were taken from the previous work with direct waves in one humidity experiment in wood [11, 12]. This effect is greater with increasing humidity up to 33% and after that we have a decrease, due to the fact that with increasing humidity the velocity in wood sample is lower and the distinction between direct air and direct waves is clearer then the water polarization effect is predominant.

This is an important result and needs to be verified with other laboratory experiments on different wood species, with different water mass content and density, in order to clarify whether this behaviour is the same. With increasing humidity, the attenuation of the signal is more when the E field is parallel to the fibre direction and the WARR method cannot be used for humidity higher than 50%, because it is impossible to detect the direct wave.

However the WARR methods functions well, when the E field is polarized in the direction perpendicular to the wood fibres.

7. FUTURE COLLABORATION WITH THE HOST INSTITUTION

The STSM was fruitful and interesting results were collected. For the future, the experimental work with the direct wave method (WARR) on different wood samples should continue, in order to clarify the effect of wood anisotropy and moisture content on GPR direct wave propagation. We hope that this work will continue in the future in the host laboratory (I2M, University of Bordeaux), in the frame of any further project, or else at the Institute of the visiting scientist in Albania (IGEWE, PUT), since there is scientific knowledge there to make the experiments, but unfortunately this is impossible for the moment because of the lack of the necessary equipment. This can hopefully be solved in the frame of COST Action TU1208 initiative *"GPR for everyone"*, where IGEUM and UPT can be provided with GPR equipment for scientific work, from the more developed countries participating in the Action.

8. FORESEEN PUBLICATIONS/ARTICLES RESULTING FROM THE STSM

The results of this scientific work were presented during the 2016 and 2017 EGU General Assemblies. Moreover, after performing further analysis and interpretation of the achieved results, and in cooperation with the Action Chair, we prepared a journal paper that was published on Geoscientific Instrumentation, Methods and Data Systems (GI), please see Ref. [13] – this is an open access paper.

REFERENCES

[1] Sbartai ZM, Laurens S, Balayssac JP, Ballivy G and Arliguie G (2006a) Effect of concrete moisture on radar signal amplitude. ACI Materials Journal 103 (6): 419-426.

[2] Sbartai ZM, Laurens S, Balayssac JP, Arliguie G, Ballivy G (2006b) Ability of the direct wave of radar ground-coupled antenna for NDT of concrete structures. NDT & E International 39 (5): 400-407.

[3] Tien Chinh Mai, Stephen Razafindratsima, Zoubir Mehdi Sbartaï, François Demontoux, Frédéric Bos (2015) Non-destructive evaluation of moisture content of wood material at GPR frequency. Construction and Building Materials 77 (2015) 213–217.

[4] Jol HM, Bristow CS (2003): GPR in sediments: advice on data collection, basic processing and interpretation, a good practice guide. – In Bristow C S, Jol H M (eds.) Ground penetrating radar in sediments. Geological Society, London Special Publications 211: 9–27.

[5] Neal A (2004): Ground-penetrating radar and its use in sedimentology: principles, problems and progress. – Earth-Science Reviews 66: 261–330.

[6] Kasal B and Tannert T (2010) In situ assessment of structural timber: state of the art report of the RILEM Technical Committee 215-AS. GPR method by Z.M. Sbartaï, Serie RILEM state of the art reports, v. 7. Heidelberg; New York: Springer.

[7] Sahin H and Nürgul A (2004) Dielectric properties of hardwood species at microwave frequencies. Journal of Wood Science 50: 375-380.

[8] Laurens S, Balayssac JP, Rhazi J, Klysz G and Arliguie G (2005) Non-destructive evaluation of concrete moisture by GPR: experimental study and direct modelling. Materials and Structures 38 (283): 827-832.

[9] Rodríguez-Abad I, Martínez-Sala R, CapuzLladró R, Díez Barra R and García-García F (2011) Assessment of the variation of the moisture content in the *Pinuspinaster* Ait. using the non destructive GPR technique. Materiales de Construcción 61(301): 143-156.

[10] Martínez-Sala R, Rodríguez-Abad I, del Val I (2013) Effect of penetration of water under pressure in hardened concrete on GPR signals Proceedings of the 7th International Workshop on Advanced Ground-Penetrating Radar, Nantes, France.

[11] Rodríguez-Abad I., Martínez-Sala R, Mené-Aparicio J (2015). Use of the direct wave amplitude to analyse timber grain at different frequencies. Universitat Politècnica de València Escuela Técnica Superior de Ingeniería de Edificación.

[12] Martínez-Sala R, Rodríguez-Abad, Diez-Barra R, Capuz-LLadró R (2013) Assessment of the dielectric anisotropy in timber using the nondestructive GPR technique. Construction and Building Materials 38, 903-911.

[13] Reci, H., Maï, T. C., Sbartaï, Z. M., Pajewski, L., and Kiri, E.: Non-destructive evaluation of moisture content in wood using ground-penetrating radar, Geosci. Instrum. Method. Data Syst., 5, 575-581, https://doi.org/10.5194/gi-5-575-2016, 2016.

73

STSM 6

CALIBRATION METHODS FOR AIR COUPLED ANTENNAS

Visiting Scientist: Vânia Marecos, LNEC, Lisbon, Portugal
(vmarecos@lnec.pt)

Host Scientist: Mercedes Solla, University of Vigo, Spain
(merchisolla@uvigo.es)

STSM Dates: 29 November - 12 December 2015

1. PURPOSE OF THE STSM

The use of GPR in transport infrastructures represents one of the most significant advances for obtaining continuous data along the road, with the advantage of operation at traffic speed and of being a non-destructive technique. Its main application, so far, has been the evaluation of layer thicknesses, which is traditionally determined by core drilling and test pits [1]. For the determination of layer thicknesses it is necessary to know the velocity of the signal, which depends on the dielectric constant of the material, and the two-way travel time of the reflected signal that is recorded by the GPR system. The calculation of the dielectric value of the materials can be done using different approaches such as: using fixed values based on experience; laboratory determination of dielectric values; applying the surface reflection method; or performing back calculation from ground truth references, such as cores and test pits [2][3][4]. The problem with using ground truth is that it is time consuming, labour intensive and intrusive to traffic [5], in addition, a drill core is not necessarily representative of the whole surveyed area. Regarding the surface reflection technique, one of the problems is that it only measures the dielectric value from the layer surface and not from the whole layer. Recent works already started to address some of these challenges proposing new approaches for GPR layer thickness measurements using multiple

antennas to calculate the average dielectric value of the asphalt layer [6][7], taking advantage of significant hardware improvements in GPR resolution and accuracy.

This STSM focused on the comparison of different methods for calibrating air coupled antennas: Coring, Surface Reflection Method (SRM) and Common Mid-Point (CMP) through the analysis of GPR data collected in a test site, in Portugal, with three test sections with different pavement solutions.

2. DESCRIPTION OF THE WORK CARRIED OUT DURING THE STSM

Different air-coupled calibration methods were compared to evaluate the applicability of each method to different pavement structures. Three methods were studied: Coring, Surface Reflection Method (SRM) and Common Mid-Point (CMP). The STSM was divided into the following tasks, which will be explained in more detail in the next sections:

- Task 1: Compilation and analysis of GPR survey data using different calibration methods: Coring, SRM and CMP
- Task 2: Comparison of calibration methods and evaluation of their application to different pavement structure solutions.
- Task 3: Preparation of a paper to be submitted to an international journal covering the main results of this research.
- Task 4. Final report of activities.

2.1 COMPILATION AND ANALYSIS OF GPR SURVEY DATA USING DIFFERENT CALIBRATION METHODS: CORING, SRM AND CMP

The data was collected in a test site in Portugal and three test sections with different pavement solutions were evaluated (Fig. **1 –** Structure of the test sections). For each cell, two parallel survey lines with a length of 1.00 m, spaced 0.30 m apart, were made Fig. **2 –** . Two control points were defined for each profile, located at 0.30 m and 0.60 m from the start of the survey line. The location of the

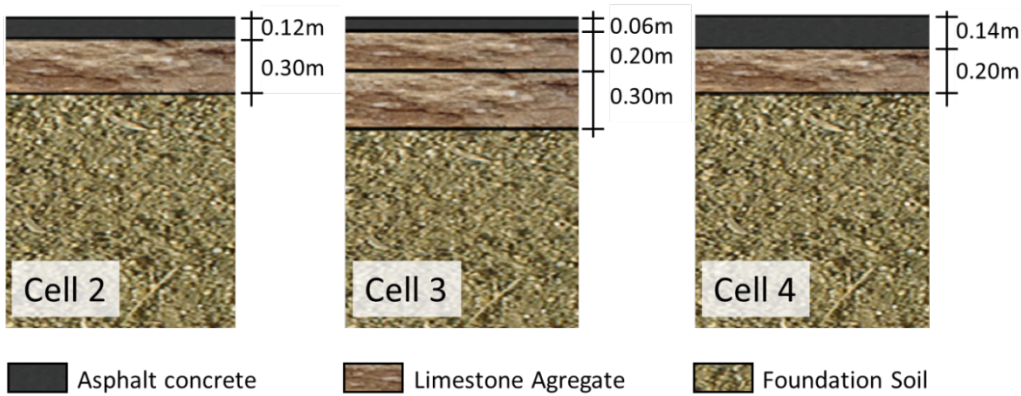survey lines, the direction of the surveys and the control points are presented in Fig. **2** – b.
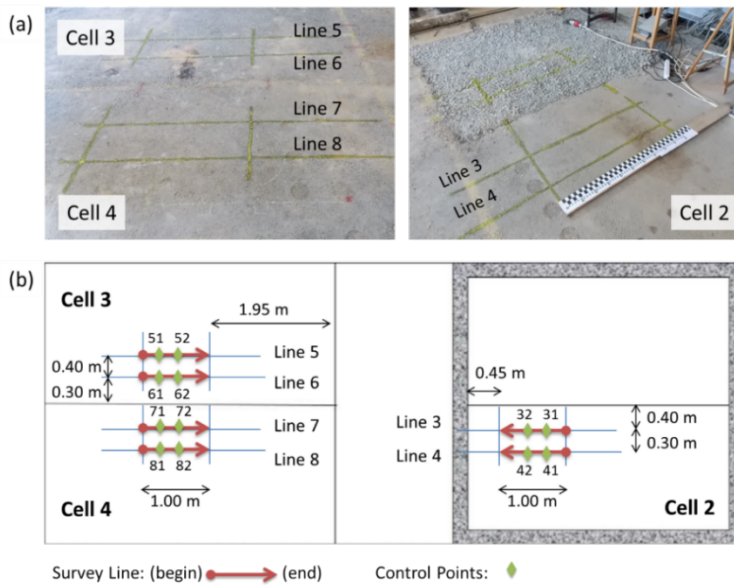

Fig. 1 – Structure of the test sections.

Fig. 2 – (a) Test site, (b) survey lines and control points.

Two pairs of air-coupled bistatic antennas with central frequencies of 1.0 GHz and 1.8 GHz – see Figure 3 – and a SIR 20 acquisition unit, both from GSSI, were employed in the tests. The

GPR data were acquired with both frequencies along the survey lines in a dynamic mode (scan by distance) and also in static mode (scan by time) over the control points. The air-coupled antennas were suspended at about 0.45-0.50 m from the surface. The setup used for the acquisition is presented in Table I.

Fig. 3 – Ground Penetrating Radar systems with air-coupled antennas.

TABLE I – GPR ACQUISITION SETUP

Antennas		Air-coupled		Units
Frequency		1.0	1.8	GHz
Time Window		20	12	ns
Samples per Trace		1024	1024	samples/scan
Trace interval	Dynamic mode	0.02	0.02	m
	Static mode	60	60	scan/s

Prior to the tests a file was collected for each cell and for both antennas using a metal plate above the pavement surface acting as a perfect reflector of the GPR signals. These data were later used while calculating the dielectric constant through the surface reflection method. For the 1.8 GHz air-coupled antenna, GPR data was also collected varying the distance between the transmitter and the receiver antenna. The first set of measurements was made over the control points using the classic method of the Common Mid-Point with air-coupled antennas – see Figure 4 left. The separation between the antennas was increased from 0.34 m up to 1.00 m with increments of 0.02 m – see Figure 4 right.
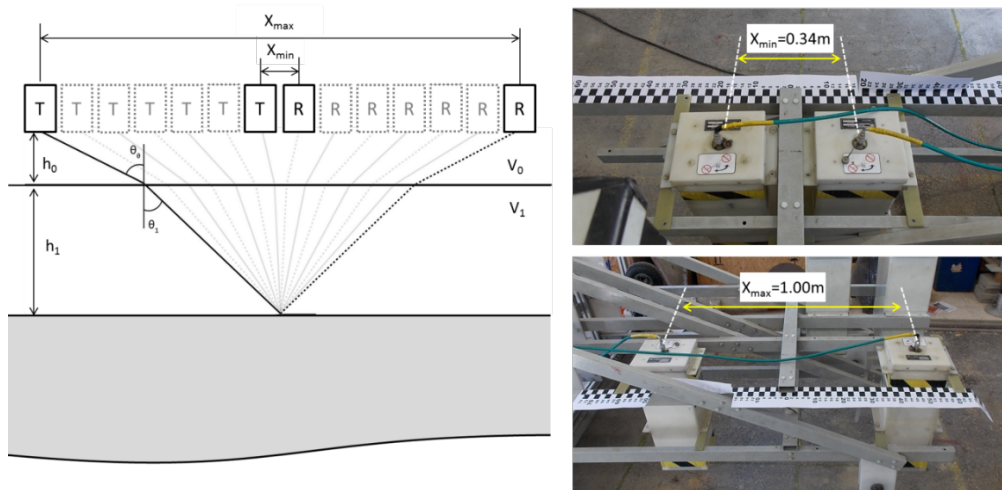

Fig. 4 – CMP configuration over the control points (static mode).

For the second approach using the CMP method the acquisition was made in a dynamic mode and for each survey line the GPR data was recorded using three different antenna separations. The setups considered distances between the receiver and the transmitter antennas of 0.28 m, 0.67 m and 1.00 m, respectively – see Figure 5.
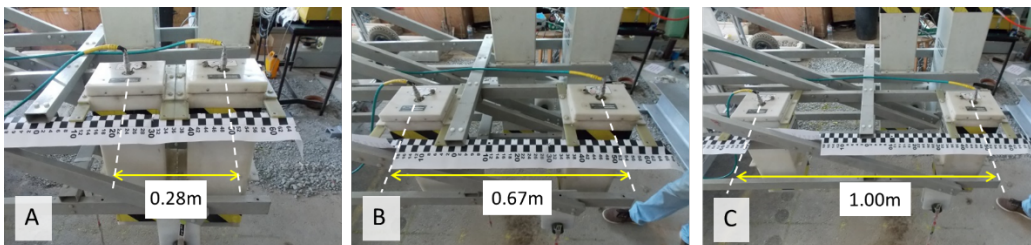

Fig. 5 – CMP configuration along survey lines (dynamic mode).

After the GPR survey 12 drill cores were extracted at the control points in order to obtain real thickness data for the bituminous layer Figure 6. The measured thicknesses are presented in Table II.

Fig. 6 – Extraction of drill cores.

TABLE II – DRILL CORES AND TEST PITS THICKNESSES

Cell	Survey Line	Control Point	Thickness (m) Asphalt Concrete
2	3	31	0.112
		32	0.115
	4	41	0.117
		42	0.115
3	5	51	0.064
		52	0.055
	6	61	0.055
		62	0.053
4	7	71	0.133
		72	0.134
	8	81	0.135
		82	0.128

The data were processed with Road Doctor Pro 2.5 and ReflexW. The analysis of the processed data showed that it was not possible, with the setup used within the tests, to obtain results from the CMP calibration method in a dynamic mode, essentially due to limitations of resolution of the data. Further tests should be implemented in the near future to try to overcome these limitations. Therefore, and considering the GPR tests performed, the following calibration methods were selected to be studied within this STSM – see Table III.

2.2 COMPARISON OF CALIBRATION METHODS AND EVALUATION OF THEIR APPLICATION TO DIFFERENT PAVEMENT STRUCTURE SOLUTIONS.

The GPR data was processed using three different methodologies for calibration, the algorithms used in the calculation and the main results for each method are presented below. The comparison of

the results obtained for each calibration method is presented in Section 3 of this report.

(i) Coring

The coring calibration method can be used to calculate the dielectric value of the asphalt layer at selected points where the layer thickness is known. For the application of this method at each control point the layer thickness of the asphalt layer was measured from the core drills. Then the two-way travel time of the reflected signal was determined from the GPR static data collected. The velocity of the propagation of the wave through the bituminous layer was calculated accordingly to equation 1 and finally the dielectric value was estimated using equation 2:

$$d = v\frac{t}{2} \qquad (1) \qquad\qquad V \cong \frac{c}{\sqrt{\varepsilon}} \qquad (2)$$

where c represents the speed of light in vacuum (0.3 m/ns). The results of the velocities and the dielectric values for the asphalt layer by the Coring method are presented in Table IV for the 1.0 GHz and the 1.8 GHz air-coupled systems, respectively.
The 1.0 GHz antennas provided higher dielectric values (and more homogeneous) than the 1.8 GHz antennas.

TABLE III – SELECTED AIR-COUPLED ANTENNAS CALIBRATION METHODS

Calibration Method	Acquisition Mode	Antenna Frequency	
		1.0 GHz	1.8 GHz
Coring	Static	x	x
	Dynamic	-	-
SRM	Static	x	x
	Dynamic	x	x
CMP	Static	-	x
	Dynamic	-	-
x: selected calibration methods to be studied			

TABLE IV – VELOCITIES OF PROPAGATION AND DIELECTRIC VALUES OBTAINED FROM CORING

Cell	Line	Control Point	Core thickness (m)	t (ns)		Velocity (m/ns)		ε	
				1.0 GHz	1.8 GHz	1.0 GHz	1.8 GHz	1.0 GHz	1.8 GHz
2	3	31	0.112	1.986	1.926	0.113	0.116	7.1	6.7
		32	0.115	1.947	1.995	0.118	0.115	6.4	6.8
	4	41	0.117	2.042	1.977	0.115	0.118	6.9	6.4
		42	0.115	2.001	1.961	0.115	0.117	6.8	6.5
3	5	51	0.064	1.045	0.941	0.122	0.136	6.0	4.9
		52	0.055	0.986	0.874	0.112	0.126	7.2	5.7
	6	61	0.055	0.920	0.888	0.120	0.124	6.3	5.9
		62	0.053	0.887	0.821	0.119	0.129	6.3	5.4
4	7	71	0.133	2.351	2.167	0.113	0.123	7.0	6.0
		72	0.134	2.286	2.276	0.117	0.118	6.5	6.5
	8	81	0.135	2.192	2.085	0.123	0.129	5.9	5.4
		82	0.128	2.192	2.061	0.117	0.124	6.6	5.8

Figure 7 shows the asphalt layer thickness profiles from Coring calculated using the average values of the velocity of propagation from the control points.

(ii) Surface Reflection Method

The Surface Reflection Method can be used when air coupled antennas are employed and relies on the comparison of the amplitude from the pavement surface with the amplitude from a metal plate reflection.

The dielectric value for the surface layer (ε_a) can be determined using the following algorithm:

$$\varepsilon_a = \left[\frac{1 + \left[\frac{A_1}{A_m}\right]}{1 - \left[\frac{A_1}{A_m}\right]} \right]^2 \qquad (3)$$
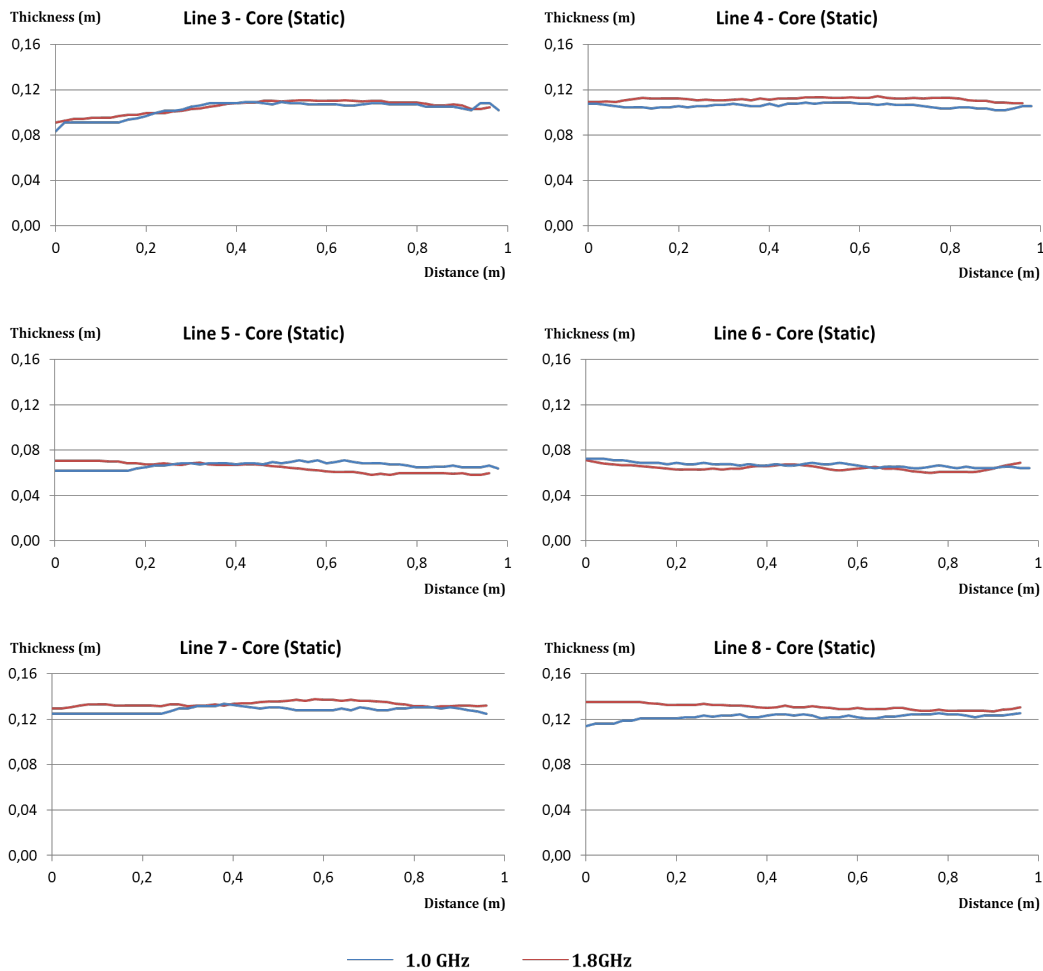
Fig. 7 – Asphalt layer thickness profiles calculated
with Coring calibration.

where A_1, A_m are the amplitudes of the reflections from the surface and from a metal plate (100% reflection case), respectively.

The amplitude of the reflection from the metal plate was obtained from the calibration files collected before the GPR tests. One A_m was determined for each pair of antenna frequency and cell. From the GPR dynamic data acquired along the survey lines

83

we gathered the amplitudes of the reflection of the surface and the two-way travel time through the asphalt layer. With both reflection amplitudes (A_1, A_m) the dielectric values along the survey lines were estimated with Equation 3. For the transformation of the collected profiles into layer thickness profiles Equation 1 was applied, whereas the wave velocity speed was calculated from Equation 2.

The results of the velocities and the dielectric values for the asphalt layer obtained from the Surface Reflection Method, over the Control Points, are presented in Table V for the 1.0 GHz and the 1.8 GHz air coupled systems, respectively.

The 1.0 GHz antennas provided higher dielectric values for Cells 3 and 4 (and more homogeneous) than the 1.8 GHz antennas.

TABLE V – VELOCITIES OF PROPAGATION AND DIELECTRIC VALUES OBTAINED FROM SRM

Cell	Line	Control Point	t (ns)		Velocity (m/ns)		ε	
			1.0 GHz	1.8 GHz	1.0 GHz	1.8 GHz	1.0 GHz	1.8 GHz
2	3	31	1.836	1.828	0.126	0.115	5.7	6.8
		32	1.856	1.910	0.128	0.124	5.5	5.8
	4	41	1.855	1.887	0.125	0.120	5.8	6.2
		42	1.875	1.921	0.130	0.133	5.4	5.1
3	5	51	1.172	1.043	0.128	0.137	5.5	4.8
		52	1.172	0.937	0.128	0.130	5.5	5.3
	6	61	1.132	0.996	0.133	0.137	5.1	4.8
		62	1.113	1.008	0.130	0.132	5.3	5.2
4	7	71	2.247	2.180	0.123	0.130	5.9	5.3
		72	2.227	2.273	0.124	0.129	5.8	5.4
	8	81	2.051	2.098	0.125	0.135	5.8	5.0
		82	2.031	2.051	0.123	0.137	5.9	4.8

In Cell 2 it was noted some variation, around the control points, of the surface amplitude measured with the 1.8 GHz antenna, which influenced the dielectric value with more relevance at survey line 3.

Figure 8 shows the asphalt layer thickness profiles determined with the velocities of propagation calculated at each point of the survey line using the Surface Reflection Method.
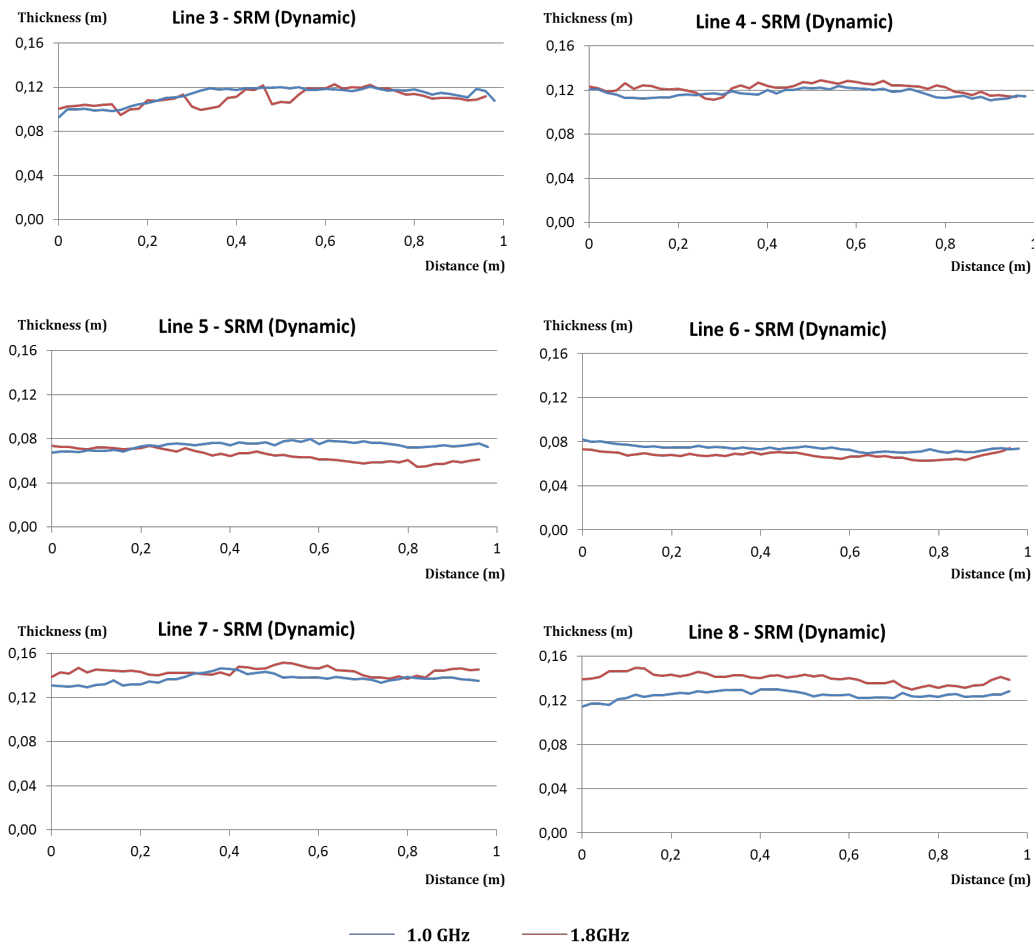

Fig. 8 – Asphalt layer thickness profiles calculated with SRM calibration

85

(iii) Common Mid-Point Method

The CMP method is widely used to estimate the electromagnetic wave velocity using ground-coupled antennas. Figure 9 shows the application of the CMP method varying the distance between the ground-coupled antennas (a), identifying the types of waves that are generated during the survey (b) from the direct waves on air and on ground, to the reflected waves and its representation in the radargrams (c). For the present case air-coupled antennas were used Figure 4 and some adaptation to the processing of the data had to be undertaken, since the electromagnetic waves differ from the usual CMP analysis. The air-direct wave loses strength as the air-coupled antennas are separated and it is difficult to identify its reflection on the radargrams and also the direct ground wave does not exist as the antennas are suspended above the ground and the "ground" is the air itself.
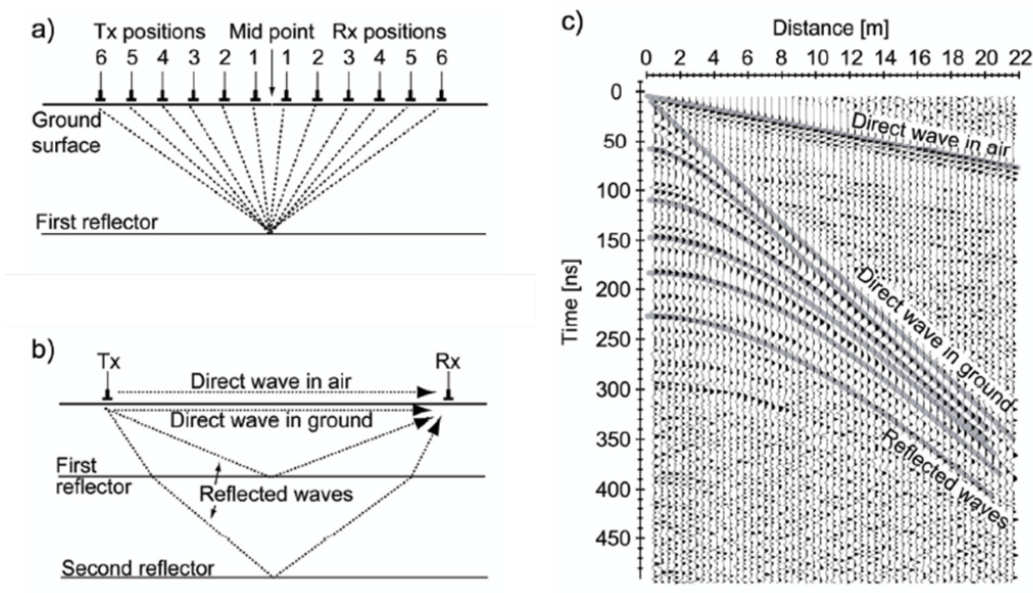
Fig. 9 – Example of CMP method using ground-coupled antennas

The processing of the CMP data was made using the Reflex program. The first stage was to correct the start time of the signal and since we do not have the direct wave we used the first reflection which must have a velocity of 0.3 m/ns (the velocity of the electromagnetic wave on the air). This was made by setting the shot position to 0 m and the receivers from 0.34 to 1.00 m and fitting the air/ground reflection using a velocity of 0.3 m/ns. Figure 10 illustrates the signal before (a) and after (b) the start time correction.

(a) Before start time correction   (b) After start time correction
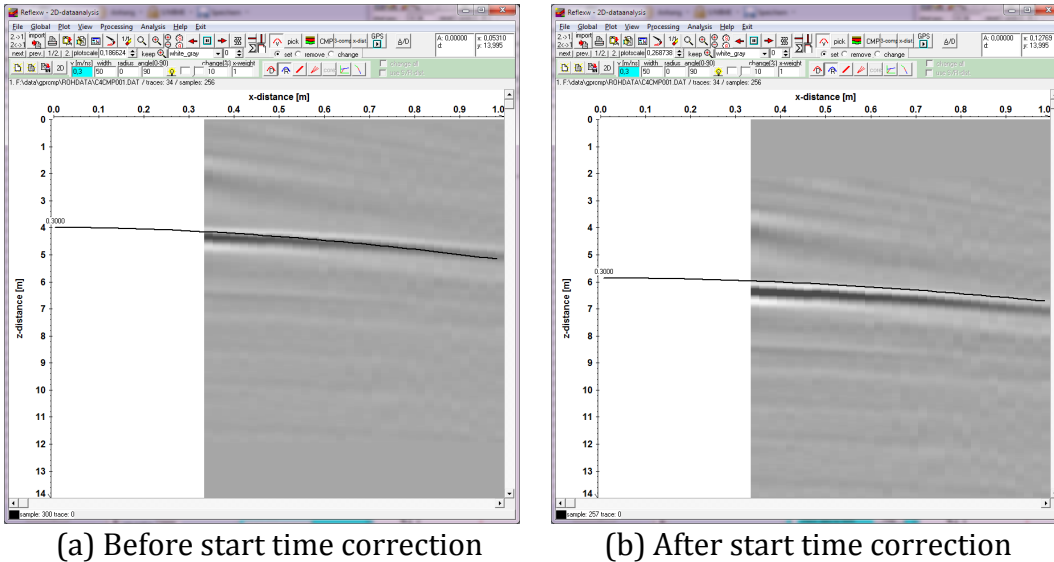
Fig. 10 – CMP signal start time correction

Using these modified data we selected the CMP-velocity analysis to determine the velocity of the propagation of the wave within the first layer. Because of the huge velocity contrast of the layers (air vs ground) we could not use the semblance analysis (that generates mean velocities) as the resulting layer velocity could become smaller than 0, which is not realistic, and a warning message appears. So in this case we use the manual velocity adaptation and adjust the reflection varying the boundary and the velocity of the hyperbolas of the CMP-velocity analysis – see Figure 11.
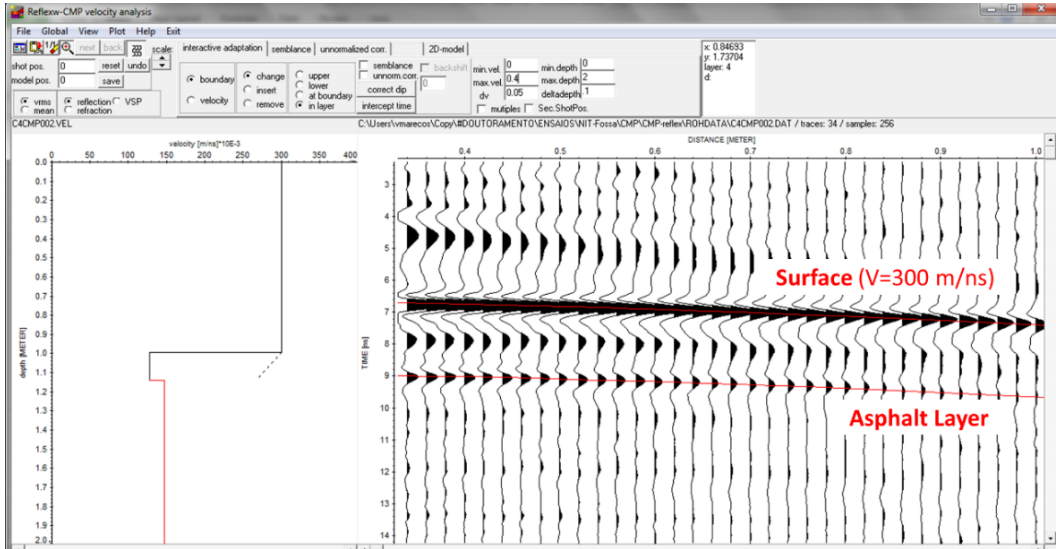
Fig. 11 – CMP-Velocity analysis (Example)

The results of the velocities, the dielectric values and the thickness for the asphalt layer obtained from the Common Mid-Point Method, over the Control Points, are presented in Table VI for the 1.8 GHz air-coupled systems.

Lower dielectric values were obtained for Cells 3 and 4 with the latter being more homogeneous. Figure 12 shows the asphalt layer thickness profiles from Common Mid-Point Method calculated using the average values of the velocity of propagation from the control points.

3. Description of the main results obtained during the STSM

Table VII resumes the dielectric values calculated from all the calibration methods studied: Coring (1.0 GHz and 1.8 GHz), Surface Reflection Method (1.0GHz and 1.8 GHz) and Common Mid-Point Method (1.8 GHz). The dielectric values are, in general, higher for the lower frequencies, ranging from 5.1 to 7.2 for the 1.0 GHz antennas and from 4.8 to 7.8 for 1.8 GHz antenna setup.

TABLE VI – Velocities of propagation and dielectric values obtained from CMP

Cell	Line	Control Point	t (ns) 1.8 GHz	Velocity (m/ns) 1.8 GHz	ε 1.8 GHz	Thickness (m) 1.8 GHz
2	3	31	1.896	0.116	6.7	0.110
		32	1.938	0.109	7.6	0.106
	4	41	1.980	0.108	7.8	0.107
		42	1.956	0.118	6.4	0.116
3	5	51	0.980	0.137	4.8	0.067
		52	0.935	0.124	5.9	0.058
	6	61	0.891	0.137	4.8	0.061
		62	0.907	0.121	6.2	0.055
4	7	71	2.186	0.137	4.8	0.150
		72	2.285	0.128	5.5	0.146
	8	81	2.127	0.134	5.0	0.142
		82	2.091	0.132	5.2	0.138

For the 1.8 GHz antennas the SRM provided the lower average dielectric values for all cells, as for the CMP method it gave the highest variability (Standard Deviations of 0.64, 0.71 and 0.30 for cells 2, 3 and 4 respectively). A more detailed statistical analysis is presented in Table VIII.

Figure 13 shows the asphalt layer thickness calculated on the control points from the GPR data measured with the 1.8 GHz air-coupled antennas. This figure allows the comparison of SRM and CMP calibration with the actual thicknesses obtained from coring (ground truth).

Table IX presents the error (%) evaluated as the difference between both thicknesses obtained from each calibration method, at the same control point, and normalized to the coring measures.
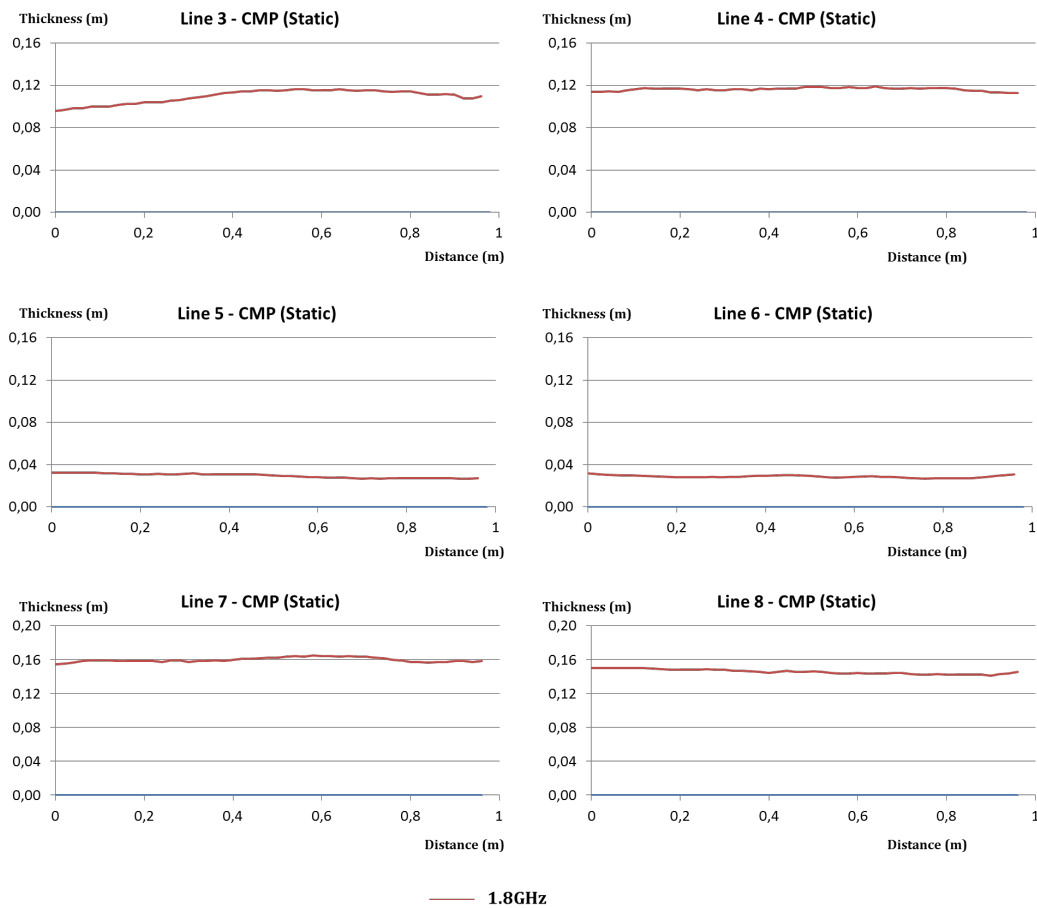
Fig. 12 – Asphalt layer thickness profiles calculated with CMP calibration.

The maximum error (26%) was obtained with the Surface Reflection Method at control point 62 that had the thinner layer of asphalt concrete. The worst results of the SRM were registed Cell 3. The maximum error for the Common Mid-Point Method was obtained at control point 71 and it was 13% (half of the maximum error from SRM). With the exception of Cell 2 the estimation of the thickness for both SRM and CMP calibration methods is higher than the actual thickness of the layer.

TABLE VII – DIELECTRIC VALUE OBTAINED BY USING
THE DIFFERENT CALIBRATION METHODS

Cell	Line	Point	Ɛ - Dieletric value				
			Coring 1.0 GHz	SRM 1.0 GHz	Coring 1.8 GHz	SRM 1.8 GHz	CMP 1.8 GHz
2	3	31	7.1	5.7	6.7	6.8	6.7
		32	6.4	5.5	6.8	5.8	7.6
	4	41	6.9	5.8	6.4	6.2	7.8
		42	6.8	5.4	6.5	5.1	6.4
3	5	51	6.0	5.5	4.9	4.8	4.8
		52	7.2	5.5	5.7	5.3	5.9
	6	61	6.3	5.1	5.9	4.8	4.8
		62	6.3	5.3	5.4	5.2	6.2
4	7	71	7.0	5.9	6.0	5.3	4.8
		72	6.5	5.8	6.5	5.4	5.5
	8	81	5.9	5.8	5.4	5.0	5.0
		82	6.6	5.9	5.8	4.8	5.2

TABLE VIII – STATISTICAL ANALYSIS OF THE DIELECTRIC VALUE OBTAINED
BY THE DIFFERENT CALIBRATION METHODS.

Cell	Statistical Property	Ɛ - Dieletric value				
		Coring 1.0 GHz	SRM 1.0 GHz	Coring 1.8 GHz	SRM 1.8 GHz	CMP 1.8 GHz
2	Average	6.8	5.6	6.6	6.0	7.1
	STDevation	0.29	0.18	0.18	0.71	0.64
3	Average	6.5	5.4	5.5	5.0	5.4
	STDevation	0.52	0.19	0.43	0.26	0.71
4	Average	6.5	5.9	5.9	5.1	5.1
	STDevation	0.45	0.06	0.46	0.28	0.30
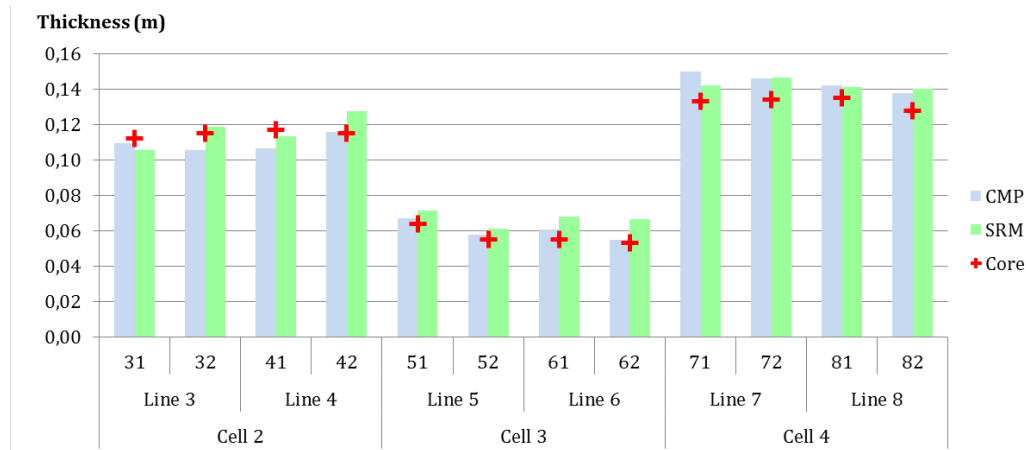
Fig. 13 – Asphalt layer thickness obtained by the different calibration methods for the 1.8 GHz air-coupled antennas.

TABLE IX – ASPHALT LAYER THICKNESS ERROR OBTAINED BY THE DIFFERENT CALIBRATION METHODS

Cell	Line	Point	Thickness (m)			Error (%)	
			Core	SRM	CMP	SRM	CMP
2	3	31	0,112	0,105	0,110	-6%	-2%
		32	0,115	0,119	0,106	3%	-8%
	4	41	0,117	0,114	0,107	-3%	-9%
		42	0,115	0,127	0,116	11%	1%
3	5	51	0,064	0,071	0,067	12%	5%
		52	0,055	0,061	0,058	11%	5%
	6	61	0,055	0,068	0,061	24%	11%
		62	0,053	0,067	0,055	26%	3%
4	7	71	0,133	0,142	0,150	7%	13%
		72	0,134	0,147	0,146	9%	9%
	8	81	0,135	0,141	0,142	5%	5%
		82	0,128	0,140	0,138	9%	8%

4. FUTURE COLLABORATION WITH THE HOST INSTITUTION

The STSM strengthened the cooperation between the visiting and host scientists.

5. FORESEEN PUBLICATIONS/ARTICLES RESULTING FROM THE STSM

Based on the results of this STSM, enriched by complementary tests, a journal paper was published on Construction and Building Materials, please see Ref. [8]. Previously, the STSM results were presented at the GI3.1 Session organised by COST Action TU1208 "Civil Engineering Applications of GPR" during the EGU GA 2016, held in Vienna, Austria, on April 17 – 22, 2016.

ACKNOWLEDGEMENT

REFERENCES

[1] Varela-Gonzalez, M.; Solla, M., Martínez-Sánchez, J.; Arias, P. A semi-automatic processing and visualisation tool for ground-penetrating radar pavement thickness data. Automation in Construction. Vol. 45, Sept. 2014, pp. 42–49.

[2] Morey, R. GPR for evaluating subsurface conditions for transportation facilities. National Cooperative Highway Research Program. Synthesis Report No. 255, Transportation Research Board, National Academy Press, Washington DC, USA, 1998.

[3] Jol, H. – Editor. Ground Penetrating Radar Theory and Applications, 1st Edition. Elsevier Science, December 2008.

[4] Daniels, D. J. Ground penetrating radar. 2nd edition, The Institution of Electrical Engineers, London, UK, 2009.

[5] Maser, K. R.; Scullion T. Automated Detection of Pavement Layer Thicknesses and Subsurface Moisture Using Ground Penetrating Radar. Transportation Research Board Paper, 1991.

[6] McRobbie, S.; Baltazart, V.; Elsworth, N.; Antunes, M.L.; Marecos, V.; Hamrouche, R., Saarenketo, T.; Krarup, J. Monitoring structural and surface conditions. TRIMM project Deliverable 4.3, 2014.

[7] Leng, Z. Al-Qadi, I. An innovative method for measuring pavement dielectric constant using the extended CMP method with two air-coupled GPR systems – NDT & E International. Sept. 2014.

[8] Marecos, V., Solla, M., Fontul, S., Antune, V. Assessing the pavement subgrade by combining different non-destructive methods. Construction and Building materials, pp. 76-85, 2017.

STSM 7

A STUDY OF THE ACCURACY OF THE SAP-DoA LOCATION TECHNIQUE APPLIED TO GPR DATA
AND COMPARISON WITH THE STANDARD HYPERBOLA APPROACH

Visiting Scientist: Simone Meschino, Airbus, Germany (ECI),
(simone.meschino@gmail.com)

Host Scientist: Lara Pajewski, Roma Tre University, Rome, Italy
(lara.pajewski@gmail.com)

STSM Dates: 4 - 9 January 2016

1. PURPOSE OF THE STSM

This STSM contributed to the achievement of the objectives of Working Group 3 of the COST Action TU1208. It was a continuation of the work that we started during a previous mission (April 3rd – 10th, 2015) [1], which results were meanwhile presented during the "IEEE 15th Mediterranean Microwave Symposium (MMS)", Lecce (Italy), Nov. 2015 [2].

Directions of Arrival (DoA) techniques enable an antenna array to estimate the number of incident signals and their arrival directions. A Sub-Array Processing (SAP) approach can be adopted for the detection of targets lying in the near field of an antenna array. In particular, the receiver array can be partitioned in several sub-arrays, such that the field scattered by the targets can be assumed to be locally planar at each sub-array. Then, by applying DoA estimation algorithms, it is possible to predict the dominant direction of the incoming signal at each sub-array. By triangulating all DoAs estimated by the sub-arrays, a pattern of crossings can be obtained. This pattern can be filtered in order to remove a noisy background of unwanted crossings [3]. Subsequently, the number of targets and their positions can be estimated.

95

Our first STSM focused on the use of SAP-DoA approaches for the location of reinforcing elements in concrete. As a first step, we reviewed our previous work on SAP-DoA techniques and suitably modified our Matlab codes, in order to be able to use them for the processing of the Fourier-transform of Ground- Penetrating Radar (GPR) radargrams. A second task was concerned with overcoming the limits of DoA algorithms, which are designed by considering a narrowband signal model: we worked on extending the approach to the case of an ultra wideband signal.

Because of the limited time at our disposal, we opted for a simple solution of the latter issue – there was still room for further improvement. Finally, we performed preliminary tests on synthetic data, calculated by using gprMax. In particular, we worked with the reference data of TU1208 Concrete Cells 1.1-1.3 [4] (see Figure 1.1) and we also simulated enlarged versions of these cells. As expected, we obtained more accurate results when the distance between objects was larger and their interaction weaker. Based on the results that we obtained during the first STSM, during the second STSM we focused on the following tasks:

- We analysed more in depth the results obtained for the enlarged versions of Cells 1.1-1.3 and obtained additional results, in order to assess in a more comprehensive way the accuracy and limits of our approach in the presence of multiple scatterers versus the distance between them (Days 1-3).
- We compared the accuracy of our method and the standard time-domain hyperbola approach (Days 4-5).

At the end of the second STSM, we also planned our future activities. We decided to test our approach on experimental data: in particular, we planned to process some sections of the TU1208 dataset coming from measurements performed at the IFSTTAR Geophysical Test Site (Nantes, France). We also desired to improve our approach during a future STSM, in order to exploit in a smarter and more advanced way the multi-frequency information enclosed in the GPR data - which is what we actually did during a

STSM performed in 2017. During that third and final STSM we also implemented a graphical-user interface and wrote a user manual, so that our codes could be released for free public download by the end of the Action.
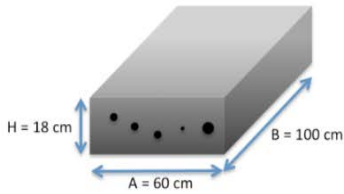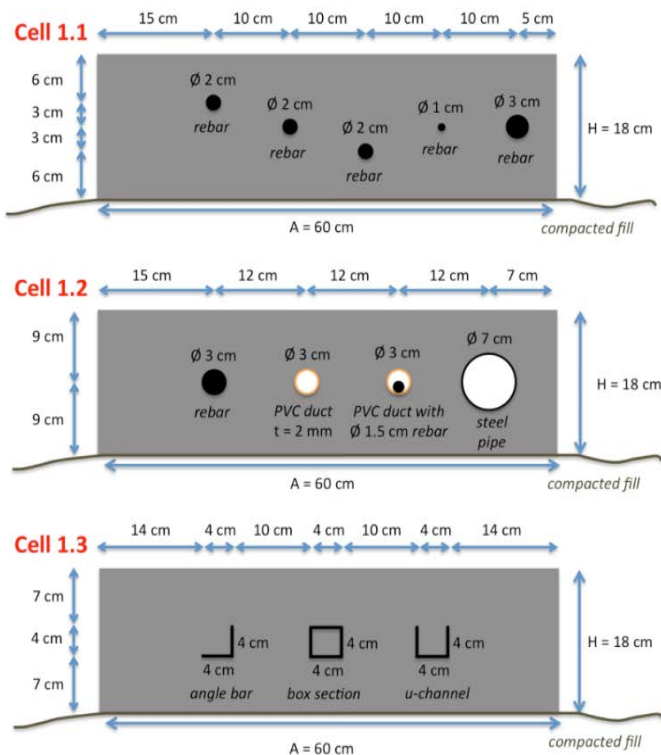

Fig. 1.1 – Original simulation scenario described in [3].

2. DESCRIPTION OF THE WORK CARRIED OUT DURING THE STSM AND OF THE MAIN RESULTS OBTAINED

2.1 SIMULATION, BY USING GPRMAX AND E²GPR, OF ENLARGED VERSION OF THE TU1208 CONCRETE CELLS

The identification of buried cables, pipes, conduits, and other cylindrical utilities, is an important task in civil engineering and is nowadays extensively studied. Most commonly employed

approaches are based on the use of electromagnetic sensing such a GPR systems, in order to extract information about the scenario and localise the sought objects. Nevertheless, innovative techniques must still be developed in order to mitigate the drawbacks of existing approaches, especially when real-time operations are needed.

As recalled in Section 1, during the first STSM we applied our SAP-DoA approach to the TU1208 Concrete Cells 1.1-1.3 proposed in [4] and to enlarged versions of them where the distance between the objects was increased of 10 cm.

During the second STSM, we carried out further simulations by using the electromagnetic simulator gprMax and the additional tool E^{2}GPR [5-6], where we gradually enlarged the cells with a 5-cm step. For each Cell, five versions are now available, as shown in Figures 2.1 - 2.6 and resumed in Tables I - III: the original cells, and cells where the distance between objects is increased by 5 cm, by 10 cm, by 15 cm, and finally by 20 cm.

2.2 THE HYPERBOLA APPROACH: DEVELOPMENT OF A MATLAB PROCEDURE FOR THE FITTING OF HYPERBOLAS IN GPR RADARGRAMS

When the radar signal impinges on circular-section rebar embedded in concrete, it is scattered and reflected due to the discontinuity of permittivity. As the GPR antenna is shifted along the surface of a concrete layer, the presence of circular-section rebar is translated into the radargram as a hyperbola. The scattering properties of rebar strongly depend on the polarization of the electromagnetic field emitted by the radar and by the size of the rebar with respect to the incident wavelength.

Everything becomes much more complicated when the section of rebar elements is not circular. As for the polarization, if the electromagnetic field emitted by the radar is linearly polarized, rebar reflections can be maximized by varying the antenna orientation. These issues have significant implications for rebar detection, survey design, and data interpretation.
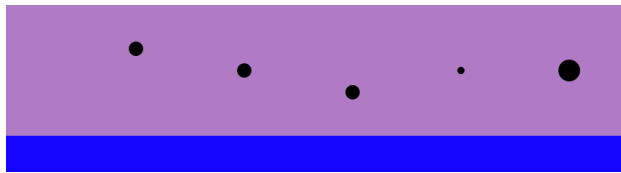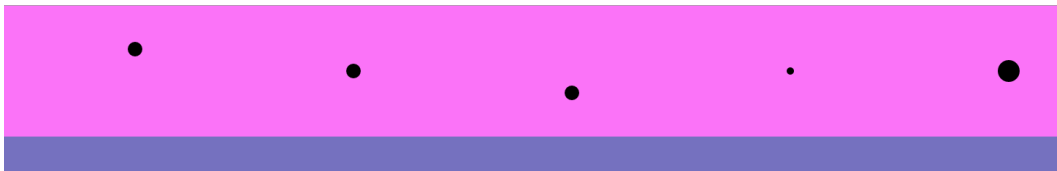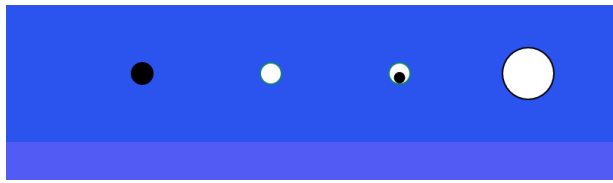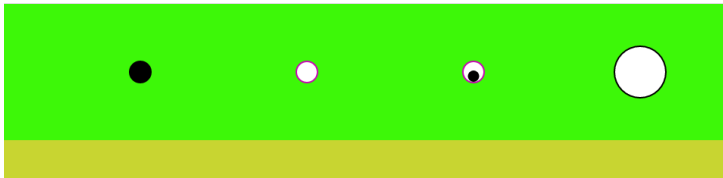
(a)
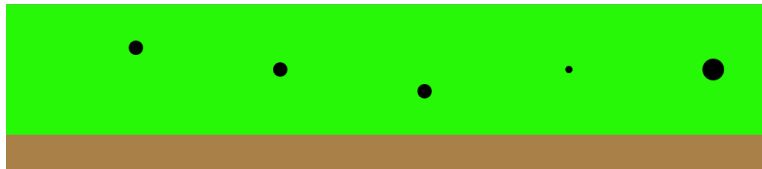
(b)

(c)

(d)

Fig. 2.1 – Geometry of enlarged versions of Cell 1.1. The cell is enlarged of 5 cm (a), 10 cm (b), 15 cm (c), and 20 cm (d) with respect to the original cell. Therefore, the distance between the axes of adjacent elements is 15 cm in (a), 20 cm in (b), 25 cm in (c) and 30 cm in (d).
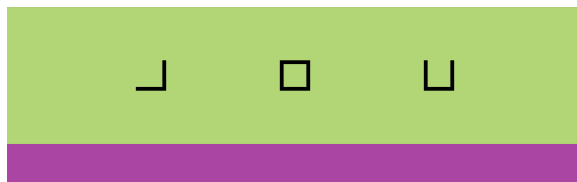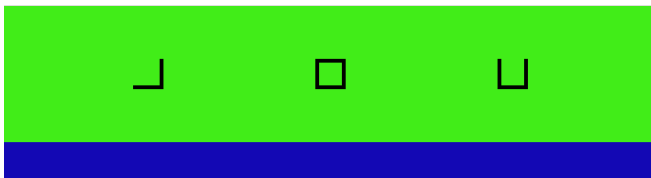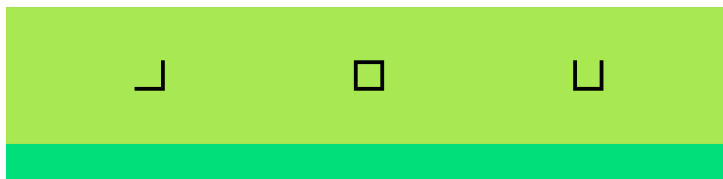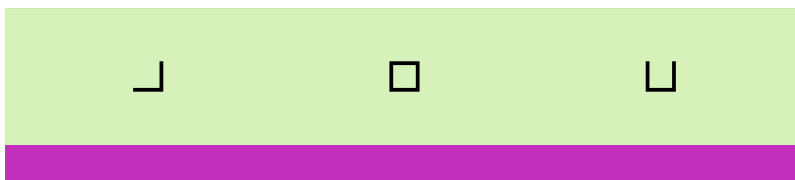
(a)

(b)

(c)

(d)

Fig. 2.2 – Geometry of enlarged versions of Cell 1.2. The cell is enlarged of 5 cm (a), 10 cm (b), 15 cm (c), and 20 cm (d) with respect to the original cell. Therefore, the distance between the axes of adjacent elements is 17 cm in (a), 22 cm in (b), 27 cm in (c) and 32 cm in (d).

(a)

(b)

(c)

(d)

Fig. 2.3 – Geometry of enlarged versions of Cell 1.3. The cell is enlarged of 5 cm (a), 10 cm (b), 15 cm (c), and 20 cm (d) with respect to the original cell. Therefore, the distance between the axes of adjacent elements is 14 cm in (a), 19 cm in (b), 24 cm in (c) and 29 cm in (d).
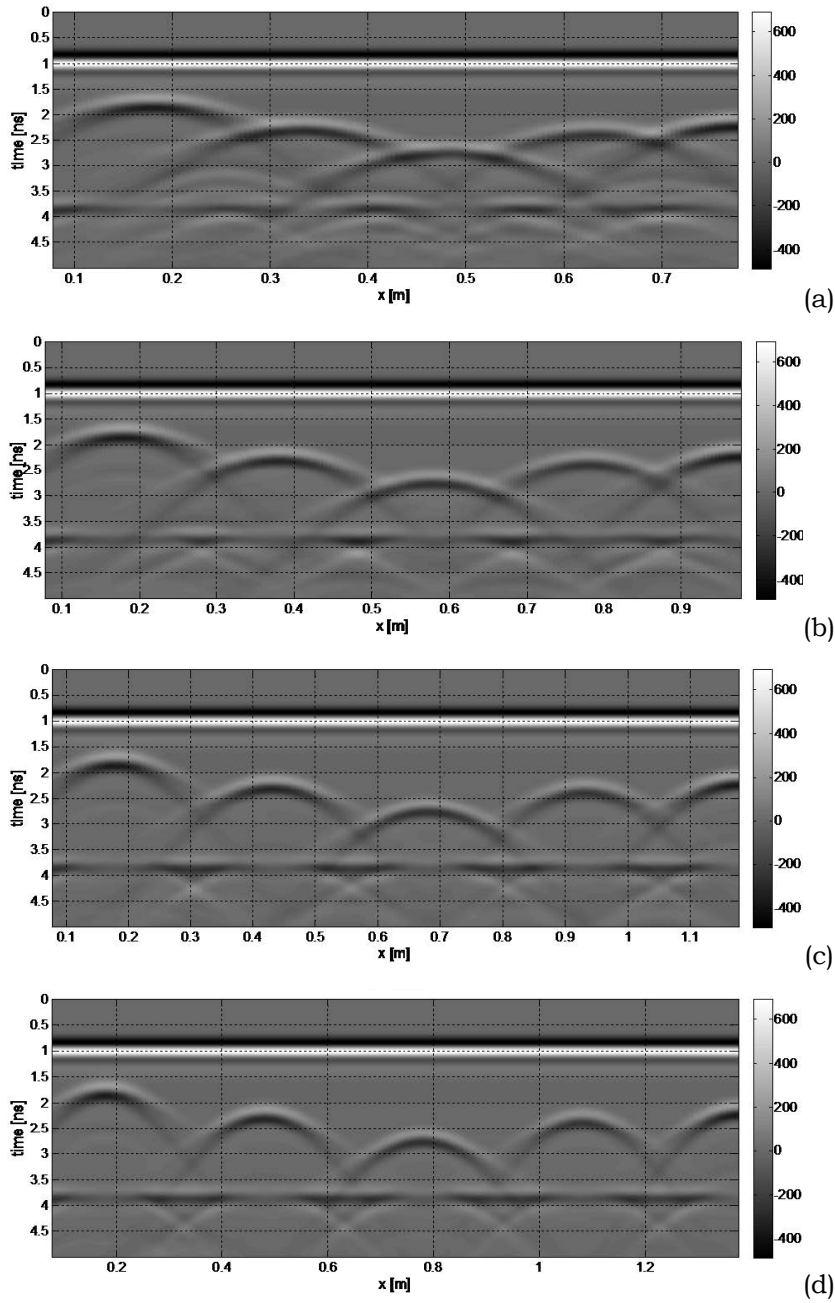
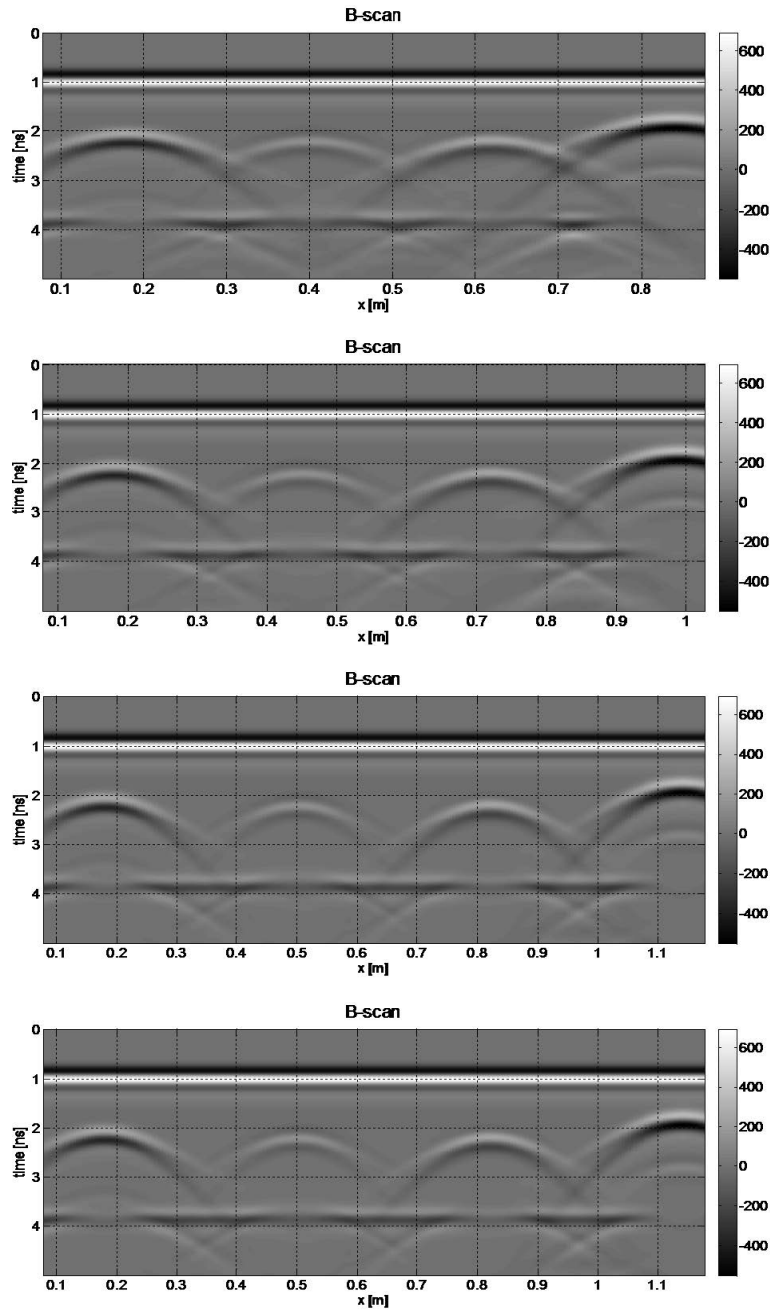**Fig. 2.4** – Radargrams for enlarged Cells 1.1 (a)-(d).

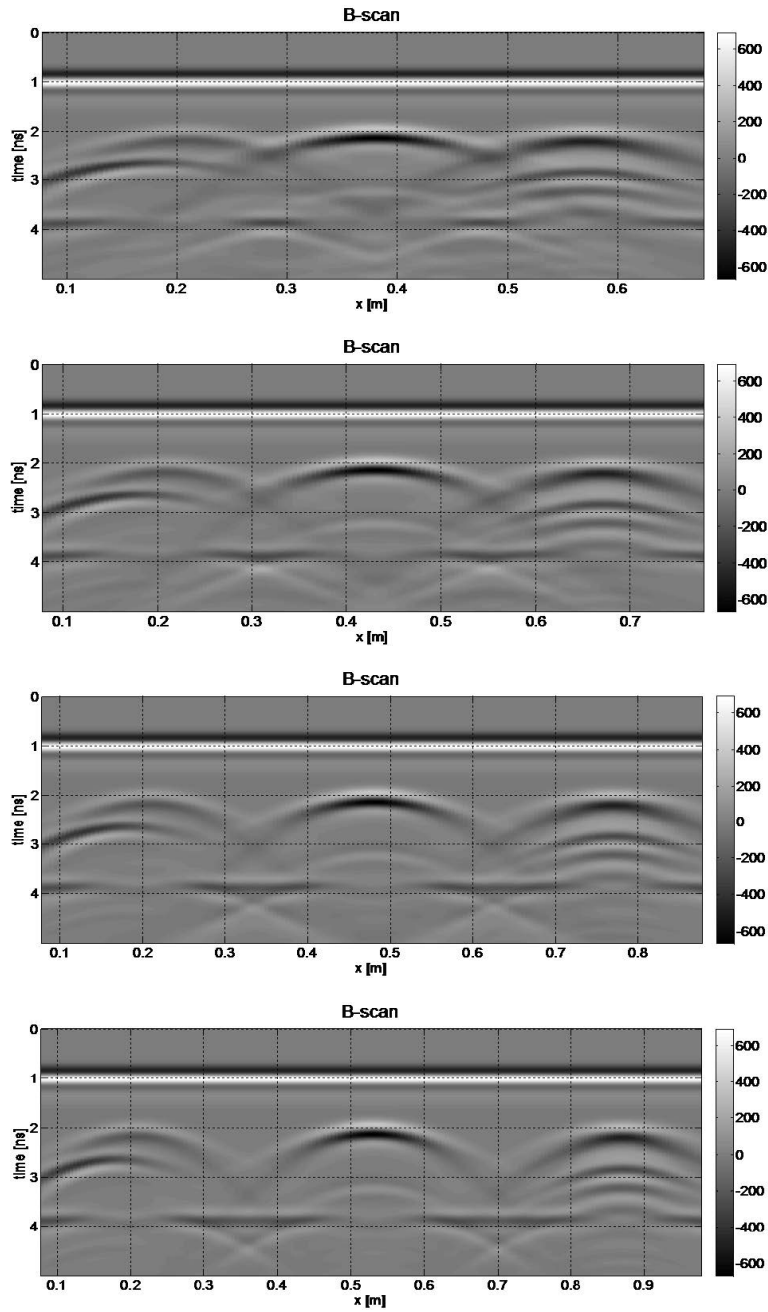**Fig. 2.5** – Radargrams for enlarged Cells 1.2 (a)-(d).

Fig. 2.6 – Radargrams for enlarged Cells 1-3 (a)-(d).

TABLE I – TEST SCENARIO FOR CELL 1-1.

CELL 1-1 a)			
Object	**Centre position [m]**	**Radius [m]**	**Material**
No. 1: Left edge	(0.18, 0.17)	0.01	pec
No. 2: Left	(0.33, 0.14)	0.01	pec
No. 3: Centre	(0.48, 0.11)	0.01	pec
No. 4: Right	(0.63, 0.14)	0.005	pec
No. 5: Right edge	(0.78, 0.14)	0.015	pec
Cell dimensions: 0.86 x 0.28 cm^2		**No. of A-Scans**: 140	
CELL 1-1 b)			
Object	**Centre position [m]**	**Radius [m]**	**Material**
No. 1: Left edge	(0.18, 0.17)	0.01	pec
No. 2: Left	(0.38, 0.14)	0.01	pec
No. 3: Centre	(0.58, 0.11)	0.01	pec
No. 4: Right	(0.78, 0.14)	0.005	pec
No. 5: Right edge	(0.98, 0.14)	0.015	pec
Cell dimensions: 1.06 x 0.28 cm^2		**No. of A-Scans**: 180	
CELL 1-1 c)			
Object	**Centre position [m]**	**Radius [m]**	**Material**
No. 1: Left edge	(0.18, 0.17)	0.01	pec
No. 2: Left	(0.43, 0.14)	0.01	pec
No. 3: Centre	(0.68, 0.11)	0.01	pec
No. 4: Right	(0.93, 0.14)	0.005	pec
No. 5: Right edge	(1.18, 0.14)	0.015	pec
Cell dimensions: 1.26 x 0.28 cm^2		**No. of A-Scans**: 220	
CELL 1-1 d)			
Object	**Centre position [m]**	**Radius [m]**	**Material**
No. 1: Left edge	(0.18, 0.17)	0.01	pec
No. 2: Left	(0.48, 0.14)	0.01	pec
No. 3: Centre	(0.78, 0.11)	0.01	pec
No. 4: Right	(1.08, 0.14)	0.005	pec
No. 5: Right edge	(1.38, 0.14)	0.015	pec
Cell dimensions: 1.46 x 0.28 cm^2		**No. of A-Scans**: 260	

GENERAL SETUP of the simulation
Dielectric constant medium 1: 6 (concrete)
Dielectric constant medium 3: 16 (compacted fill)
Spacing: 5E-3 m
Time window: 5e-9 sec
Centre frequency: 1500 MHz (Ricker pulse)

Most commercial GPR antennas are dipole antennas radiating a linearly-polarized field, with the electric field oriented along the long axis of the dipole. In a co-polarized antenna configuration, both receiving and transmitting antennas have the same polarization properties: rebar yield strong reflections when oriented parallel to the long axis of the dipoles, weak reflections when oriented orthogonal to the axis of the antennas. A cross-polarized antenna configuration is less sensitive to smooth planar targets and more sensitive to targets that yield depolarized energy.

It is therefore very important to consider polarization when planning and executing a GPR field survey, as the sensitivity of cross-pole and co-pole antenna arrangements are different depending on the type of target and subsurface conditions. Optimization of antenna orientation, to take advantage of signal polarization, is a significant feature for a successful location of reinforcing bars in the radargrams. Note that all simulations presented in Section 2.1, both the receiving and transmitting antennas are parallel to the rebar axis.

One of the most commonly used methods for the estimation of rebar size in concrete from GPR data is the hyperbola approach. In order to be able to compare this approach with our SAP-DoA method, we implemented a Matlab procedure for hyperbola fitting. This is based on a Minimum Mean Square Error technique [7].

Let us consider an ideal vertical transverse-axis hyperbola with coefficients a and b, centred at the origin of a xy Cartesian reference system. The equation for such hyperbola is:

$$\frac{x^2}{a^2} + \frac{y^2}{b^2} = 1 \tag{1}$$

TABLE 2 - TEST SCENARIO FOR CELL 1-2.

CELL 1-2 a)			
Object	**Centre position [m]**	**Radius [m]**	**Material**
No. 1: Left edge	(0.18, 0.14)	0.015	pec
No. 2: Left	(0.35, 0.14)	0.015	pvc
	(0.35, 0.14)	0.013	free space
No. 3: Right	(0.52, 0.14)	0.015	pvc
	(0.52, 0.14)	0.013	free space
	(0.52, 0.1345)	0.0075	pec
No. 4: Right edge	(0.69, 0.14)	0.035	pec
	(0.69, 0.14)	0.033	free space
Cell dimensions: 0.81 x 0.28 cm2		**No. of A-scans**: 13	
CELL 1-2 b)			
Object	**Centre position [m]**	**Radius [m]**	**Material**
No. 1: Left edge	(0.18, 0.14)	0.015	pec
No. 2: Left	(0.4, 0.14)	0.015	pvc
	(0.4, 0.14)	0.013	free space
No. 3: Right	(0.62, 0.14)	0.015	pvc
	(0.62, 0.14)	0.013	free space
	(0.62, 0.1345)	0.0075	pec
No. 4: Right edge	(0.84, 0.14)	0.035	pec
	(0.84, 0.14)	0.033	free space
Cell dimensions: 0.96 x 0.28 cm2		**No. of A-scans**: 160	
CELL 1-2 c)			
Object	**Centre position [m]**	**Radius [m]**	**Material**
No. 1: Left edge	(0.18, 0.14)	0.015	pec
No. 2: Left	(0.45, 0.14)	0.015	pvc
	(0.45, 0.14)	0.013	free space
No. 3: Right	(0.72, 0.14)	0.015	pvc
	(0.72, 0.14)	0.013	free space
	(0.72, 0.1345)	0.0075	pec
No. 4: Right edge	(0.99, 0.14)	0.035	pec
	(0.99, 0.14)	0.033	free space
Cell dimensions: 1.11 x 0.28 cm2		**No. of A-scans**: 190	

CELL 1-2 d)			
Object	**Centre position [m]**	**Radius [m]**	**Material**
No. 1: Left edge	(0.18, 0.14)	0.015	pec
No. 2: Left	(0.5, 0.14) (0.5, 0.14)	0.015 0.013	pvc free space
No. 3: Right	(0.82, 0.14) (0.82, 0.14)	0.015 0.013	pvc free space
No. 4: Right edge	(1.14, 0.14) (1.14, 0.14)	0.035 0.033	pec free space
Cell dimensions: 1.26 x 0.28 cm2			
No. of A-scans: 220			
GENERAL SETUP			
Dielectric constant medium 1: 6 (concrete)			
Dielectric contant medium 2: 16 (compacted fill)			
Dielectric constant medium 3: 3 (pvc)			
Spacing: 5E-3 m			
Time window: 5e-9 sec			
Centre frequency: 1500 MHz (Ricker pulse)			

Let us call (x_i, y_i), with $i = 1, 2, 3,...n$, the coordinates of n points along a curve. If the curve is a perfect hyperbola, then all the points (x_i, y_i) satisfy Equation (1) and the error due to hyperbola-fitting of the curve is zero. For real field hyperbolic signatures in a radargram, (x_i, y_i) do not perfectly lie on a hyperbola. For any point (x_i, y_i), the error e can be defined as the difference between the left and right hand sides of the Eq. (1). Thus the square error e^2 is:

$$e^2 = \sum_{i=1}^{n} \left(1 - \frac{x_i^2}{a^2} + \frac{y_i^2}{b^2} \right)^2 \qquad (2)$$

Eq. (2) is a function of the parameters a and b. These parameters are to be determined such that the square error e^2 is minimised and the best-fitting hyperbola is found.

TABLE III – TEST SCENARIO FOR CELL 1-3.

CELL 1-3 a)			
Object	**Object position [m]**	**Shape**	**Material**
No. 1: Left edge	X: from 0.17 to 0.21 Y: from 0.12 to 0.16	L-shaped	pec
No. 2: Centre	X: from 0.36 to 0.4 Y: from 0.12 to 0.16	Square-shaped	pec
No. 3: Right edge	X: From 0.55 to 0.59 Y: From 0.12 to 0.16	U-shaped	pec
Cell dimensions: 0.76 x 0.28 cm^2			
No. of A-scans: 120			
CELL 1-3 b)			
Object	**Object position [m]**	**Radius**	**Material**
No. 1: Left edge	X: from 0.17 to 0.21 Y: from 0.12 to 0.16	L-shaped	pec
No. 2: Centre	X: from 0.41 to 0.45 Y: from 0.12 to 0.16	Square-shaped	pec
No. 3: Right edge	X: From 0.65 to 0.69 Y: From 0.12 to 0.16	U-shaped	pec
Cell dimensions: 0.86 x 0.28 cm^2			
No. of A-scans: 140			
CELL 1-3 c)			
Object	**Object position [m]**	**Radius**	**Material**
No. 1: Left edge	X: from 0.17 to 0.21 Y: from 0.12 to 0.16	L-shaped	pec
No. 2: Centre	X: from 0.46 to 0.5 Y: from 0.12 to 0.16	Square-shaped	pec
No. 3: Right edge	X: From 0.75 to 0.79 Y: From 0.12 to 0.16	U-shaped	pec
Cell dimensions: 0.96 x 0.28 cm^2			
No. of A-scans: 160			

CELL 1-3 d)			
Object	**Object position [m]**	**Shape**	**Material**
No. 1: Left edge	X: from 0.17 to 0.21 Y: from 0.12 to 0.16	L-shaped	pec
No. 2: Centre	X: from 0.51 to 0.55 Y: from 0.12 to 0.16	Square-shaped	pec
No. 3: Right edge	X: From 0.85 to 0.89 Y: From 0.12 to 0.16	U-shaped	pec

Cell dimensions: 1.06 x 0.28 cm^2
No. of A-scans: 180
GENERAL SETUP
Dielectric constant medium 1: 6 (concrete)
Dielectric constant medium 2: 16
Spacing: 5E-3 m
Time window: 5e-9 sec
Centre frequency: 1500 MHz (Ricker pulse)

Centre frequency: 1500 MHz (Ricker pulse)

The optimal values of a and b are obtainable by differentiating e^2 with respect to the parameters and by equating the differentials to zero. That is, by solving the equations:

$$\sum_i y^2{}_i - \sum_i \frac{y^2{}_i}{a^2} + \sum_i \frac{x^2{}_i y^2{}_i}{b^2} = 0 \qquad (3)$$

$$\sum_i x^2{}_i - \sum_i \frac{x^2{}_i}{b^2} + \sum_i \frac{x^2{}_i y^2{}_i}{a^2} = 0 \qquad (4)$$

Eq. (3) and (4) can be solved for a and b and the following expressions can be obtained:

$$a^2 = \frac{\sum_i x_i^4 \sum_i y_i^4 - (\sum_i x_i^2 y_i^2)^2}{\sum_i x_i^4 \ \sum_i y_i^2 - (\sum_i x_i^2 y_i^2)\sum_i x_i^2} \qquad (7)$$

$$b^2 = \frac{(\sum_i x^2{}_i y^2{}_i) \ \sum_i x_i^4 - (\sum_i x^2{}_i y^2{}_i)^2}{(\sum_i x^2{}_i y^2{}_i)\sum_i y_i^2 - \sum_i x_i^2 \sum_i y_i^4} \qquad (8)$$

The fitting algorithm was implemented in a MATLAB environment. The procedure hyperfit.m that we wrote is reported in the following.

hyperfit.m

```matlab
function [a,b]=hyperfit(x,t)
%Input
% x horizontal distance coordinates (m)
% t vertical time coordinates (ns)
%Output
% a fitting coefficient (a)
% b fitting
coefficient (b)
P=sum(x.^2);
Q=sum(t.^2);
R=sum(x.^4);
S=sum(t.^4);
T=sum((x.^2).*
(t.^2));
a=sqrt((R.*S-T.^2)/(R.*Q-T.*P));
b=sqrt((T.*R-T.^2)/(Q.*T-P.*S));
yData = sqrt( ( (x./a).^2 - 1 ) .* (b.^2) );
%Plot
result
hold
on;
plot( xData, mean(yData) - (yData -
mean(yData)),'g','LineWidth',2 ); axis ij
%Label
axes
xlabel( 'x
[m]' );
ylab
grid on

end
```

The input data can be extracted from a synthetic or experimental B-Scan by using the function **bscan2D.m** reported in [1] and by

implementing a dedicated script for each simulation setup. To give an example, the script for Cell 1.1 a) is reported in the following.

cell_11a.m

```
% Cell 1-1 a)
% Object position:
% % x   y
% #1 (0.18, 0.17)
% #2 (0.33, 0.14)
% #3 (0.48, 0.11)
% #4 (0.63, 0.14)
% #5 (0.78, 0.14)
%
% % cell dimension: 0.86
x 0.28 cm^2 clear
clc
load E_1-
1_piu5.mat
c_m_s =
299792500;
epsr = 6;                    % Dielectric constant
of ground.  offset = 0.05;
peak_time = [];
E_new = E(1000:3000,:);
scan_E =
zeros(size(E_new));
for k =
1:size(E_new,2)
    [ak,bk] = findpeaks(E_new(:,k));
    eval(sprintf('%s.%s%d = %s;','peak_time','t',k,'bk'));
    [rk,ck] = max(ak);
    scan_E(bk(ck),k) =
    100;
end

figure
(1001)
images
c(E);

figure(102)
```

```
[C,h] =
contourf(scan_E)
; close 102
CC = find(C(2,:)<20);
C(:,CC) = [];
[xsortdata,xsort] =
sort(C(1,:));
xdata = linspace(rxposition(1)-
offset,rxposition(end)-
offset,length(xsortdata));
ydata = (1000 + C(2,xsort)).*Header.dt.*1E9;
% cell_1-1_piu5
x1 = xdata(1:ds

y1 = ydata(1:dsearchn(xsortdata',38));
x2 = xdata(dsearchn(xsortdata',39):dsearchn(xsortdata',71));
y2 = ydata(dsearchn(xsortdata',39):dsearchn(xsortdata',71));
x3 = xdata(dsearchn(xsortdata',72):dsearchn(xsortdata',92));
y3 = ydata(dsearchn(xsortdata',72):dsearchn(xsortdata',92));
x4 =xdata(dsearchn(xsortdata',93):dsearchn(xsortdata',122));
y4 =ydata(dsearchn(xsortdata',93):dsearchn(xsortdata',122));
x5=xdata(dsearchn(xsortdata',123):dsearchn(xsortdata',140));
y5=ydata(dsearchn(xsortdata',123):dsearchn(xsortdata',140));
```

the two vectors (xdata,ydata) are used as input for the function **hyperfit.m**.

For each object the representative data have to be extracted, as shown in Figure 2.7. In particular, in such figure we show how the relevant point data have been extracted (by using the Matlab code reported above) in order to calculate the hyperbola fitting curve by using the hyperfit.m function. This procedure leads to the representation of the B-scan vs the obtained data (hyperbola fitting curve), shown in Figure 2.8. Finally, Figure 2.9 shows the extracted B-scan data (green) and the hyperbola fitted data.
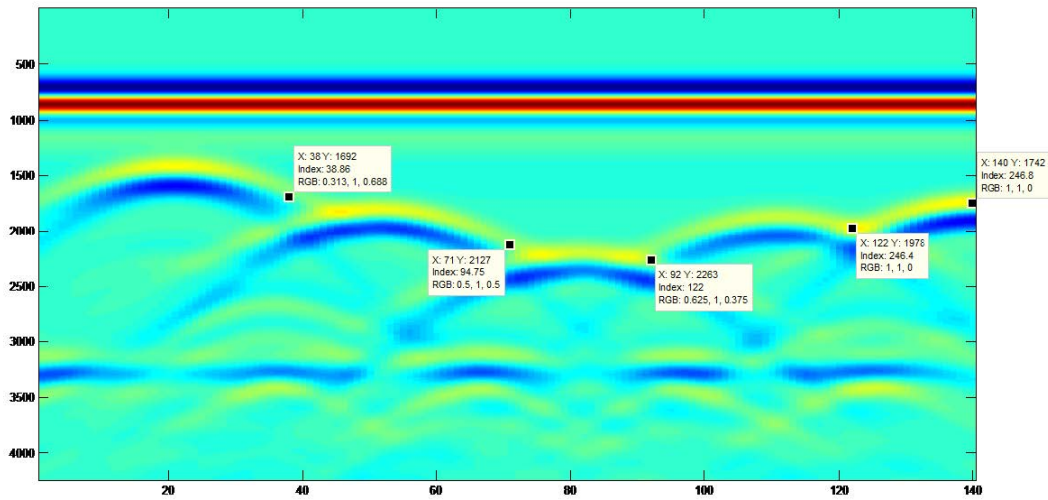
Fig. 2.7 – Extraction of object position data: Cell 1.1a.
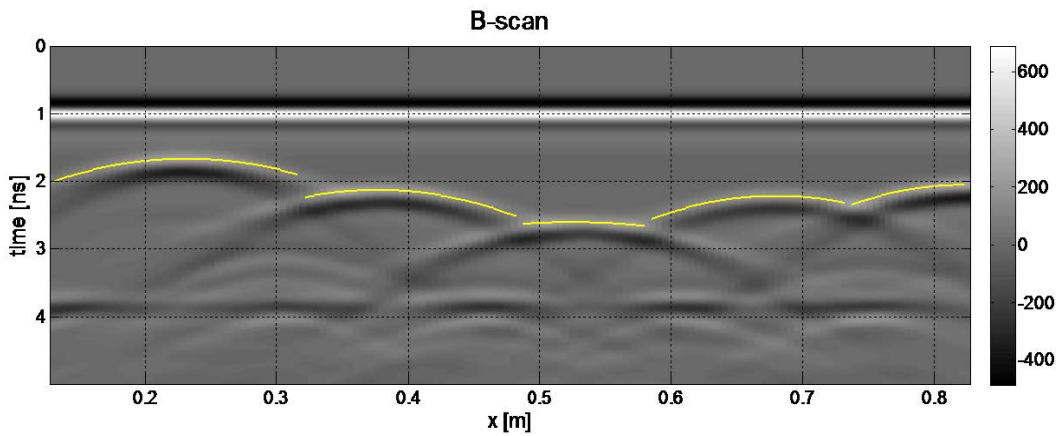
Fig. 2.8 – Hyperbolic data fitting on B-scan data: Cell 1.1a.
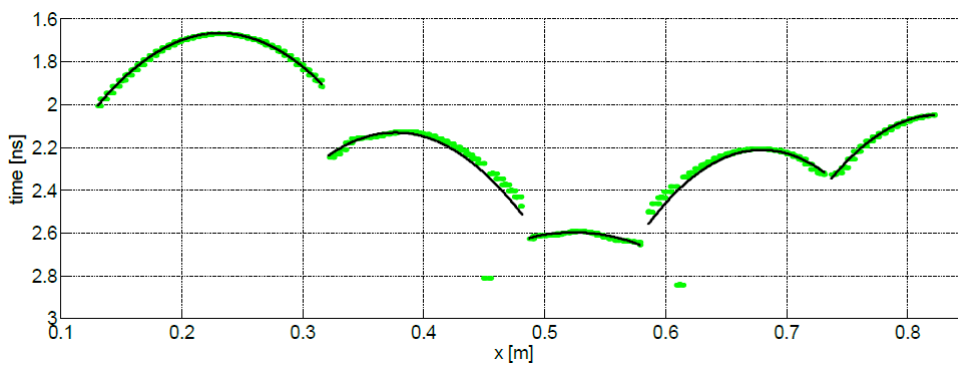
Fig. 2.9 – Hyperbola data fitting vs data extracted by using the Matlab routine: Cell 1.1a.

2.3 REBAR LOCALISATION WITH THE SAP-DoA TECHNIQUE AND WITH THE STANDARD HYPERBOLA APPROACH

Table IV shows the localization results for Cell 1.1, for all the considered versions of it. In particular, the position error is reported (actual position - estimated position) for the hyperbolic fitting and for the SAP-DOA estimations. In Figure 2.10, the error is plotted as a function of the horizontal distance between adjacent objects.

As expected, the SAP-DOA method error decreases when the objects are more distant one to another. For Cell 1.1, the hyperbolic fitting estimation is much more robust than the SAP-DOA methods, when objects are closer than 30 cm. We wish to investigate what happens when the rebar size becomes larger: in such case, both the hyperbolic fitting estimation and the SAP-DoA approach will show a worse behaviour, due to the fact that the objects will not anymore lie in the far-field of the antennas.

Table V shows the localization results for Cell 1.2, for all the considered versions of it. In Figure 2.11, the rms error is plotted as a function of the horizontal distance between adjacent objects.

Again, the SAP-DOA method error is higher than the hyperbolic fitting estimation. Moreover, in this case, we observe

TABLE IV – CELL 1-1: COMPARING LOCATIONS ESTIMATED BY MEANS OF HYPERBOLIC FITTING AND THOSE ESTIMATED BY THE SAP-DOA APPROACH.

CELL 1-1 a)		
Object	**Hyp. Position error [m]**	**SAP-DOA position error**
No. 1: Left edge	(-0.002, -0.008)	(-0.0063, -0.0014)
No. 2: Left	(0.003, -0.01)	(0.0695, 0.03)
No. 3: Centre	(0.006, -0.011)	(0.15, 0.0259)
No. 4: Right	(8.6E-5, -0.005)	(0.173, 0.06)
No. 5: Right	(0.007, -0.015)	(0.1264, 0.0247)
CELL 1-1 b)		
Object	**Hyp. Position error [m]**	**SAP-DOA position error**
No. 1: Left edge	(0.0001, -0.008)	(-0.0095, -0.0148)
No. 2: Left	(-0.0012, -0.01)	(0.0388, -0.0287)
No. 3: Centre	(0.001, -0.011)	(0.0268, -0.0441)
No. 4: Right	(0.0031, -0.005)	(0.0605, -0.0321)
No. 5: Right	(0.007, -0.015)	(0.0671, -0.0347)
CELL 1-1 c)		
Object	**Hyp. Position error [m]**	**SAP-DOA position error**
No. 1: Left edge	(-0.0012, -0.008)	(0.0217, -0.011)
No. 2: Left	(-0.003, -0.01)	(0.0336, -0.0138)
No. 3: Centre	(-0.002, -0.011)	(0.0295, -0.0178)
No. 4: Right	(0.003, -0.005)	(0.0322, -0.0124)
No. 5: Right	(0.007, -0.015)	(0.0147, -0.01)
CELL 1-1 d)		
Object	**Hyp. Position error [m]**	**SAP-DOA position error**
No. 1: Left edge	(-0.0063, -0.008)	(0.0182, -0.006)
No. 2: Left	(-0.0015, -0.01)	(0.0239, -0.003)
No. 3: Centre	(-0.003, -0.011)	(0.029, -0.0118)
No. 4: Right	(0.0126, -0.0045)	(0.0316, -0.0024)
No. 5: Right	(0.007, -0.0155)	(0.0077, -0.01)
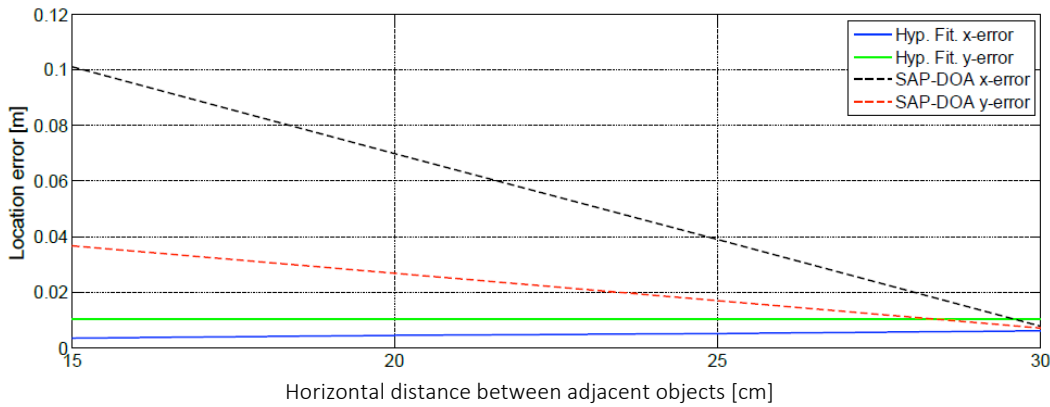
Fig. 2.10 – RMS estimation error versus object mutual distance for Cell 1.1 a-d.

that the SAP-DOA depth error increases by increasing the distance among the objects. This is due to the presence of dielectric objects with cavities in this case study and is consistent with the A-scans reported in [1] for the original not enlarged cell (see the unusual time delays of the reflections by empty objects, there).

Table VI shows the localization results for Cell 1.3, for all the considered versions of it. In Figure 2.12, the rms error is plotted as a function of the horizontal distance between adjacent objects. As objects of Cell 1.3 do not have a circular section, the center position has been considered as the mean x, y point. In this case study, the SAP-DOA method seems to be more robust than the hyperbolic fitting estimation. This is due to the fact that, in this case, objects have non-circular section. This result shows that the SAP-DOA method can be used successfully to detect targets in concrete different than pipes and tubes: in such cases the hyperbola approach cannot be adopted, whereas our SAP-DoA method can still provide a useful estimation of the target size.

TABLE V – CELL 1-2: COMPARING LOCATIONS ESTIMATED BY MEANS OF HYPERBOLIC FITTING AND THOSE ESTIMATED BY THE SAP-DOA APPROACH.

CELL 1-2 a)		
Object	**Hyp. Position error [m]**	**SAP-DOA position**
No. 1: Left edge	(-4.72E-4, 0.0149)	(-0.0163, 0.0055)
No. 2: Left	(-0.0018, 0.0054)	(0.073, 0.026)
No. 3: Centre	(0.003, 0.0064)	(0.0672, -0.04)
No. 4: Right	(2.8E-5, 0.0338)	(0.006, -0.0437)
CELL 1-2 b)		
Object	**Hyp. Position error [m]**	**SAP-DOA position**
No. 1: Left edge	(-0.019, 0.00147)	(0.0219, 0.007)
No. 2: Left	(0.0951, 0.068)	(0.0142, -0.0081)
No. 3: Centre	(0.01, 0.059)	(0.0244, -0.0009)
No. 4: Right	(0.02, 0.038)	(0.0341, 0.0234)
CELL 1-2 c)		
Object	**Hyp. Position error [m]**	**SAP-DOA position**
No. 1: Left edge	(-0.0043, 0.0148)	(0.0213, -0.0014)
No. 2: Left	(-0.0032, 0.0051)	(0.0211, 0.0306)
No. 3: Centre	(0.0165, 0.0043)	(0.02, -0.0241)
No. 4: Right	(-0.0015, 0.0037)	(0.0444, 0.0424)
CELL 1-2 d)		
Object	**Hyp. Position error [m]**	**SAP-DOA position**
No. 1: Left edge	(-0.0127, 0.015)	(0.0088, 0.0147)
No. 2: Left	(0.0015, 0.01)	(0.0266, 0.0719)
No. 3: Centre	(0.003, 0.011)	(0.0253, 0.0299)
No. 4: Right	(-0.0126, 0.0045)	(0.028, 0.0293)

3. CONCLUSIONS

In this STSM, the accuracy of the SAP-DoA localization technique was investigated, versus the distance between the sought objects. Moreover, the technique was compared with the standard hyperbola approach, which is commonly employed for the interpretation of GPR data.
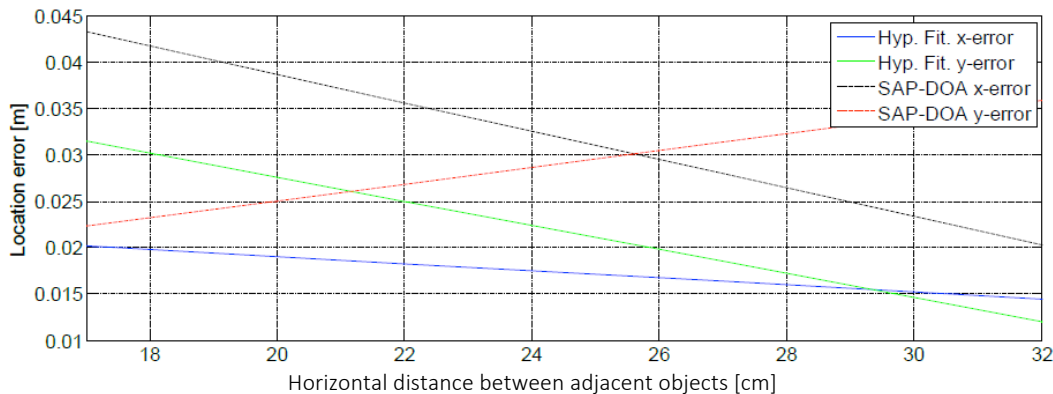
Fig. 2.11 – RMS estimation error versus object mutual distance for Cell 1.2 a-d (4 simulated cases).

We applied the SAP-DoA technique to the synthetic reference data of TU1208 Cells 1.1-1.3 and to new enlarged version of these cells. In these scenarios, several metallic and dielectric targets embedded in concrete are considered; such targets have different shapes and they are embedded at different depths in the hosting cells. Matlab functions and scripts have been developed, to extract the time-distance information from the B-scan and perform the hyperbolic interpolation.

As expected, the accuracy of the SAP-DoA techniques improves when the distance between the reinforcing elements embedded in the cell is increased and their electromagnetic interaction becomes weaker. Moreover, the accuracy of the hyperbolic interpolation method is higher when circular-section cylindrical objects are sought. Nevertheless, the situation is different for the localisation of objects with non-cylindrical shape. In this case, the hyperbola approach cannot be employed whereas the SAP-DOA method can still provide interesting results.

Regarding the detection and localization of objects with non-cylindrical shape, the SAP-DOA method proved a significant precision in estimating the object position, compared with the traditional hyperbolic fitting estimation method.

119

TABLE VI – CELL 1-3: COMPARING LOCATIONS ESTIMATED BY MEANS OF HYPERBOLIC FITTING AND THOSE ESTIMATED BY THE SAP-DOA APPROACH.

CELL 1-3 a)		
Object	**Hyp. Position error [m]**	**SAP-DOA position**
No. 1: Left edge	(-0.0938, 0.0236)	(0.0082, -0.0111)
No. 2: Left	(-0.0013, 0.0211)	(0.0205, 0.0034)
No. 3: Centre	(-0.0014, 0.0186)	(0.0266, 0.023)
CELL 1-3 b)		
Object	**Hyp. Position error [m]**	**SAP-DOA position**
No. 1: Left edge	(-0.0987, 0.0135)	(0.0191, -0.0055)
No. 2: Left	(0.0492, 0.0211)	(0.0187, 0.0874)
No. 3: Centre	(0.108, 0.0188)	(0.0269, -0.0099)
CELL 1-3 c)		
Object	**Hyp. Position error [m]**	**SAP-DOA position**
No. 1: Left edge	(-0.0069, 0.092)	(0.0161, 0.0015)
No. 2: Left	(2.9E-4, 0.021)	(0.0264, 0.0399)
No. 3: Centre	(-0.014, 0.0189)	(0.0205, -0.0019)
CELL 1-3 d)		
Object	**Hyp. Position error [m]**	**SAP-DOA position**
No. 1: Left edge	(-0.1571, 0.0251)	(0.0134, 0.0078)
No. 2: Left	(-0.011, 0.0169)	(0.0251, 0.0243)
No. 3: Centre	(0.074, 0.0145)	(0.0419, 0.0077)

3 FUTURE COLLABORATION WITH THE HOST INSTITUTION

Thanks to this STSM, a fruitful collaboration with the host institution could continue and be strengthened.

Our plans for future work include:

- Testing our SAP-DoA approach on experimental data. We wish to process some sections of the TU1208 dataset coming from measurements performed at the IFSTTAR Geophysical Test Site (Nantes, France).
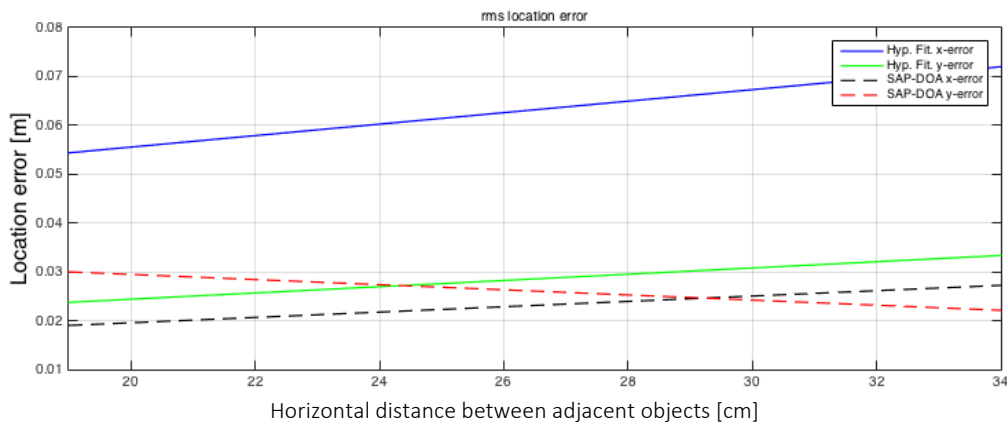
Fig. 2-12 – RMS estimation error versus object mutual distance for Cell 1.3 a-d (4 simulated cases).

- Compare the accuracy of our approach and of the hyperbola approach for the localisation of circular-section objects with size larger than the central wavelength emitted by the radar.
- Combine the SAP-DoA approach with Support-Vector-Machine (SVM) techniques, in cooperation with the University of Genoa. These techniques are expected to increase the robustness of our approach with respect to the distance between sought targets, as they are more powerful than standard DoA algorithms in coping with electromagnetic interactions between objects.

As already mentioned, a third and final STSM was carried out about one year after this report was written, during Year 4 of the Action. During that STSM, we were able to improve the approach and exploit in a more advanced way the multi-frequency information enclosed in the GPR data. Furthermore, we implemented a graphical-user interface for our codes and wrote a user manual. We intend to release our software tool for free public download.

Afterwards, we started comparing our approach with a different technique, based on neural networks and on an innovative algorithm for the analysis of hyperbolic patterns. Such technique was developed by a Serbian research team and the results of the comparison will be soon published on an invited paper, on the Journal of Environmental and Engineering Geophysics.

4 FORESEEN PUBLICATIONS/ARTICLES RESULTING FROM THE STSM

The results of this STSM were presented during the 2016 European Geosciences Union General Assembly [8].
As already mentioned in Section 3, the work continued during a STSM carried out in Year 4. Then, the results of our research efforts were published in two open access journal papers, please see Refs. [9, 10].

ACKNOWLEDGEMENT

REFERENCES

[1] S. Meschino, L. Pajewski, "Application of a SAP-DoA Method to GPR data, for the Localisation of Scatterers in Concrete", Short Term Scientific Missions – Year 2, COST Action TU1208, L. Pajewski, M. Marciniak, S. Lambot, Eds., Aracne Editrice, Rome, Italy, May 2015, ISBN 978-88-548-8488-5.
[2] S. Meschino, L. Pajewski, "Application of a SAP-DoA method to GPR data for the location of reinforcing elements in concrete", IEEE 15th Mediterranean Microwave Symposium (MMS), Nov. 2015.
[3] S. Meschino, L. Pajewski, and G. Schettini, " A SAP-DOA Method for the Localization of Two Buried Objects," International Journal of Antennas and Propagation, Special Issue on "Inverse Scattering and Microwave Tomography in Safety, Security, and Health", Int. Journal of Antennas and Propagation, A-ID 702176, 2013.

[4] L. Pajewski, A. Giannopoulos, "Electromagnetic modelling of Ground Penetrating Radar responses to complex targets", Short Term Scientific Missions and Training Schools – Year 1, COST Action TU1208, L. Pajewski & M. Marciniak, Eds., Aracne Editrice, Rome, Italy, May 2014, ISBN 978-88-548-7225-7, pp. 7-45.

[5] Giannopoulos, A. (2005). Modelling ground penetrating radar by GprMax, Construction and Building Materials, 19(10), 755-762.

[6] D. Pirrone, L. Pajewski, "E2GPR - Edit your geometry, execute GprMax2D and plot the results!," 2015 IEEE 15th Mediterranean Microwave Symposium (MMS), Lecce, 2015, pp. 1-4, doi: 10.1109/MMS.2015.7375414

[7] Bello. Y. Idi and Md. N. Kamarudin, "Utility Mapping with Ground Penetrating Radar: an Innovative Approach", Journal of American Science, Vol. 7(1). 2011.

[8] S. Meschino, L. Pajewski, and M. Marciniak, "Development of SAP-DoA techniques for GPR data processing within COST Action TU1208," Geophysical Research Abstracts, vol. 18, European Geosciences Union (EGU) General Assembly 2016, 17-22 April 2016, Vienna, Austria, article ID EGU2016-12565-1, 2 pp.

[9] S. Meschino and L. Pajewski, "SPOT-GPR: A Freeware Tool for Target Detection and Localization in GPR Data Developed within the COST Action TU1208," Journal of Telecommunications and Information Technology, Vol. 2017(3), pp. 43-54, September 2017.

[10] S. Meschino and L. Pajewski, "A practical guide on using SPOT-GPR, a freeware tool implementing a SAP-DoA technique," Ground Penetrating Radar, Vol.1(1), pp. 104-122, January 2018.

STSM 8

AN EDUCATIONAL PACKAGE TO TEACH GPR IN THE UNIVERSITY

Visiting Scientist: Vega Perez-Gracia, Universitat Politecnica de Catalunya, Barcelona, Spain (vega.perez@upc.edu)

Host Scientist: Lara Pajewski, Roma Tre University, Rome, Italy (lara.pajewski@gmail.com)

STSM Dates: 22 February - 26 February 2016

1. PURPOSE OF THE STSM

The main objective of the STSM was to bring forward the Education Pack initiative. This is structured in modules and its draft structure is as follows:

Module 1: GPR basic principles
- Introduction to GPR
- History of GPR
- Overview on GPR applications
- Electromagnetic properties of media

Module 2: GPR systems and antennas
- Introduction to radar systems
- GPR systems
- GPR antennas

Module 3: GPR applications.
- Civil engineering
  - Overview on civil-engineering applications of GPR
  - Roads
  - Bridges and tunnels
  - Railways
  - Buildings
  - Utilities
  - Water content

- Construction materials
- Archaeology and cultural heritage
- Humanitarian applications
  - Detection of unexploded landmines
  - Localisation of people trapped under debris and avalanches
  - Forensics
- Water management
- Geology and sedimentology
- Geotechnical applications
- Planetary exploration

Module 4: GPR data processing and interpretations
- Data processing
- Electromagnetic modelling

Module 5: GPR surveys
- Practical hints for effective GPR inspections
- GPR limits
- Recommendations for the safety of people and equipment during GPR prospecting
- Guidelines
- Integration of GPR and geomatic, remote sensing

Advanced topics:
- Notes on imaging and inversion techniques
- …

Glossary (translated in different languages)

For each submodule, slides for a 1h 30min lecture are being prepared, along with additional material to deepen the comprehension of the topics and multimedia material. A template for the slides was prepared and Members were asked to contribute to the various modules by preparing the lectures or else by making available their teaching material. A huge amount of material was collected. Our STSM objectives were: to examine and organise the teaching material made available by Action Members; to improve the lecture template; and to prepare the slides for some lectures.

Additionally, part of the STSM was devoted to implementing and executing a realistic electromagnetic model of a column, for which experimental data collected by the visiting scientist were available. This activity was not foreseen in the STSM workplan.

2. DESCRIPTION OF THE WORK CARRIED OUT DURING THE STSM

2.1 EDUCATION PACK

As mentioned in Section 1, we examined all the teaching material made available by Action Members and tried to organise it. Then, we improved the lecture template. For example, we improved the way in which References are presented and additional material is listed. We decided to include photos and short biographies of the Authors at the end of each lecture. Most of the time was devoted to preparing slides. Alessio Ventura (Roma Tre University) and Santo Prontera (Sapienza University) participated to the preparation of the slides. We focused on the following submodules (among parentheses, we indicated the current status of the submodule, after the STSM):

Module 1:
Introduction to GPR (to be improved)
Module 2:
GPR antennas (rather complete)
Module 3:
Overview on the civil-engineering applications of GPR (to be improved).
Bridges and Tunnels (rather complete).
Buildings (rather complete).
Module 4:
Electromagnetic modelling (rather complete).

The status of the Education Pack was subsequently presented during the Fifth General Meeting in Lisbon, Portugal (March 2-4, 2016).

2.2 ELECTROMAGNETIC MODELLING OF COLUMNS

As mentioned in Section 1, we devoted part of the STSM to simulate a masonry column of the "Hospital de Sant Pau" in Barcelona, Spain. For this column, experimental data previously collected by the visiting scientist were available.

The GPR assessment of some columns in the old buildings of the "Hospital de Sant Pau" was carried out by the visiting scientist, as a preliminary stage of a structural analysis of the buildings preceding their complete restoration. One column was removed from its original place and moved to the laboratory of the Universitat Politecnica de Catalunya, to carry out further experiments and investigations.

The column survey presented two main difficulties: the first one was to adapt the B-scans to the shape of the columns – see Figure 1; the second one was related to the large number of irregular scatterers inside the columns, because the columns were built by using irregular pieces of bricks, arranged in a sort of "star" configuration.

The experimental radargrams obtained for these columns are not easy to be interpreted, due to their complicated structure. Inside the columns there is a metallic tube and, in some parts of the radar images, the tube seems to disappear. The diameter of the columns is 64 cm. The metallic tube inside the columns (a drainage pipe) has a 8-cm diameter.

Externally, the column is composed by 12 cm × 6 cm rectangular glazed fired clay breaks. Inside the column, the irregularly-distributed bricks were bounded with portland cement.

Radar data were acquired along the column and also along perimetral radar lines schemes - see Figure 2. The distance between the perimetral lines was 3 cm, and the distance between the lines along the column was 5 cm.

A commercial Ramac radar (Mala Geoscience) was used in the test, with a 1.6-GHz centre frequency antenna. The position of the antenna on the column was determined with a survey-wheel odometer.

a)

b)
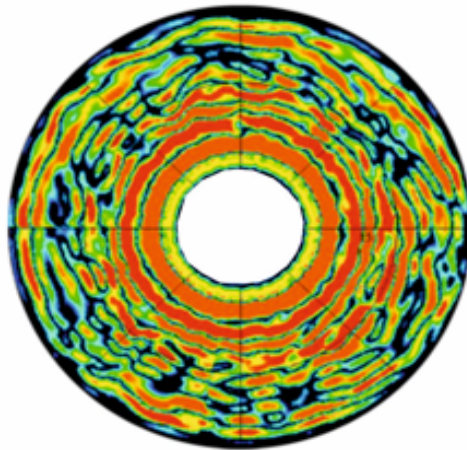
c)

Fig. 1 – (a) Section of a surveyed column. (b) Photo of a surveyed column.
(c) A radargram obtained on a perimetric radar line
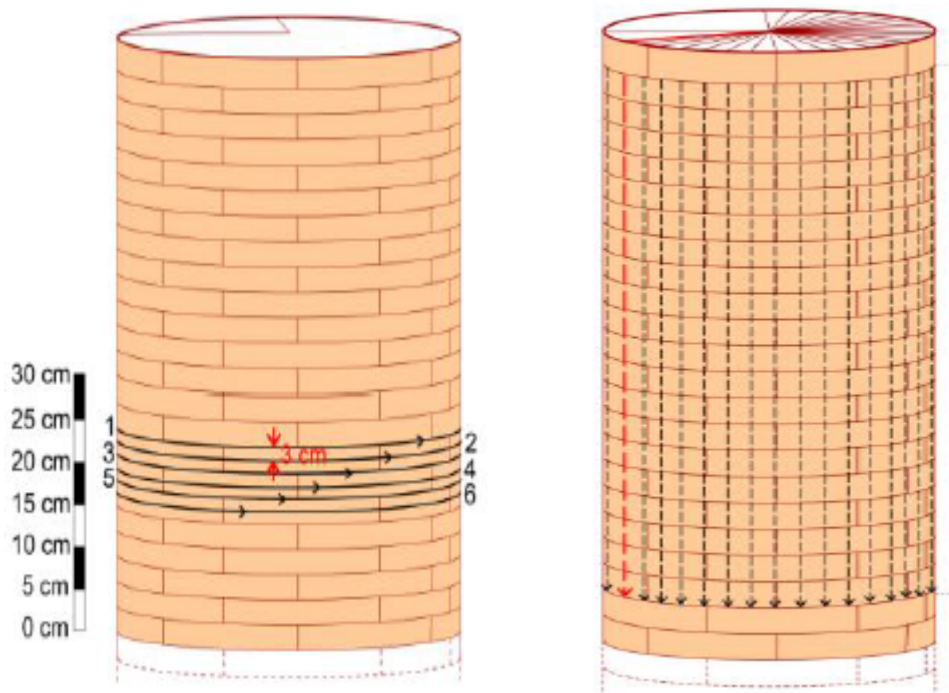
Fig. 2 – Radar lines. The distance between horizontal lines (perimetral) was 3 cm. The distance between vertical lines (along the column) was 5 cm.

During the radar acquisition, the sampling frequency was 86,200 MHz, obtaining 672 samples per trace. The spatial sampling was 0.002 m, and the temporal window was 8 ns.

Some preliminary tests in the columns of the building indicated that the average wave velocity was about 10 cm/ns. These tests were carried out with direct measurements, knowing the diameter of the column and obtaining the reflection on a metallic target placed on the opposite side of the antenna.

Later and more accurate measurements, using a specimen under laboratory conditions (this specimen was one of the columns that was moved to the laboratory), indicate that the average velocity could be higher, close to 13 cm/ns.

Two examples of the radar images obtained in both type of radar lines are shown in Figure 3. In these data, under the first arrival, heterogeneous anomalies highlight the irregular structure of the column.

During the STSM, a series of electromagnetic models were implemented and executed, for the column moved to the laboratory. The TU1208 free tools gprMax and E^{2}GPR were used [1, 2]. The purpose of the simulations was to support and ease the interpretation of the experimental radargrams.

The first model was a realistic one, where we tried to reproduce the section of the column in the best possible way, by using available photos of the column. The geometry of a horizontal section of the column and the synthetic B-Scan are reported in Figure 4.

The subsequent models were simplified and more regular from the geometrical point of view, they helped us to understand the scattering phenomena occurring inside the column. An example of such simplified models is presented in Figure 5.

In all our models, we assumed for concrete and bricks a relative permittivity equal to 7 and 11, respectively. The relative permeability was equal to 1. The conductivity of materials was neglected at this stage. Improved simulations will adopt a Debye model of the media, in order to take into account their conductivity and frequency-dispersive properties. The spatial discretisation step of the model was 1 mm; consequently, the time discretisation was calculated by using the Courant condition. We employed Perfectly Matched Layers with 20 layers in our models. The pulse emitted by the GPR had a Ricker time shape and its spectrum was centred on 1600 MHz. The source was a line of current and the model of the receiver was neglected.

The simulations of the column were performed with the help of Daniele Pirrone (Roma Tre University, TU1208 WG Member).

a)

b)

c)
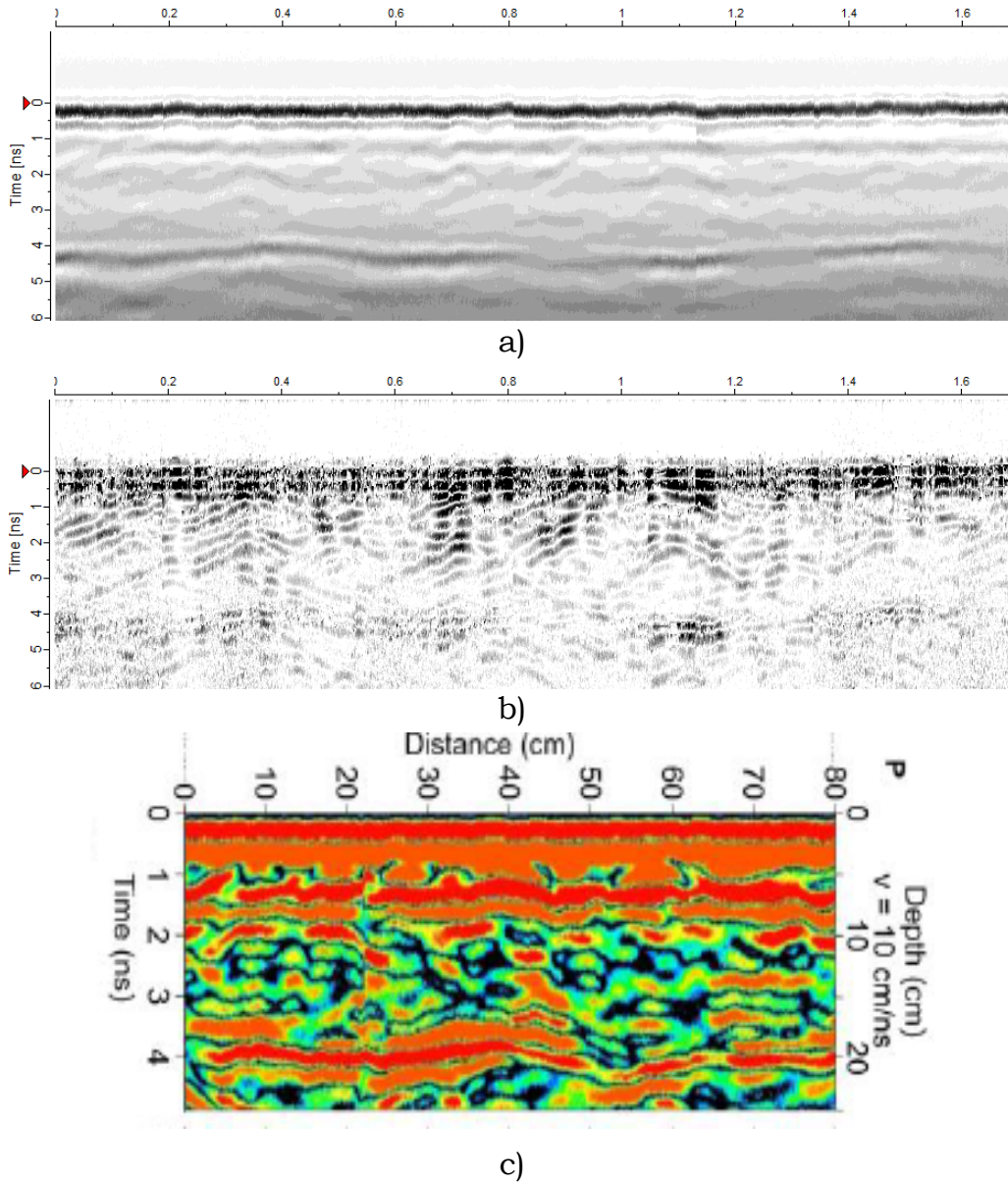
Fig. 3 – a) Radar data from a perimetric profile. b) Radar data from the perimetric profile after the processing with a background removal and a gain function. b) Radar data from a longitudinal profile

.

Finally, part of the STSM was spent to finalise the class scheduling and organisation of the Training School on Non-Destructive Techniques (NDT) for civil engineering, held in Barcelona two weeks after the STSM.

4. FUTURE COLLABORATION WITH THE HOST INSTITUTION

Future collaboration will be focused on:
1) Working on the Education Pack.
2) Completing the work related to the simulation of columns.

5. FORESEEN PUBLICATIONS/ARTICLES RESULTING FROM THE STSM

The Education Pack will be published on the website of the Action. This material will be available in open access for all users and we believe it will help to promote training of GPR throughout Europe and beyond.

When the comparison between experimental results collected on columns and synthetic results calculated with gprMax and E^{2}GPR will be completed, a paper will be prepared and submitted to a scientific peer-reviewed journal.

ACKNOWLEDGEMENT

REFERENCES

[1] Giannopoulos, A. (2005). Modelling ground penetrating radar by GprMax, Constr. Building Materials, 19(10), 755-762.
[2] D. Pirrone, L. Pajewski, "E2GPR - Edit your geometry, execute GprMax2D and plot the results!," 2015 IEEE 15th Mediterranean Microwave Symposium (MMS), Lecce, 2015, pp. 1-4, doi: 10.1109/MMS.2015.7375414.

a)

b)
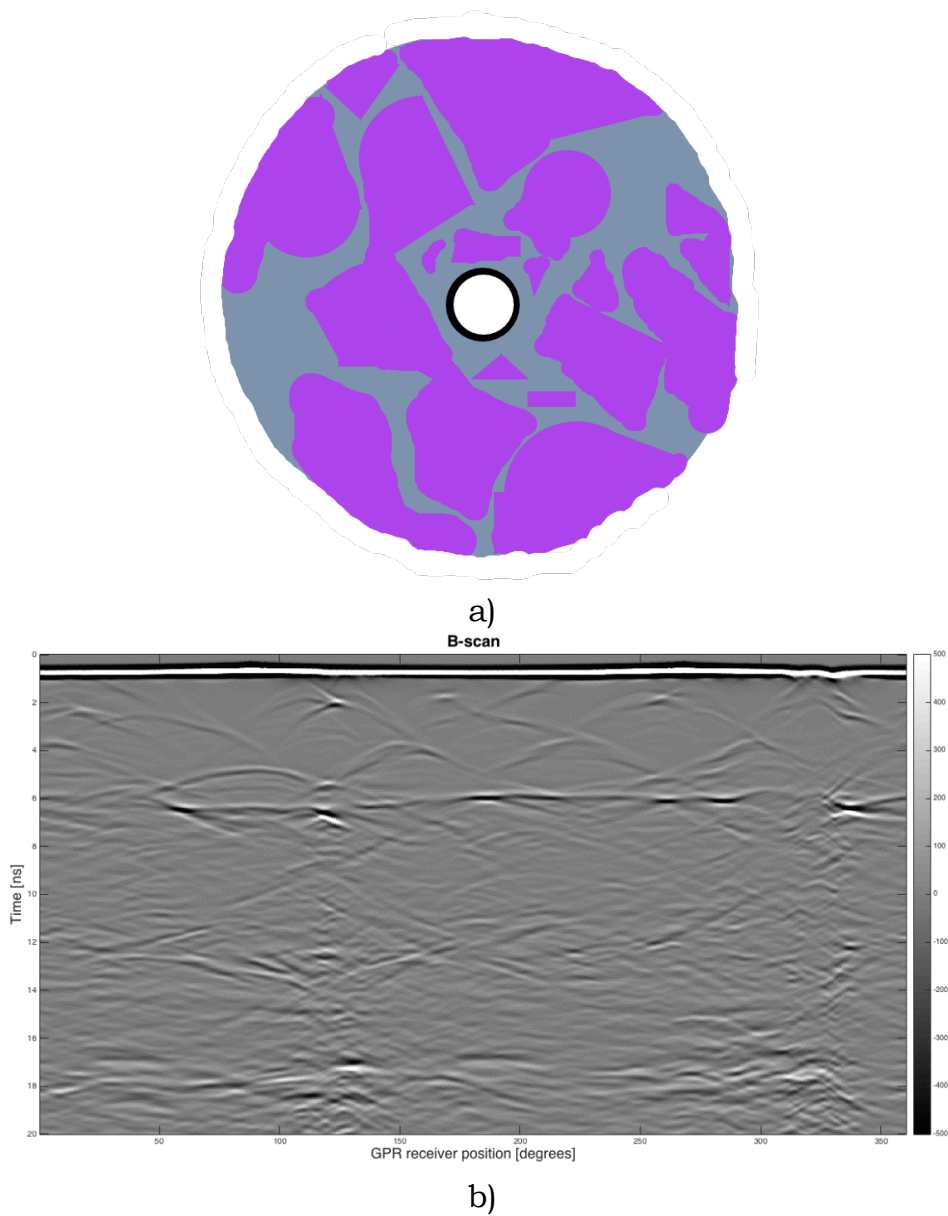
Fig. 4 – (a) A section of the modelled column – realistic model. (b) Synthetic radargram.
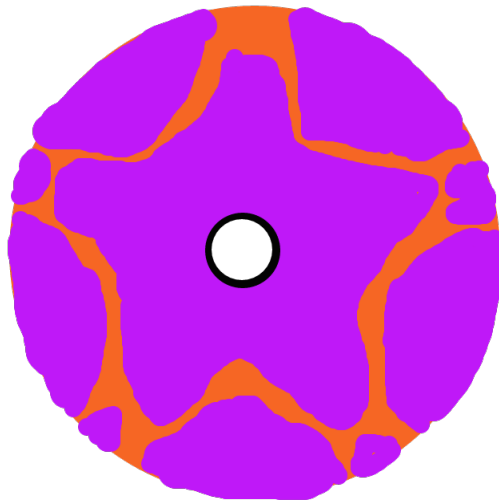
a)
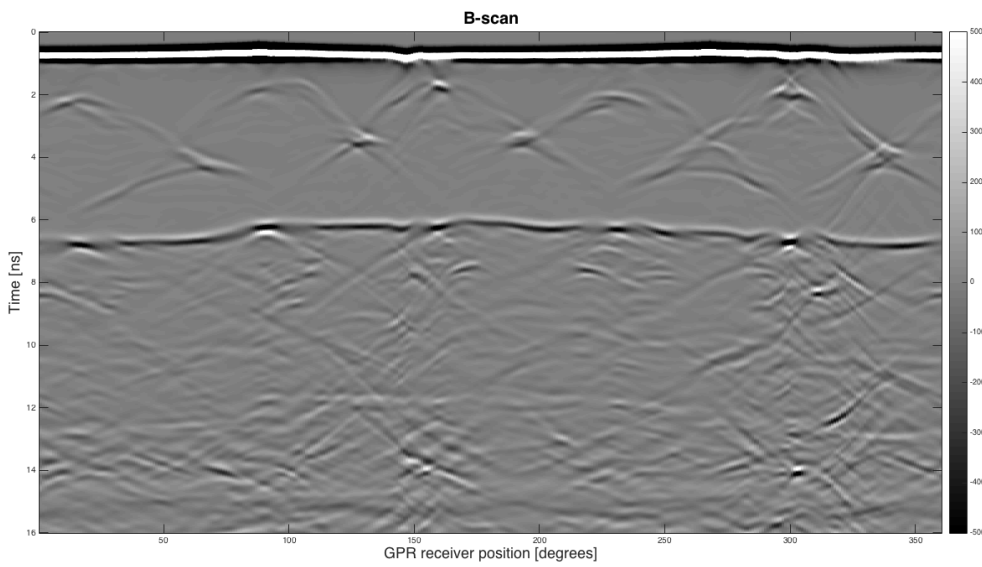
b)

Fig. 5 – (a) A section of the modelled column – simplified model. (b) Synthetic radargram.

STSM 9

GPR IN CIVIL ENGINEERING: DISSEMINATING INFORMATION TO STAKEHOLDERS AND END USERS

Visiting Scientist: Patrizio Simeoni, Transport Infrastructure Ireland, Dublin, Ireland (xdebianx@gmail.com)

Host Scientist: Lara Pajewski, Roma Tre University, Rome, Italy (lara.pajewski@gmail.com)

STSM Dates: 31 March – 4 April 2016

1. PURPOSE OF THE STSM

The COST Action TU1208 aims to promote, throughout Europe, a wider and more effective use of the GPR technique in the monitoring of both infrastructures and structures, as it is stated in the Memorandum of Understanding. In order to achieve such objective, the Action is carrying out dissemination activities at different levels and is developing guidelines for a correct use of GPR in various civil-engineering tasks. The dissemination activities include a series of initiatives devoted to explaining GPR basic principles and civil-engineering applications to stakeholders and end-users. Strategies for a stronger stakeholders and end-users' involvement in the COST Action were extensively discussed during the Third General Meeting in London [1].

During the Fifth General Meeting in Lisbon, a working team started mapping GPR European stakeholders/end-users profiles. In parallel, dissemination seminars started taking place in different Countries, in particular the first successful seminar was held in Lisbon in occasion of the Fifth General Meeting and it was attended by more than 100 representatives from private companies and local authorities, further seminars are planned in Italy, Czech Republic, Croatia, Greece, Romania and Poland.

In the described framework, this STSM aimed at achieving two objectives: the first one was to organize and improve all the relevant material collected during the Fifth General Meeting of COST Action TU1208 in Lisbon, according to the Stakeholders engagement steps described and agreed in [1]; the second objective was a strategy for the development of multimedia material concerning Ground Penetrating Radar (GPR) conceived to disseminate both GPR basic principles and civil-engineering applications of this technique.

2. DESCRIPTION OF THE WORK CARRIED OUT DURING THE STSM

The work performed during this STSM was mainly carried out by Mr Patrizio Simeoni and Dr Lara Pajewski. It also benefitted from the contribution of Mr Santo Prontera (TU1208 WG Member, Sapienza University, Italy).

The work started with a review and finalisation of the Stakeholders profile table, created in Portugal during the Fifth General Meeting, as well as of a report containing such table and resuming the results of the Lisbon seminar [2].

The original table was constituted of a list of Stakeholders profiles relevant for GPR and grouped by "application field". In occasion of the STSM, it was recognised the importance of adding two columns, the first one indicating the Working Group relevant for every specific application field and a second one containing the available TU1208 resources for such field that could be provided to both Stakeholders and end-users. In the latter column, the following questions were answered:

- Are guidelines being prepared, under preparation or out of scope for this application?
- Is the state of art completed, in progress or out of scope for this application?
- Are there TU1208 Case Studies available?
- Will flyers be prepared?
- Is this application relevant for TU1208?

The table, when completed, was merged back into the original report, to avoid a dispersion of information. After completing this task, a first instance of the table, containing Stakeholders profiles in Italy, was prepared with the double objective of starting an actual Stakeholder mapping and to provide an example to Members in other Countries showing how the table should be filled in. The table prepared, which is available as "Annex A" to this report, is going to be sent to all TU1208 MC members, along with the draft of the report [2]. The table will be filled by MC members collecting information about all Stakeholders in their Countries, this will permit TU1208 to feed Stakeholders/final users with useful information about GPR applications or seminars.

During the STSM it was also observed that the material available on the TU1208 website, even when relevant, is not in a form which is useful to Stakeholders and final users who are mainly interested in Case Studies. It was therefore decided to re-organise the relevant information and add to the website a new page including a list of TU1208 Case Studies. For each case study, the items listed below will be provided:

1. Case Study site.
2. Complete reference details of the paper or report where the Case Study is presented and described.
3. Contact of a member of the TU1208 COST Action who contributed to the paper and is available to provide further information and/or answer to questions/doubts about the Case Study proposed.
4. Additional information/comments. The table is going to be published on the above-mentioned new page of the TU1208 website and it will evolve in time. The table is identified by a version so that Stakeholders and end-users may be able to verify newer/different releases present on the website. The so called "Case Studies" table, in its actual version, is attached as "Annex B" to this report. This draft version won't be released on the website; the table will be published only after having formally reviewed its contents, and after having added

at least few more Case Studies. Moreover, the fourth column (links and comments) present in the draft version, that was included with the only objective of helping the review process, will be removed or strongly modified before publishing.

Finally, a flyer template was developed. The idea is to realise a series of flyers presenting the most important civil-engineering applications of GPR, plus a flyer on COST Action TU1208 and on GPR basic principles.

Few software tools (e.g. Microsoft Publisher) were initially considered but finally it was decided to design the flyer by employing Microsoft PowerPoint because this instrument is commonly used by most of the researchers and engineers involved in TU1208.

It was decided that the flyer page format will be an A4 and that each flyer will include 4 pages, therefore the flyer itself was developed as an A3 page. The flyer-template content was chosen according to common strategies applied in flyers designed by commercial Companies and in particular:

1. Front page, for which the content is Application dependent, is constituted by:

    a. Top Banner containing COST Logo (header).
    b. Title of the Application.
    c. Subtitle.
    d. Picture.
    e. Short description.
    f. Footer containing TU1208 website link.

2. Back page, for which the content is generic and applicable to all flyers, is constituted by:

    a. Top Banner (header).
    b. Description of COST and its primary objectives.
    c. Description of TU1208 and its primary objectives.
    d. Relevant Contacts.

e. Footer containing COST website link.

3. Internal pages, having application dependent content, in this case the only fixed/non modifiable part is the top banner (or header).

The proposed flyer template, filled with some random data to help visualising the final product, is attached as "Annex C" to this report.

The actual flyers will be created from the template described above with the cooperation of other experts involved in TU1208. The table in [2] describes all Case Studies scenarios (or application fields) for which flyers are planned or relevant. The flyers will be hosted in the TU1208 website in pdf or jpg format and will be sent via email.

Flyers will also be printed for hand-made distribution, therefore a folder was designed to contain them, the prototype of the folder is attached as "Annex D" to this report.

3. DESCRIPTION OF THE MAIN RESULTS OBTAINED DURING THE STSM

The main objective of this STSM was to setup a cooperation in order to produce material that will be used to improve stakeholders and final users' awareness on the TU1208 activities. The objective was achieved by designing and realising tables and strategies as described in the Section 2. Five working-days, planned for this STSM, were obviously not sufficient to complete all the activities started, but they were enough to setup the activities and tune the different ideas to make it possible for the researchers involved in this task to continue working in their respective labs. Such coordination could not be achieved without carrying out this STSM.

4. FUTURE COLLABORATION WITH THE HOST INSTITUTION

A future and continuous collaboration with the host institution is a mandatory requirement for the success of the heavy task started during the STSM, this will be achieved through regular planning and review of the status of the Stakeholder engagement activities

listed in this report. Coordination with the host institution will be required when future dissemination activities will be planned. Mr Patrizio Simeoni and the host institution will moreover cooperate to support, coordinate and review actual flyers that will be designed with the help of other TU1208 members.

5. FORESEEN PUBLICATIONS/ARTICLES RESULTING FROM THE STSM

A tangible result of this STSM will be the publication of the Case Study table on the TU1208 website. A final paper describing the Strategy adopted for dissemination by TU1208 and all results achieved will be written when the Stakeholder Engagement and Dissemination Activity will be completed. This final article will hopefully help other COST Actions to try and start an analogous process. The paper will describe the overall activity started in London in occasion of the Third General Meeting and in which this STSM was a major milestone, it will contain results achieved and issues encountered during the development of this task.

ACKNOWLEDGEMENT

REFERENCES

[1] F.Frezza, L. Pajewski, P.Simeoni, "Strategies for Stakeholders involvement in the GPR COST Action," Proceedings of the Third COST Action TU1208 General Meeting, London, UK, March 2015.
[2] P. Simeoni, S. Fontul, L. Pajewski, K. Dimitriadis, S. Stan "Stakeholders Engagement Status – Draft," Fifth COST Action TU1208 General Meeting, Lisbon, Mar, 2016.

ANNEX A

LIST OF STAKEHOLDERS FOR UTALY

The following table has to be filled with the Stakeholders relevant in ITALY. A full description of the activity is illustrated in [1] and [2].

Application Field	Stakeholders	Comments and available TU1208 resources	WG	Actual Stakeholders	
				Institution	Contact
Archeology and cultural heritage	- Museum authorities - Authorities for archeology and cultural-heritage management	GPR is useful for both preservation and restoration. TU1208 guidelines are being prepared. TU1208 state of the art is being completed. TU1208 case studies are available. TU1208 flyer is planned.	WG4	Ministero dei Beni e delle Attività Culturali e del Turismo	tel. 066723.5338 .5339 .5340 .5283 http://www.beniculturali.it/mibac/opencms/MiBAC/sito-MiBAC/MenuServizio/Contatti/index.html
				Area Didattica di Beni Culturali Dipartimento di Studi Umanistici - Università degli Studi Roma Tre	Tel.: +39.06.5733.8628; Fax: +39.06.5733.8587 didattica.beniculturali@uniroma3.it http://umanistici.lms.uniroma3.it/rm3ben/
				Istituto Superiore per la Conservazione ed il Restauro (ISCR)	Tel. 06 67236300 Fax 06 67236409 is-cr.segreteria@beniculturali.it http://www.icr.beniculturali.it/pagina.cfm?usz=1&uid=5
				Comando Carabinieri Tutela Patrimonio Culturale	Roma, Piazza Sant'Ignazio, 152 Tel. +39.06.6920301 fax +39.06.69203069 Sito web: www.carabinieri.it E-mail: tpc@carabinieri.it http://www.beniculturali.it/mibac/export/MiBAC/sito-MiBAC/MenuServizio/TutelaCulturale/index.html
					GRS LAB grs-lab@itabc.cnr.it

Application area	Stakeholders	Status	WG	Institution	Contact
				CNR Consiglio Nazionale delle Ricerche	http://www.itabc.cnr.it/pagine/grs-lab SURVEY LAB info@itabc.cnr.it http://www.itabc.cnr.it/pagine/survey-lab ARCHMAT LAB info@itabc.cnr.it http://www.itabc.cnr.it/pagine/archmat-lab ARCHEO LAB info@itabc.cnr.it http://www.itabc.cnr.it/pagine/archeo-lab
				C.S.R. Restauro Beni Culturali (COMPANY)	Laboratorio Via U. Biancamano 35 00185 ROMA (RM) tel./fax 06 77207745 http://www.csrrestauro.it/home/
				Institution	**Contact**
Buildings	- Local authorities - Private restoration companies - Public restoration companies - Constructors - Construction materials providers	TU1208 guidelines are being prepared. TU1208 state of the art is available. TU1208 case studies are available.	WG2	ASTALDI	Astaldi S.p.A. Via Giulio Vincenzo Bona, 65 - 00156 Roma (Italia) tel: +39 06 417661 fax: +39 06 41766652 investor.relations@astaldi.com e-mail: businessdevelopment@astaldi.com http://www.astaldi.it/il_gruppo/contatti3/
				GRANDI LAVORI FINCOSIT SPA	Grandi Lavori Fincosit S.p.A. Piazza Fernando De Lucia, 60/65 00139 Roma Tel. +39 06 881 711 Telefax +39 06 881 3051 Email glf@glf.it http://www.glf.it/ita/index.php?option=com_content&view=article&id=91&Itemid=1
				Institution	**Contact**
Transport infrastructure (roads, bridges,	- Road authorities	TU1208 guidelines are being prepared.	WG2	FER – Ferrovie Emilia Romagna	Via Zandonai, 4 44124, Ferrara Email: info@fer.it http://www.fer.it/?page_id=11

			Institution	Contact
tunnels, railways)	- Road maintainers	TU1208 state of the art is available.	Trentino trasporti s.p.a.	Via Innsbruck 65 - 38121 Trento - Tel. 0461 031000 - Fax 0461 031207 patrimonio@ttspa.it - PEC: patrimonio@pec.ttspa.it http://www.ttspa.it/Contatti
	- Railway authorities - Bridge/tunnel authorities	TU1208 case studies are available.	Società per l'Ammodernamento e la Gestione delle Ferrovie e Tramvie Vicentine S.p.A.	Viale Milano, 138 - 36100 Vicenza ftv@ftv.vi.it – PEC: ftv@legalmail.it http://www.ftv.vi.it/it/contatti/contatti
		TU1208 flyers are planned.	Ferrovie dello Stato Italiane s.p.a.	Piazza della Croce Rossa, 1,00161 Roma, Italia http://www.fsitaliane.it/
	- Transport authorities		Rete Ferroviaria Italiana	http://www.rfi.it/
	- Construction materials providers		ITALFERR s.p.a	via V. G. Galati, 71 - 00155 Roma italferr@italferr.it http://www.italferr.it/italferr.html
			GRANDISTAZIONI	Via G. Giolitti, 34 - 00185 Roma Telefono: +39 06 478 411 Fax: +39 06 48 23 915 Piazza Luigi di Savoia, 1/23 - 21124 Milano Telefono: +39 02 66 73 511 Fax: +39 02 66 73 52 50 http://www.grandistazioni.it/grandistazioni.html info@grandistazioni.it
Airport runways (WG2)	- Airport authorities		Pavimental s.p.a.	Pavimental S.p.A. Via Giuseppe Donati, 174 00159 Roma, Italia Email: mail@pavimental.it http://www.pavimental.it/index.php
	- Runway maintainers	TU1208 case studies are available.	Vitali infrastrutture	Vitali S.p.A. via Lombardia, 2/a 20068 - Peschiera Borromeo (MI) info@vitalispa.it http://infrastrutture.vitalispa.it/contatti
	- Construction materials providers		TeMa Technologies and Materials s.r.l.	TeMa Via dell'Industria, 21	31029 Vittorio Veneto (TV) info@temacorporation.com http://www.temacorporation.com/it
			InCONCRETO	http://www.inconcreto.net/index.php http://www.inconcreto.net/Articolo/780/Pavimentazione_aeroportuale_in_calcestruzzo.html

Application	Stakeholders	TU1208 status	Institution	Contact
tunnels, railways)	- Road maintainers	TU1208 state of the art is available.	Trentino trasporti s.p.a.	Via Innsbruck 65 - 38121 Trento - Tel. 0461 031000 - Fax 0461 031207 patrimonio@ttspa.it - PEC: patrimonio@pec.ttspa.it http://www.ttspa.it/Contatti
	- Railway authorities	TU1208 case studies are available.	Società per l'Ammodernamento e la Gestione delle Ferrovie e Tramvie Vicentine S.p.A.	Viale Milano, 138 - 36100 Vicenza ftv@ftv.vi.it – PEC: ftv@legalmail.it http://www.ftv.vi.it/it/contatti/contatti
	- Bridge/tunnel authorities		Ferrovie dello Stato Italiane s.p.a.	Piazza della Croce Rossa, 1,00161 Roma, Italia http://www.fsitaliane.it/
	- Transport authorities	TU1208 flyers are planned.	Rete Ferroviaria Italiana	http://www.rfi.it/
	- Construction materials providers		ITALFERR s.p.a	via V. G. Galati, 71 - 00155 Roma italferr@italferr.it http://www.italferr.it/italferr.html
			GRANDISTAZIONI	Via G. Giolitti, 34 - 00185 Roma Telefono: +39 06 478 411 Fax: +39 06 48 23 915 Piazza Luigi di Savoia, 1/23 - 21124 Milano Telefono: +39 02 66 73 511 Fax: +39 02 66 73 52 50 http://www.grandistazioni.it/grandistazioni.html info@grandistazioni.it
			Institution	**Contact**
Airport runways	- Airport authorities	TU1208 case studies are available.	Pavimental s.p.a.	Pavimental S.p.A. Via Giuseppe Donati, 174 00159 Roma, Italia Email: mail@pavimental.it http://www.pavimental.it/index.php
	- Runway maintainers		Vitali infrastrutture	Vitali S.p.A. via Lombardia, 2/a 20068 - Peschiera Borromeo (MI) info@vitalispa.it http://infrastrutture.vitalispa.it/contatti
	- Construction materials providers		TeMa Technologies and Materials s.r.l.	TeMa Via dell'Industria, 21	31029 Vittorio Veneto (TV) info@temacorporation.com http://www.temacorporation.com/it
			InCONCRETO	http://www.inconcreto.net/index.php http://www.inconcreto.net/Articolo/780/Pavimentazione_aeroportuale_in_calcestruzzo.html

WG2

Category	Description	Note	WG	Institution	Contact
				Pavimenti-Web	IMREADY Srl Strada Cardio 4 47891 Galazzano – RSM info@imready.it http://www.pavimenti-web.it/Pavimenti.php
				CONCRETE SOLUTION ITALIA	Via dell' Alpino, 7 46037 Bagnolo San Vito (MN) info@concretesolutionitalia.com http://www.concretesolutionitalia.it/
				B. NORD PAVI 2000	Via dell'Artigiano, 11, I-32026 Mel (BL) http://www.bnordpavi.it/?aeroportuali info@bnordpavi.it
				BMB SYSTEM s.r.l	Via Don Milani 15 a/b 26862 Guardamiglio (LO) staff@bmbsystem.it http://www.bmbsystem.it/
				Institution	**Contact**
Dams	Dam maintainers	Not covered by TU1208.	WG2	Studio Pietrangeli	Studio Ing. G. Pietrangeli S.R.L.	Via Cicerone 28 Rome tel. +39 06 3210880, fax +39 06 3227276, e-mail: info@pietrangeli.it http://www.pietrangeli.it/dighe/progettazione-dighe.htm
				ITINERA s.p.a.	ITINERA S.P.A. Via Balustra, 15 - 15057 Tortona (AL) Tel. +39 0131.8691 - Fax +39 0131.869279 - Email itineraspa@itinera-spa.it - PEC itineraspa@legalmail.it http://www.itinera-spa.it/
				TREVI s.p.a.	Trevi S.p.A. Via Dismano, 5819 47522 Cesena - Italy trevi@trevispa.com segreteriaitalia@trevispa.com http://www.trevispa.com/viewdoc.asp?co_id=87
				VIANINI LAVORI	Sede Legale Via Montello 10 – 00195 Roma Tel. +39 06 374921 Fax +39 06 3728546 http://www.vianinigroup.it/page.php?cat=13
				Institution	**Contact**
Utilities	Local authorities and service providers for communications gas, electricity,	TU1208 guidelines are being prepared. TU1208 state of the art is available.	WG2	Gas Natural Distribuzione Italia S.p.A.	Via Sardegna - Z.I. Acquaviva delle Fonti (BA) accessoretegndi@legal.gasnaturaldistribuzioneitalia.com http://www.gasnaturaldistribuzione.com/it/1285085161867/inizio.html
				Depur Padana Acque s.r.l.	Viale Maestri del Lavoro, 45100 z.i. Borsea – Rovigo info@depurpadana.it

			Institution	Contact
	water supply and sewage,	TU1208 case studies are available. TU1208 flyer is planned.	ENI s.p.a	http://www.depurpadana.com/index.cfm?lingua=IT ENI Piazzale Enrico Mattei , 00144, Roma info@enicorporateuniversity.eni.it http://www.eni.com/it_IT/prodotti-servizi/energia-elettrica/energia-elettrica.shtml
Environment (trees in urban and forested areas, water resources, agriculture, geological structures, glaciers, pollution)	- National authorities	TU1208 state of the art is available for soil characterisation, management of water resources.	Azienda forestale speciale consorziale Trento - Sopramonte	Via Belenzani, 19 - 38122 Trento PEC progstat.comune.tn@cert.legalmail.it http://www.comune.trento.it/Aree-tematiche/Aziende-e-societa-partecipate/Aziende-speciali/Patrimonio-forestale/Azienda-forestale-speciale-consorziale-Trento-Sopramonte
			Ministero delle Politiche agricole alimentari e forestali	Via XX Settembre, 20 - 00187 Roma urp@politicheagricole.it https://www.politicheagricole.it/flex/cm/pages/ServeBLOB.php/L/IT/IDPagina/8
	- Natural resources management	TU1208 state of the art is being prepared for trees.	Ministero dell'Ambiente e della Tutela del Territorio e del Mare	Via Cristoforo Colombo, n. 44 00147 - Roma (Italia) URP@minambiente.it http://www.minambiente.it/
		TU1208 case studies are available.	Ministero dello Sviluppo Economico	Via Molise 2 00187 Roma urp.comunicazioni@mise.gov.it http://www.sviluppoeconomico.gov.it/index.php/it/contatti
			ARPAT	Agenzia regionale per la protezione ambientale della Toscana http://www.arpat.toscana.it/ urp@arpat.toscana.it

			Institution	Contact
Oil Industry	Main oil companies	Not covered by TU1208. GPR may be useful for oil transport networks rather than for oil extraction sites.	Not applicable	

				Institution	Contact
Aerospace (planetary exploration, inspection of rockets and space stations)	- European Space Agency - National airspace institutions	TU1208 case studies are available for the inspection of rockets and space stations.	WG4	ASI Agenzia Spaziale Italiana	Via del Politecnico snc 00133 Roma, Italia Tel: +39 06 8567.1 http://www.asi.it/it PEC: asi@asi.postacert.it urp@asi.it
				Electronics Aerospace s.r.l.	Via appia antica, 177 81100 Caserta Info@electronics-aerospace.com http://www.electronics-aerospace.com/home.html
				Finmeccanica S.p.a.	Piazza Monte Grappa n. 4 - 00195 Roma info@finmeccanica.com http://www.finmeccanica.com/
				ELETTRONICA s.p.a.	Via Tiburtina Valeria Km 13,700, 00131 Rome info@elt.it, comunicazione@elt.it http://www.elt-roma.com/index.php/it/
				SIRIO Microelettronica S.r.l.	Via Giacomo Peroni, 400/402, 00131 Tecnopolo Tiburtino (Roma info@siriomicroelettronica.it http://www.siriomicroelettronica.it/index.htm
				Institution	**Contact**
Forensic	- Technical offices of police departments - Courts	Not covered by TU1208.	WG4	Indagini scientifiche Carabinieri RIS	Ufficio Relazioni con il Pubblico Piazza Bligny, 2 - 00197 Roma carabinieri@carabinieri.it
				Institution	**Contact**
Humanitarian assistance (avalanches and earthquakes rescue, landmines detection)	- Civil Protection - Fire Fighters	These are applications still under study therefore guidelines cannot be prepared. TU1208 state of the art is available.	WG4	Protezione Civile	Dipartimento della Protezione Civile Via Ulpiano 11 - 00193 Roma Centralino 06 68201 http://www.protezionecivile.gov.it/jcms/it/homepage.wp
				Vigili del Fuoco	Piazza del Viminale, 1 - 00100 Roma http://www.vigilfuoco.it/aspx/Home.aspx

			WG	Institution	Contact
Development of GPR equipment	- All application Stakeholders may be equipment Stakeholders. - Data-processing engineers	TU1208 case studies are available. TU1208 state of the art is available for GPR systems and antennas. TU1208 design of a cheap pulsed bistatic GPR system, mainly conceived for basic training and applications, will be available. TU1208-gprMax electromagnetic models of GPR antennas are available.	WG1	IDS Ingegneria Dei Sistemi S.p.A.	Via Enrica Calabresi, 24 56121 Pisa, ITALY Phone: + 39 050 3124 1 Fax: + 39 050 3124 201 ids@idscorporation.com https://www.idscorporation.com/
Development of algorithms	- All application Stakeholders may be alogorithm Stakeholders.	TU1208 state of the art is available for electromagnetic modelling, imaging, inversion and data-processing	WG3	IDS Ingegneria Dei Sistemi S.p.A.	Via Enrica Calabresi, 24 56121 Pisa, ITALY Phone: + 39 050 3124 1 Fax: + 39 050 3124 201 ids@idscorporation.com https://www.idscorporation.com/

			Institution	Contact
	- GPR manufacturers - System engineers	techniques for GPR. TU1208-gprMax tools for electromagnetic modelling are available. TU1208 database of experimental and synthetic data is being prepared		
Education	Universities	TU1208 Education Pack.	All	Covered by education pack

[1] F.Frezza, P.Simeoni, L. Pajewski, "Strategies for Stakeholders involvement in the GPR COST Action," Third COST Action TU1208 General Meeting, Athens, Sep. 2015.

[2] P. Simeoni, S. Fontul, L. Pajewski, K. Dimitriadis S. Stan, "Stakeholders Engagement Status".

CASE STUDIES OF THE COST ACTION TU1208.

Collection of Case Studies of the COST Action TU1208 grouped by application.

In this document, some case studies related to the use of GPR in different fields are presented. This collection aims to be an aid to stakeholders and final users in the understanding of GPR applications. The document is subjected to continuous evolution and eventually more case studies will be added in the future. Changes to the document will be tracked in the relevant revision table. Contact details are made available for every case study, of people who can be contacted for more information related a specific case study.

The document will be available on the website of the Action. Also, a more effective and captivating description of the most significant case studies will be realised on such website, but this will probably done after the Action end, as currently it goes beyond Members' possibilities and the priority is on other tasks.

CASE STUDIES of the COST Action TU1208.

1. AGRICOLTURE

SITE	ARTICLE	CONTACT	LINKS AND COMMENTS
Two test areas in different agricultural fields in Flanders, Belgium.	E. Van De Vijver, J. De Pue, W. Cornelis, M. Van Meirvenne, "Comparison of air-launched and ground-coupled configurations of SFCW GPR in time, frequency and wavelet domain," Geophysical Research Abstracts, European Geosciences Union (EGU) General Assembly 2015, 12-17 April 2015, Vienna, Austria, article ID EGU2015-10038		http://gpradar.eu/onewebmedia/EGU2015-GI3-1-Abstracts.pdf

2. ARCHEOLOGY

SITE	ARTICLE	CONTACT	LINKS AND COMMENTS
Tholos Acharnon Tomb in Athens area.	S. Santos Assunçao, K. Dimitriadis, Y. Konstantakis, V. Pérez-Gracia, E. Anagnostopoulou, M. Solla, and H. Lorenzo, "Non-destructive assessment of the Ancient Tholos Acharnon Tomb Building Geometry," Geophysical Research Abstracts, European Geosciences Union (EGU) General Assembly 2014, 27 April-2 May 2014, Vienna, Austria, article ID EGU2014-13961-1	K. Dimitriadis	Mentioned in Vienna proceedings starting from page 323.
Archaeological park of Manduria, Apulia, Italy.	L. Matera, M. Ciminale, R. Persico, M. T. Giannotta, V. Desantis, A. Alessio, "Application of a reconfigurable stepped frequency system to cultural heritage prospecting," pp. 1-5, Proc. 15th International Conference on Ground Penetrating Radar (GPR 2014), Brussels, Belgium, 30 June – 4 July 2014, pp. 18-24, doi: 10.1109/ICGPR.2014.6970377 (Italy: GPR 2014)	R. Persico	http://ieeexplore.ieee.org/stamp/stamp.jsp?tp=&arnumber=6970377

3. BRIDGES

SITE	ARTICLE	CONTACT	LINKS AND COMMENTS
St'Anton Bridge, Galicia	M. Solla, H. Lorenzo, A. Novo and F.I. Rial, "Ground-Penetrating Radar Assessment of the Medieval Arch Bridge of St'Anton Galicia," Archaeological Prospection 17(4):223 - 232 - October 2010, DOI: 10.1002/arp.390.	M. Solla	Vienna proceedings page 209 (but the article is from 2010). Complete
Bridge in Aylesford, Kent, UK	A. M. Alani, K. Banks, "Applications of Non-destructive methods (GPR and 3D Laser Scanner) in Historic Masonry Arch Bridge Assessment," Geophysical Research Abstracts, European Geosciences Union (EGU) General Assembly 2014, 27 April-2 May 2014, Vienna, Austria, article ID EGU2014-2727-1	A. M. Alani	Vienna proceedings page 334. Complete
Karl-Carstens Bridge in Bremen	C. Trela, "GPR activities at the Federal Institute for Materials Research and Testing (BAM), in Germany," pp 249-263, COST Action TU1208 Civil Engineering Applications Of Ground Penetrating Radar. Working Group Progress Meeting - Proceedings Nantes, France, February 24 – 25, 2014.	C. Trela	The bridge is presented at p. 261. Slides only are available
Carracedo Bridge (Galicia, Spain)	M. Solla and X. Núñez-Nieto, "FDTD Modelling of the GPR Signal Based on Data Obtained from Other NDT Methods: an Approach for More Exhaustive Interpretation of Field Data," pp. 179-187, COST Action TU1208 Civil Engineering Applications Of Ground Penetrating Radar. Second Action's General Meeting - Proceedings Vienna, Austria, April 30 – May 2 2014.	M. Solla	Vienna proceedings page 179. This is a very valuable article anyway It may need high experience level to be understood.
Lubians Bridge (Galicia, Spain)	M. Solla and X. Núñez-Nieto, "FDTD Modelling of the GPR Signal Based on Data Obtained from Other NDT Methods: an Approach for More Exhaustive Interpretation of Field Data," pp. 179-187, COST Action TU1208 Civil Engineering Applications Of	M. Solla	Vienna proceedings page 179. This is a very valuable article anyway It may need high experience level to be understood.

SITE	ARTICLE	CONTACT	LINKS AND COMMENTS
Monforte Bridge (Galicia, Spain)	Ground Penetrating Radar. Second Action's General Meeting - Proceedings Vienna, Austria, April 30 – May 2 2014. M. Solla and X. Núñez-Nieto, "FDTD Modelling of the GPR Signal Based on Data Obtained from Other NDT Methods: an Approach for More Exhaustive Interpretation of Field Data", COST Action TU1208 Civil Engineering Applications Of Ground Penetrating Radar. Second Action's General Meeting - Proceedings Vienna, Austria, April 30 – May 2 2014.	M. Solla	Vienna proceedings page 179. This is a very valuable article anyway It may need high experience level to be understood.
Bridge on National Road Nr. 13 near Spliigen, Orisons, Switzerland.	Hugenschmidt, F. Wenk, E. Brühwiler, "GPR chloride inspection of a RC bridge deck slab followed by an examination of the results," Proc. 15th International Conference on Ground Penetrating Radar (GPR 2014), Brussels, Belgium, 30 June – 4 July 2014, pp. 456-460, doi: 10.1109/ ICGPR.2014.6970465		http://ieeexplore.ieee.org/xpl/ articleDetails.jsp?arnumber=6970465

4. GEOLOGY/GEOPHYSICS

SITE	ARTICLE	CONTACT	LINKS AND COMMENTS
Glasgow 3D subsurface geological modelling (UK)	D. Campbell, J. de Beer, D. Lawrence, M. van der Meulen, S. Mielby, D. Hay, R. Scanlon, I. Campenhout, R. Taugs, I. Eriksson, "COST Action TU1206 SUB-URBAN - A European network to improve understanding and use of the ground beneath our cities," Geophysical Research Abstracts, European Geosciences Union (EGU) General Assembly 2014, 27 April-2 May 2014, Vienna, Austria, article ID EGU2014-11333	R. Scanlon	Sub-urban project – Vienna proceeding page Relevant from slide number 18. The "article" is not easy to be read in the actual provided form.
Netherland 3D Stochastic modelling.	D. Campbell, J. de Beer, D. Lawrence, M. van der Meulen, S. Mielby, D. Hay, R. Scanlon, I. Campenhout, R. Taugs, I. Eriksson, "COST Action TU1206 SUB-URBAN - A European		Sub-urban project – Vienna proceeding page Relevant from slide number 30. The "article"

Site	Reference	Author	Note
	network to improve understanding and use of the ground beneath our cities," Geophysical Research Abstracts, European Geosciences Union (EGU) General Assembly 2014, 27 April-2 May 2014, Vienna, Austria, article ID EGU2014-11333		is not easy to be read in the actual provided form.
Static to dynamic/predictive modelling applied to Hamburg	D. Campbell, J. de Beer, D. Lawrence, M. van der Meulen, S. Mielby, D. Hay, R. Scanlon, I. Campenhout, R. Taugs, I. Eriksson, "COST Action TU1206 SUB-URBAN - A European network to improve understanding and use of the ground beneath our cities," Geophysical Research Abstracts, European Geosciences Union (EGU) General Assembly 2014, 27 April-2 May 2014, Vienna, Austria, article ID EGU2014-11333	R. Scanlon	Sub-urban project – Vienna proceeding page Relevant from slide number 31. The "article" is not easy to be read in the actual provided form.
Thur River, Austria/Europe	A. Klotzsche, J. van der Kruk, G. A. Meles , J. A. Doetsch, H. Maurer and N. Linde "Overview of crosshole GPR full-waveform inversion to characterize aquifers, Ground Penetrating Radar (GPR)", 13th International Conference on Ground Penetrating Radar (GPR). June 2010, Lecce, Italy. doi: 10.1109/ICGPR.2010.5550238.	A. Klotzsche	Vienna proceedings page 191 (IEEE article, its content need to be reviewed).
Boise River, Idaho/USA	A. Klotzsche, J. van der Kruk, G. A. Meles , J. A. Doetsch, H. Maurer and N. Linde "Overview of crosshole GPR full-waveform inversion to characterize aquifers, Ground Penetrating Radar (GPR)," 13th International Conference on Ground Penetrating Radar (GPR). June 2010, Lecce, Italy. doi: 10.1109/ICGPR.2010.5550238.	A. Klotzsche	Vienna proceedings page 191 (IEEE article, its contents need to be reviewed).
Maltese Archipelago (Mediterranean Sea 90 km south of Sicily).	S. D'Amico, "A multidisciplinary approach to investigate rock spreading, rock sliding and cultural heritage sites on the Maltese Archipelago," pp. 390-392, COST Action TU1208 Civil Engineering Applications Of Ground Penetrating Radar. Second Action's General Meeting - Proceedings Vienna, Austria, April 30 – May 2 2014.	S. D'Amico	Vienna proceedings page 390

5. HERITAGE

SITE	ARTICLE	CONTACT	LINKS AND COMMENTS
Aylesford, Kent, UK	A. M. Alani, K. Banks, "Applications of Non-destructive methods (GPR and 3D Laser Scanner) in Historic Masonry Arch Bridge Assessment," Geophysical Research Abstracts, European Geosciences Union (EGU) General Assembly 2014, 27 April-2 May 2014, Vienna, Austria, article ID EGU2014-2727-1	A. M. Alani	Vienna proceedings page 334
Maltese Archipelago (Mediterranean Sea 90 km south of Sicily).	A multidisciplinary approach to investigate rock spreading, rock sliding and cultural heritage sites on the Maltese archipelago		Vienna proceedings page 390
Petrified Forest of Evros, Greece	G. Vargemezis, N. Diamanti, P. Tsourlos, I. Fikos, "Electrical Resistivity Tomography and Ground Penetrating Radar for locating buried petrified wood sites: a case study in the natural monument of the Petrified Forest of Evros, Greece," Geophysical Research Abstracts, European Geosciences Union (EGU) General Assembly 2014, 27 April-2 May 2014, Vienna, Austria, article ID EGU2014-14298.		Vienna proceedings page 393 (presented as poster)
St. John Baptist in Parabita (near Lecce, Southern Italy).	L. Matera, M. Ciminale, R. Persico, M. T. Giannotta, V. Desantis, A. Alessio, "Application of a reconfigurable stepped frequency system to cultural heritage prospecting," pp. 1-5, Proc. 15th International Conference on Ground Penetrating Radar (GPR 2014), Brussels, Belgium, 30 June – 4 July 2014, pp. 18-24, doi: 10.1109/ICGPR.2014.6970377	R. Persico	Rome Proceedings page 63

SITE	ARTICLE	CONTACT	LINKS AND COMMENTS
Test site at the Department of Engineering of Rome Tre University in Rome, Italy (41 051' 16.02" N, 12° 28' 06.02" E)	2015, 12-17 April 2015, Vienna, Austria, article ID EGU2015-15509 F. Tosti, S. Adabi, L. Pajewski, G. Schettini, A. Benedetto, "Large-scale analysis of dielectric and mechanical properties of pavement using GPR and LFWD," Proc. 15th International Conference on Ground Penetrating Radar (GPR 2014), Brussels, Belgium, 30 June – 4 July 2014, pp. 868-873, doi: 10.1109/ICGPR.2014.6970551	L. Pajewski	http://ieeexplore.ieee.org/stamp/stamp.jsp?tp=&arnumber=6970551
Test site - pavement fatigue carrousel of IFSTTAR, Nantes (France)	J.-M. Simonin, V. Balthazart, P. Hornych, X. Dérobert, E. Thibaut, J. Sala, V. Utsi, "Case study of detection of artificial defects in an experimental pavement structure using 3D GPR systems," Proc. 15th International Conference on Ground Penetrating Radar (GPR 2014), Brussels, Belgium, 30 June – 4 July 2014, pp. 847-851, doi: 10.1109/ICGPR.2014.6970547	X. Dérobert	http://ieeexplore.ieee.org/stamp/stamp.jsp?tp=&arnumber=6970547

8. TREES

SITE	ARTICLE	CONTACT	LINKS AND COMMENTS
Louvain-la-Neuve and Brussels	J. Jezova, L. Mertens, S. Lambot, "Microwave sensing of tree trunks," Geophysical Research Abstracts, European Geosciences Union (EGU) General Assembly 2015, 12-17 April 2015, Vienna, Austria, article ID EGU2015-6264-1	S. Lambot	http://euradar.eu/onewebmedia/EGU2015-GI3-1-Abstracts.pdf
Petrified Forest of Evros, Greece	G. Vargemezis, N. Diamanti, P. Tsourlos, I. Fikos, "Electrical Resistivity Tomography and Ground Penetrating Radar for locating buried petrified wood sites: a case study in the natural monument of the Petrified Forest of Evros, Greece," Geophysical Research Abstracts, European Geosciences Union (EGU) General Assembly 2014, 27 April-2 May 2014, Vienna, Austria, article ID EGU2014-14298.		Vienna proceedings page 393 (presented as poster)

6. RAILWAY

SITE	ARTICLE	CONTACT	LINKS AND COMMENTS
Old railway substructure: Northern Line platform (Lisbon-Oporto)	S. Fontul, "GPR experience at the National Laboratory for Civil Engineering, Lisbon, Portugal" pp 211-246, COST Action TU1208 Civil Engineering Applications Of Ground Penetrating Radar. Working Group Progress Meeting - Proceedings Nantes, France, February 24 – 25, 2014.	S. Fontul	Nantes Proceedings page 234. This is a sub-article; the main article page number is way lower.

7. ROADS

SITE	ARTICLE	CONTACT	LINKS AND COMMENTS
District of Rieti	F. Tosti, F. D'Amico, A. Calvi, A. Benedetto, "On-site inspections of pavement damages evolution using GPR," Geophysical Research Abstracts, European Geosciences Union (EGU) General Assembly 2014, 27 April-2 May 2014, Vienna, Austria, article ID EGU2014-12978	F. Tosti	http://meetingorganizer.copernicus.org/EGU2014/EGU2014-12978.pdf
Belgian Road Research Centre	E. Van De Vijver, J. De Pue, W. Cornelis, M. Van Meirvenne, "Comparison of air-launched and ground-coupled configurations of SFCW GPR in time, frequency and wavelet domain," Geophysical Research Abstracts, European Geosciences Union (EGU) General Assembly 2015, 12-17 April 2015, Vienna, Austria, article ID EGU2015-10038		http://gpradar.eu/onewebmedia/EGU2015-GI3-1-Abstracts.pdf
Medway Tunnel in North Kent	M. A. Alani, K. Banks, "Medway Tunnel Road Pavement Survey Using Different Frequency GPR Antenna Systems – A Case Study," Geophysical Research Abstracts, European Geosciences Union (EGU) General Assembly	M. A. Alani	http://gpradar.eu/onewebmedia/EGU2015-GI3-1-Abstracts.pdf

9. TUNNELS

SITE	ARTICLE	CONTACT	LINKS AND COMMENTS
Medway Tunnel in North Kent	M. A. Alani, K. Banks, "Medway Tunnel Road Pavement Survey Using Different Frequency GPR Antenna Systems – A Case Study," Geophysical Research Abstracts, European Geosciences Union (EGU) General Assembly 2015, 12-17 April 2015, Vienna, Austria, article ID EGU2015-15509	M. A. Alani	http://gpradar.eu/onewebmedia/EGU2015-GI3-1-Abstracts.pdf

ANNEX C

COST
EUROPEAN COOPERATION
IN SCIENCE AND TECHNOLOGY

GPR APPLICATIONS IN RAILWAYS.
GROUND PENETRATING RADAR, A NON INVASIVE AND EFFECTIVE TECHNOLOGY.

"COST is the longest-running European framework supporting trans-national cooperation among researchers, engineers and scholars across Europe.
It is a unique means for them to jointly develop their own ideas and new initiatives across all fields in science and technology, including social sciences and humanities, through pan-European networking of nationally funded research activities. Based on a European intergovernmental framework for cooperation in science and technology, COST has been contributing - since its creation in 1971 - to closing the gap between science, policy makers and society throughout Europe and beyond. As a precursor of advanced multidisciplinary research, COST plays a very important role in building a European Research Area (ERA)."

For more information please visit www.cost.eu

"As stated in the Memorandum of Understanding, the main objective of the COST Action TU1208 is to exchange and increase scientific-technical knowledge and experience of Ground Penetrating Radar (GPR) techniques in Civil Engineering (CE). Furthermore, the Action aims at promoting, throughout Europe, a wider and more effective use of this safe and non-destructive technique in the monitoring of infrastructures and structures."

For more information please visit www.gpradar.eu

Contacts:

Chair of the Action:
Dr Lara Pajewski
"Roma Tre University", IT
lara.pajewski@uniroma3.it

Vice-Chair of the Action:
Prof Andreas Loizos
National Technical University of Athens, EL

Science Officer:
Dr Mickael Pero
COST Office, BE

Administrative Officer:
Ms Carmencita Malimban
COST Office, BE

Insert here an example of application...
This part should contain no more than 200 words describing the particular application and its objective has to be efficacy.

COST Action TU1208
Civil Engineering Applications of Ground Penetrating Radar
www.gpradar.eu

This flyer is supported by COST, (European Cooperation in Science and Technology).
COST is supported by the EU RTD Framework Programme Horizon2020.
www.cost.eu

THIS IS AN EXAMPLE OF FIRST INTERNAL PAGE.

The internal page can provide any information that the expert in a given field may find relevant. A bullet list containing few information is provided here as an example.
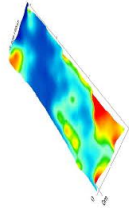
ADVANTAGES OF NON-DESTRUCTIVE TESTING.

- **Reduce** risks of incidents associated to invasive tests.
- **Reduce** costs associated with digging.

USAGE OF GPR AT DEPLOYMENT STAGE:

- Utility mapping.
- Soil mapping.

USAGE OF GPR AT MAINTAINANCE STAGE.

- Bridges cracks detection.
- Railway track line monitoring.
- Ballast state monitoring.
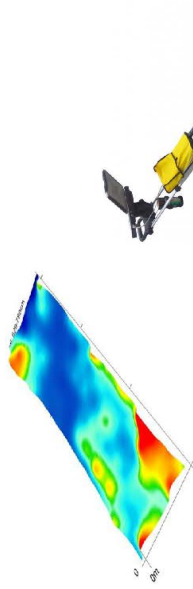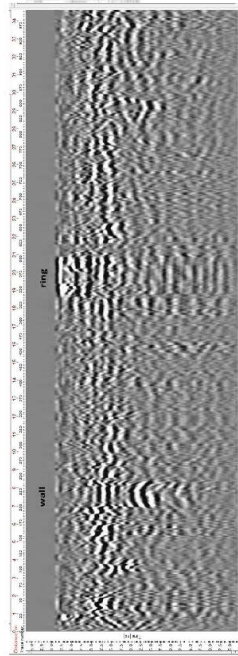
Characteristics of GPR commonly used in Railway applications.

Application	frequency	Typical penetration in wet soil	Typical penetration in dry soil
Tunnels			
Utility mapping			
Soil mapping			
Railway track line monitoring			

TABLE 2....

b	b	b	b
a	a	a	a

ANNEX D

STSM 10

COMPARISON OF FINITE-DIFFERENCE AND FINITE-INTEGRATION METHODS IN THE TIME-DOMAIN FOR THE SIMULATION OF GPR AND OTHER ELECTROMAGNETIC APPLICATIONS

Visiting Scientist: Alessio Ventura, Roma Tre University, Roma, Italy (alessioventura@hotmail.com)

Host Scientist: Antonis Giannopoulos, The University of Edinburgh, Edinburgh, UK (a.giannopoulos@ed.ac.uk)

STSM Dates: 18 April – 22 April 2016

1. PURPOSE OF THE STSM

This STSM focused on the use of different electromagnetic simulators, implementing different aproaches for spatial discretization and different numerical techniques for the solution of Maxwell's Equations, to develop accurate and realistic models of antennas in GPR scenarios. In particular, we compared the Finite-Integration Technique (FIT), implemented in the commercial tool Microwave Studio by Computer Simulation Technology (CST), and the Finite-Difference Time-Domain (FDTD) technique, implemented in the new version of gprMax, the free open-source solver developed in the University of Edinburgh as a contribution to COST Action TU1208. Furthermore, we started testing the effectiveness of gprMax for other electromagnetic applications.

2. DESCRIPTION OF THE WORK CARRIED OUT DURING THE STSM

The work carried out during the STSM was mainly concerned with the simulation of GPR antennas. In particular, before the STSM we modelled two commercial bow-tie antennas for Ground Penetrating Radar: GSSI 1.5 GHz and MALA 1.2 GHz. The Roma Tre University research team focused on modelling them by using CST Microwave Studio. The University of Edinburgh team modelled them with

gprMax and collected experimental data. During the STSM, we finalised the series of comparisons that we carried out in remote collaboration. Preliminary results of our joint work were presented in [1]. More results will be presented in [2].

Next, for simple scenarios involving a dipole and a half-space, we carried out simulations to compare gprMax and CST results with the results of integral methods developed in Croatia, by the University of Split research team. These comparisons will be presented in [2].

Finally, another aspect of this STSM was to demonstrate that is possible to achieve a good agreement between CST Microwave Studio and gprMax not only in the GPR context but also for other electromagnetic applications.

3. DESCRIPTION OF THE MAIN RESULTS OBTAINED DURING THE STSM

3.1 GPR ANTENNAS

As already mentioned, the first part of the STSM focused on finalising comparisons of synthetic data obtained by using two different tools for electromagnetic modelling of GPR scenarios: gprMax and CST Microwave Studio.

In Figures 1 and 2 the geometry of the simulated GSSI antenna is shown. In Figure 3, crosstalk results obtained with both tools are presented; the unknown parameters were optimised, in order to obtain the best agreement between the output data given by models.

In Figures 4-6, the same as in Figures 1-3 is presented for the MALA antenna.

More results can be found in [1, 2].

3.2 DIPOLE ANTENNA

Once the optimization of GSSI and MALA antennas was finalised, we focused on the simulation of a wire dipole antenna. For this simple antenna, we compared results of CST Microwave Studio, gprMax and Croatian codes implementing integral methods.
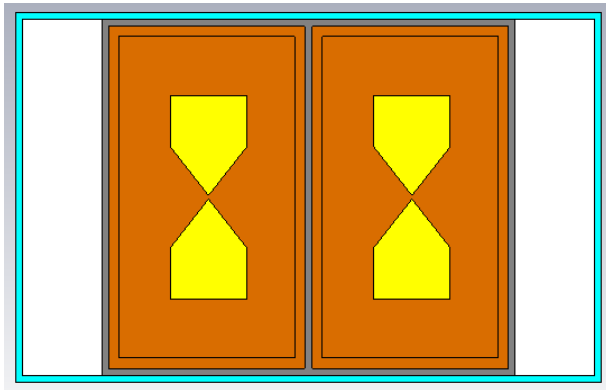
Fig. 1 –GSSI 1.5 GHz antenna modelled by using CST Microwave Studio.
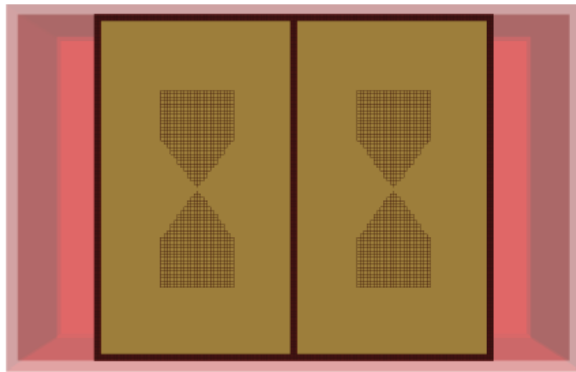
Fig. 2 –GSSI 1.5 GHz antenna modelled by using gprMsx.
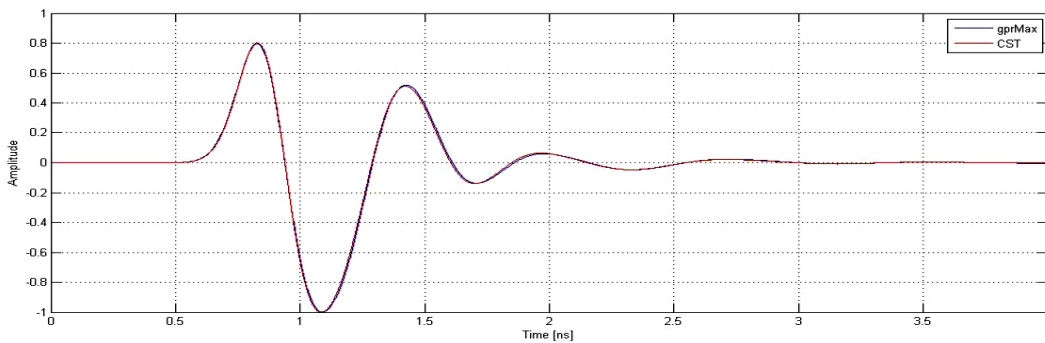
Fig. 3 – GSSI 1.5 GHz crosstalk in free space: CST and gprMax results.
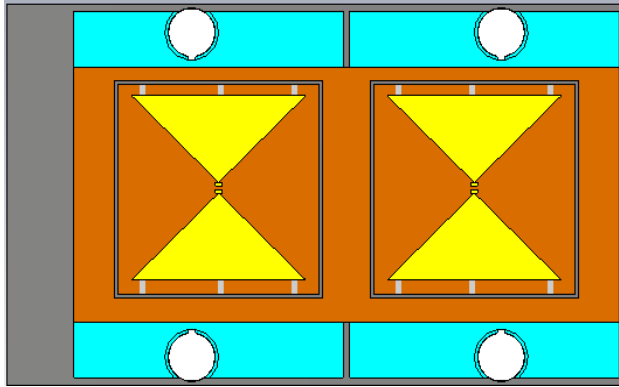
Fig. 4 – MALA 1.2 GHz modelled by using CST
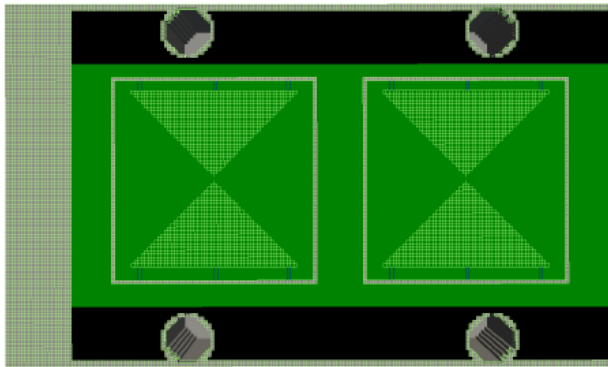
Fig. 5 – MALA 1.2 GHz modelled by using GprMax
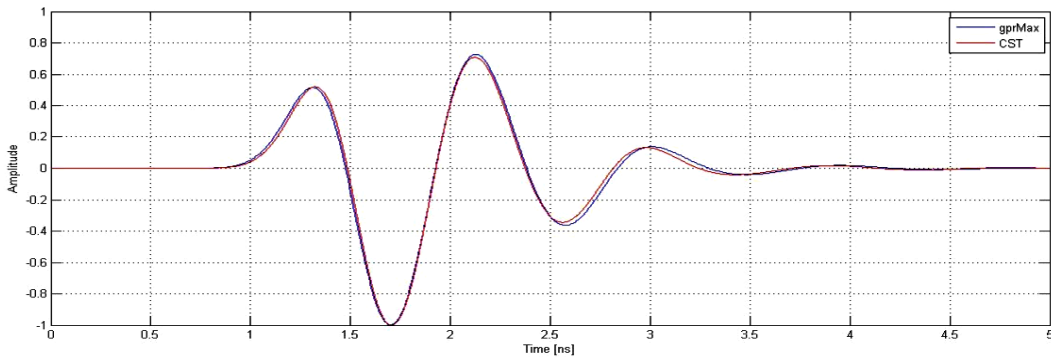
Fig. 6 – Same as in Fig. 3 for the MALA 1.2 GHz antenna.

Different simulations of the dipole were performed, in free space and over several soils with different properties:

- Lossless half-space with relative permittivity ε_r=10;
- Lossy half-space with relative permittivity ε_r= 10 and conductivity ;σ = 1 mS/m;
- Lossy half-space with relative permittivity ε_r= 10 and conductivity σ = 10 mS/m.

The CST model of the dipole is shown in Figure 7. For each scenario, we calculated the current at the centre of the dipole, and the electric field at different distances. When the half-space was present, the distance between the dipole and the soil was 0.1 m: see the geometry in Figure 8. Results were calculated at 0.5 m, 1 m and 1.5 m depth. The antenna was excited by a voltage source with a Gaussian-shaped waveform in a gap between the arms of the dipole:

$$V(t) = V_0 e^{-g^2(t-t_0)^2} \tag{1}$$

where $V_0 = 1\,V$, $g = 1.5 * 10^9$ s^{-1}, and $t_0 = 1.43 * 10^{-9}$ s.

Figures 9-24 show the results of the simulations of the above-listed scenarios for the FDTD, TDIE and FIT simulation methods.

3.3 WOODPILE EBG

Another purpose of the STSM was to show that gprMax can be successfully applied to scenarios not concerned with GPR. We decided to consider the simulation of a woodpile electromagnetic band-gap (EBG) superstrate, designed to increase the directivity of a patch antenna. Indeed, for such structure several HFSS results and experimental data are available [3, 4], recently obtained in Italy by researchers working in Sapienza and Roma Tre Universities. More time is needed to complete this activity: the gprMax model has to finalised, simulations have to be carried out in order to obtain gprMax results and compare them with HFSS results and with measurements. We are not able to present results in this report. The geometry of the considered structure is shown in Figures 25 and 26.
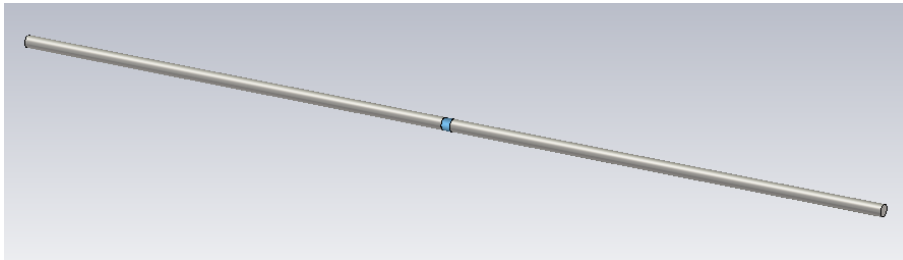
Fig. 7 – Model of the dipole in CST.
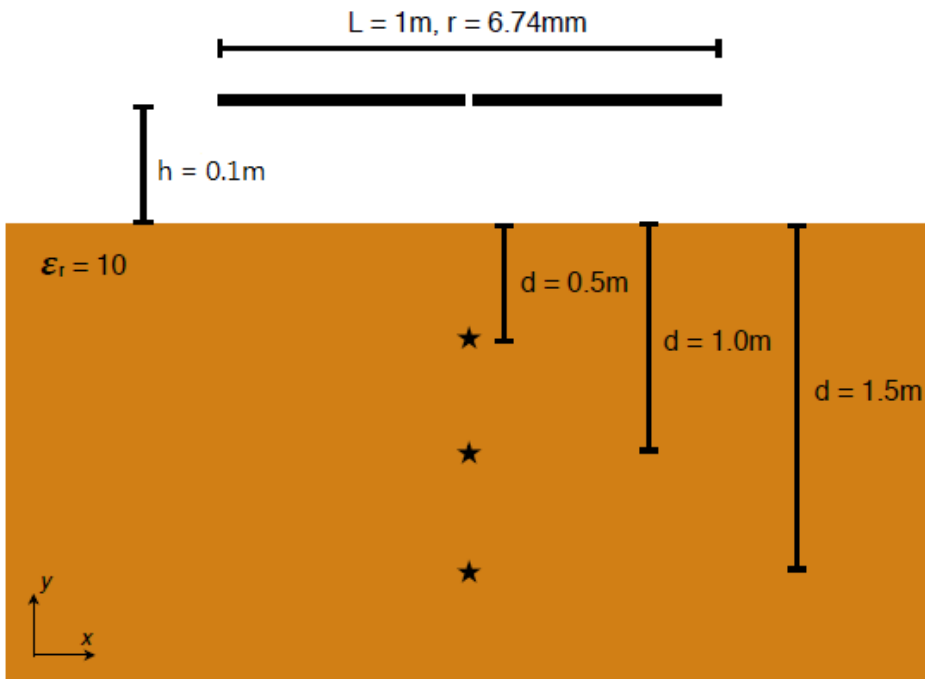
Fig. 8 – scheme of the scenario

3.4 HUMAN BODY

The final part of the STSM was devoted to developing of a human body model in gprMax, to study the interaction between electromagnetic fields and the different parts and tissues which compose the human body.
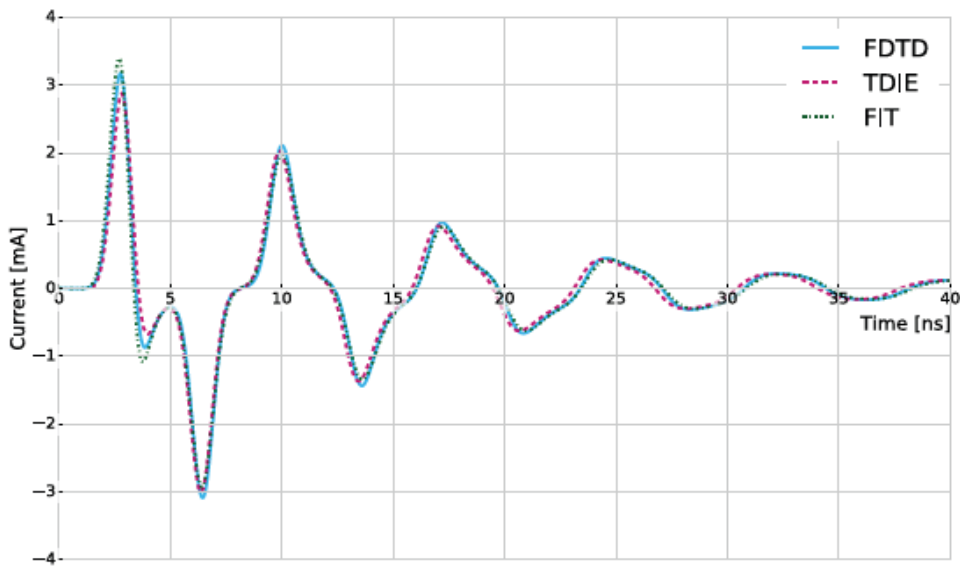
Fig. 9 – Current I_x at the centre of the dipole and in free space.
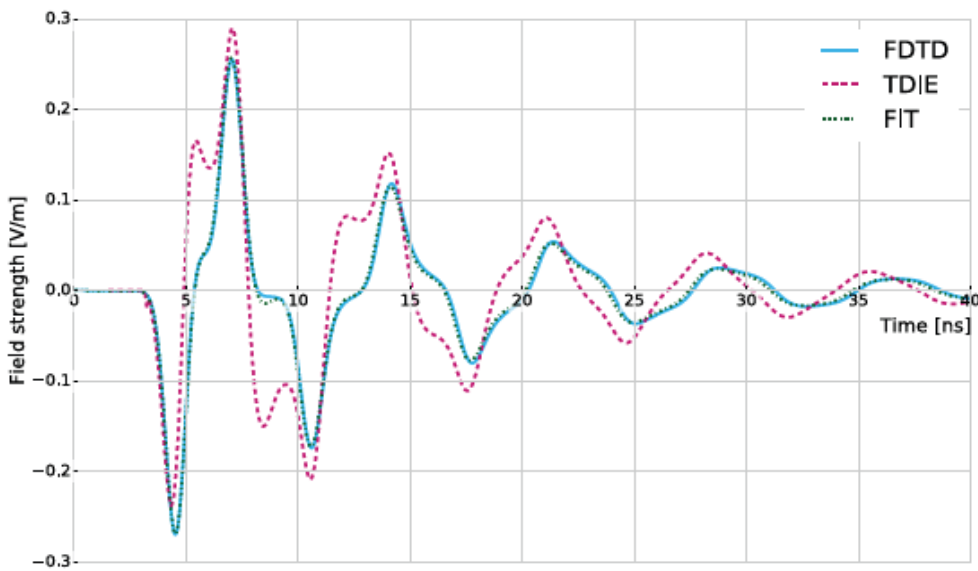
Fig. 10 – Electric field E_x at d=0.5 m from the centre of the dipole, in free space.
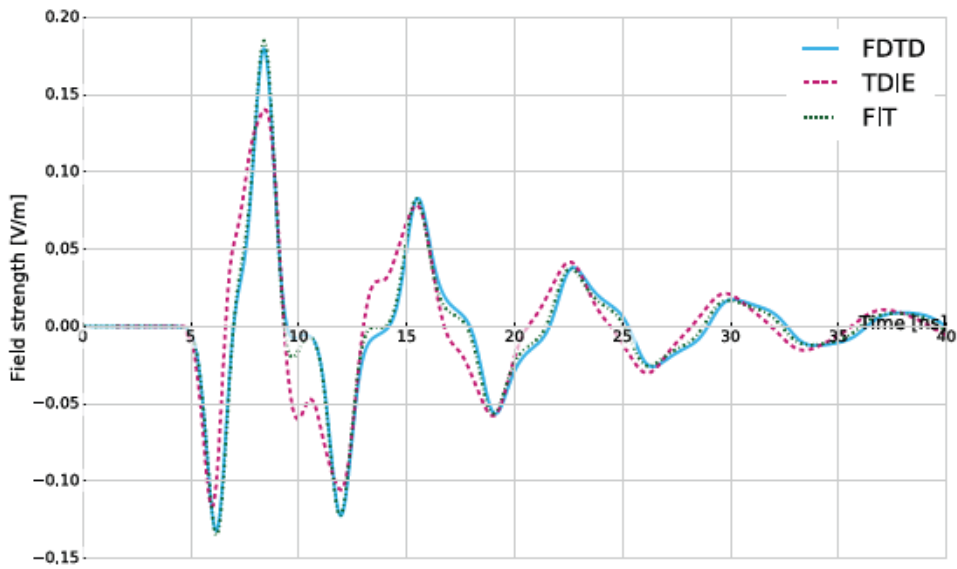
Fig. 11 – Same as in Fig. 10, with d=1.0 m.
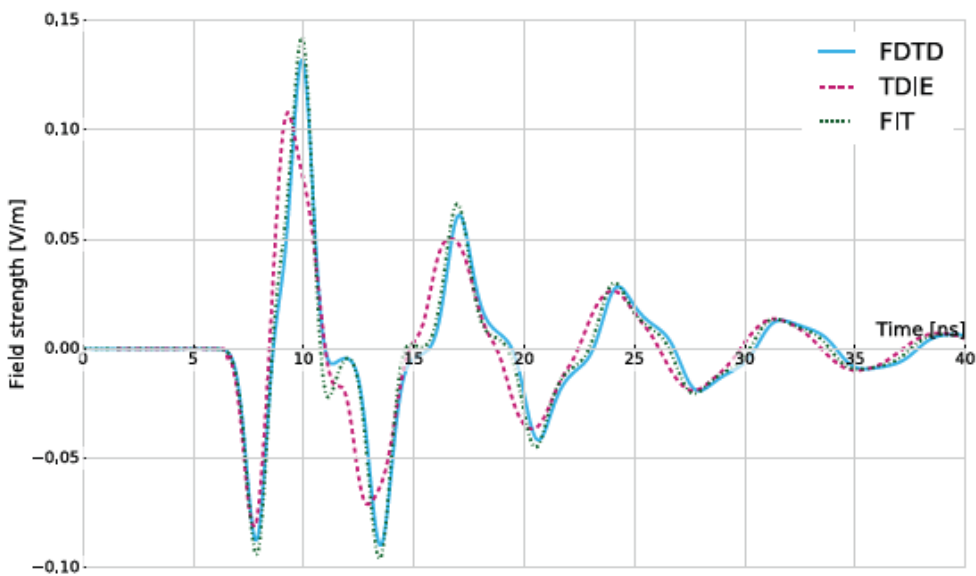
Fig. 12 – Same as in Fig. 10, with d=1.5 m.
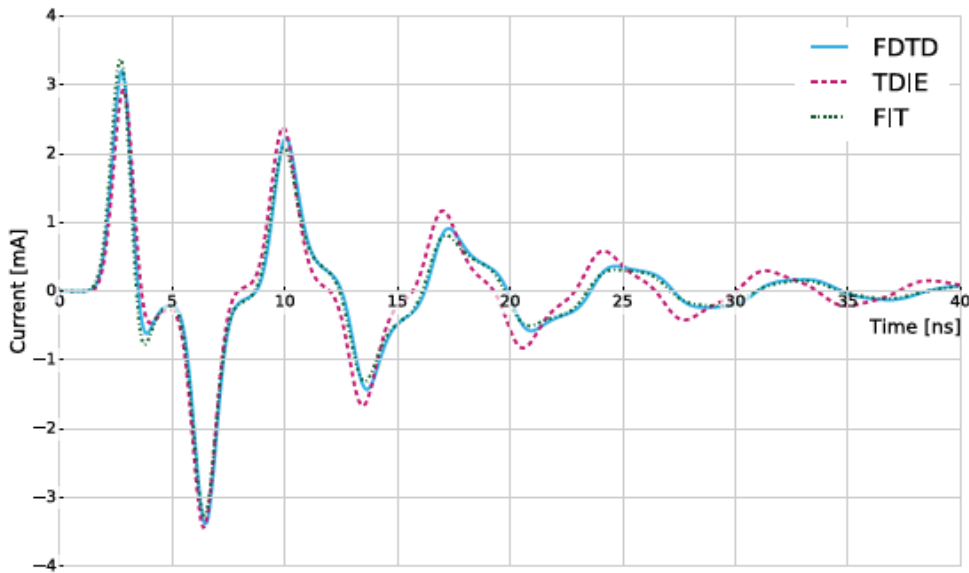
Fig. 13 – Current I_x at the centre of the dipole; the dipole is over a half-space with ε_r=10.
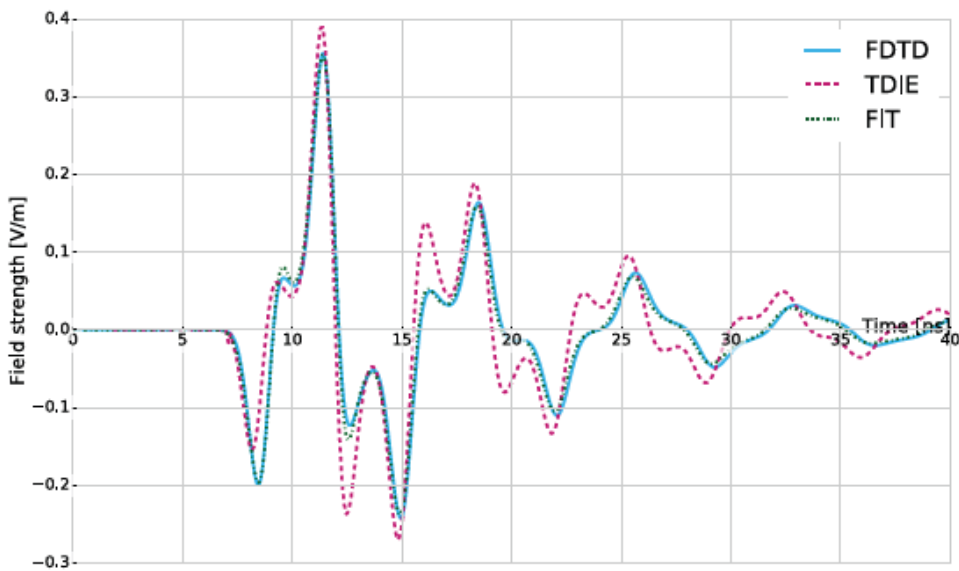
Fig. 14 – Electric field E_x at d=0.5 m inside the half-space (ε_r=10).
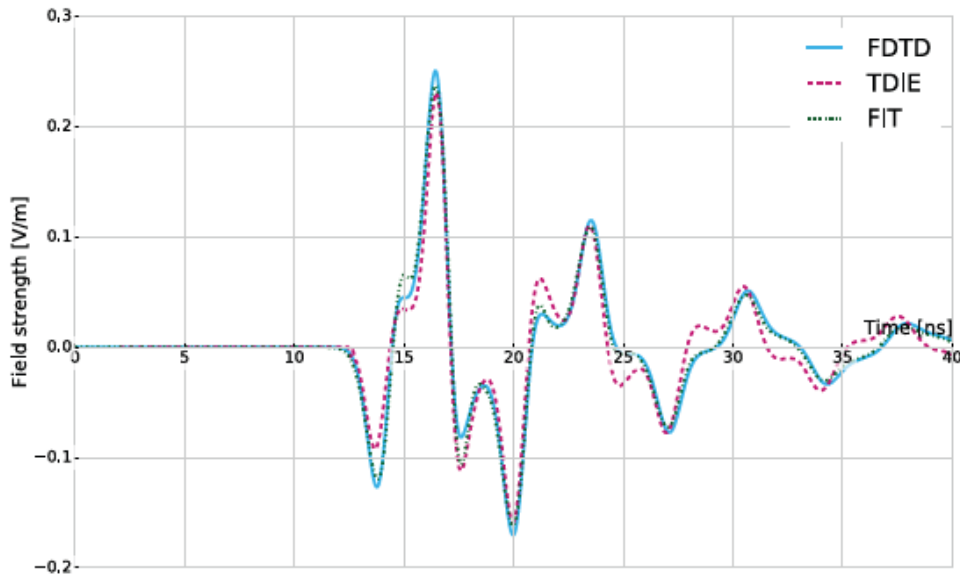
Fig. 15 – Same as in Fig. 14, with d=1.0 m.
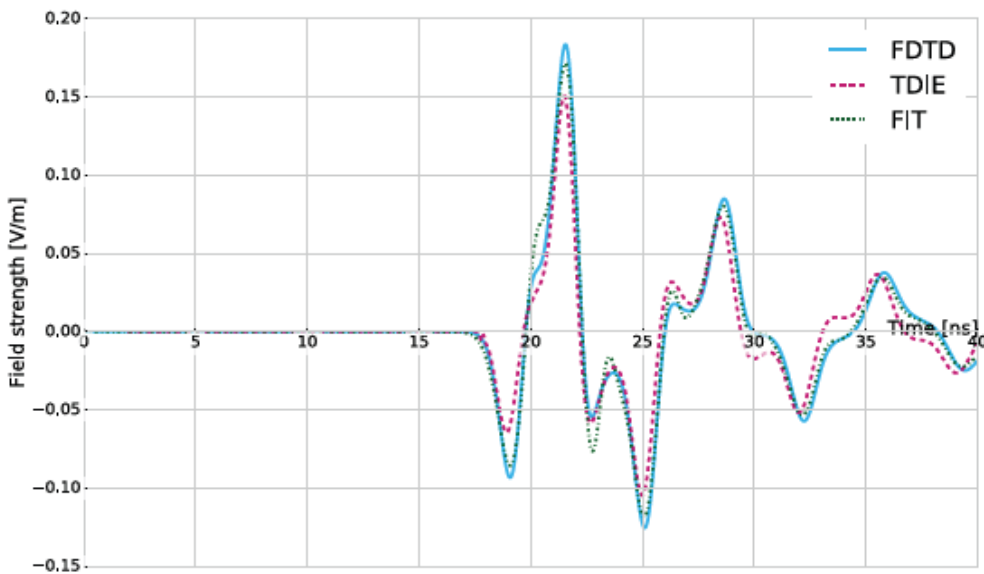
Fig. 16 – Same as in Fig. 14, with d=1.5 m.

170
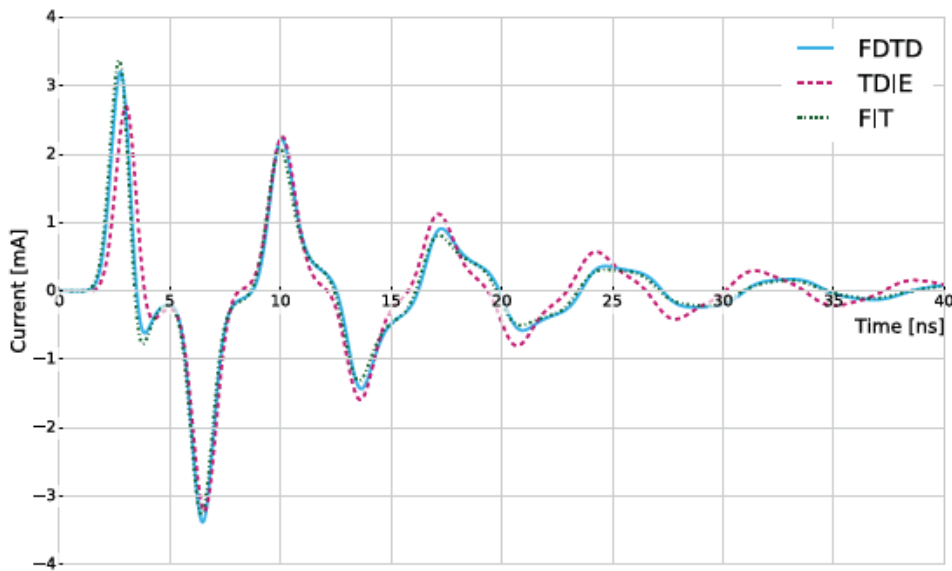
Fig. 17 – Same as in Fig. 13, with a lossy half-space (ε_r=10; σ =1 mS/m).
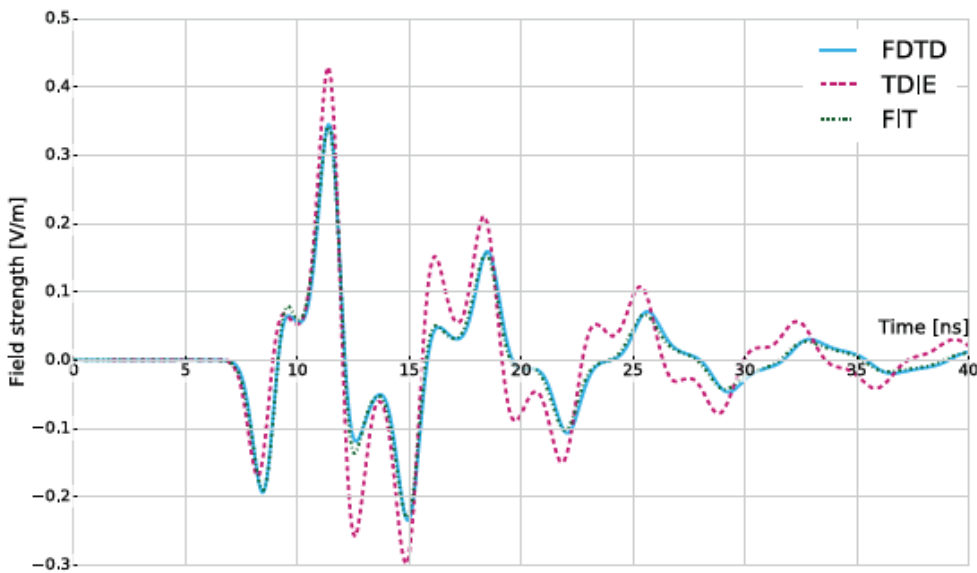
Fig. 18 – Same as in Fig. 14, with a lossy half-space (ε_r=10; σ =1 mS/m).
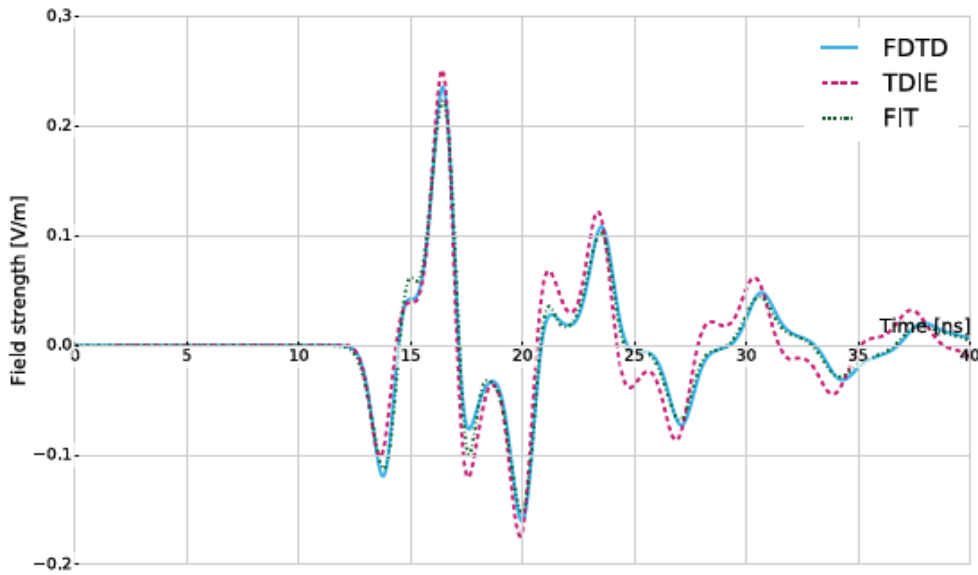
Fig.19 – Same as in Fig. 18, with d=1.0 m.
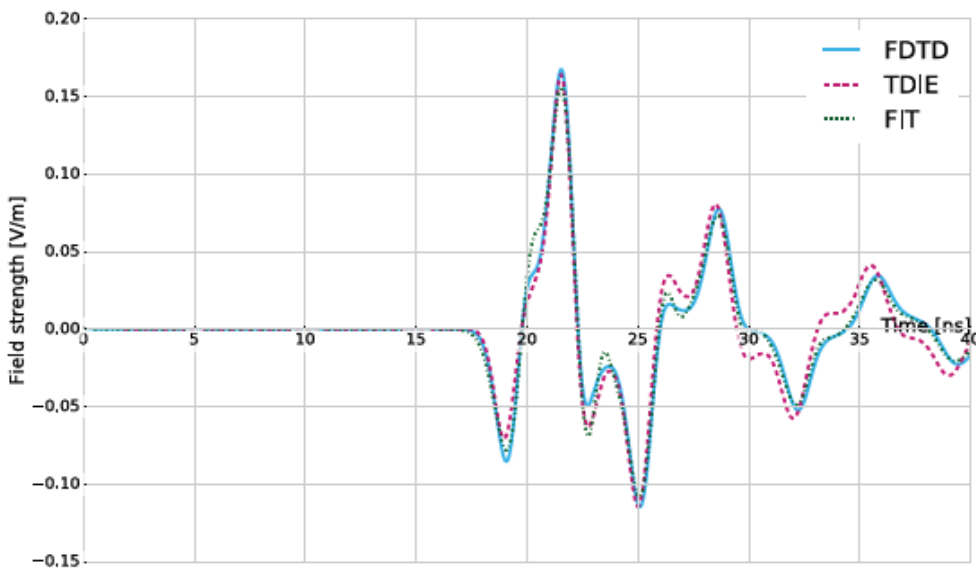
Fig. 20 – Same as in Fig. 18, with d=1.5 m.

172
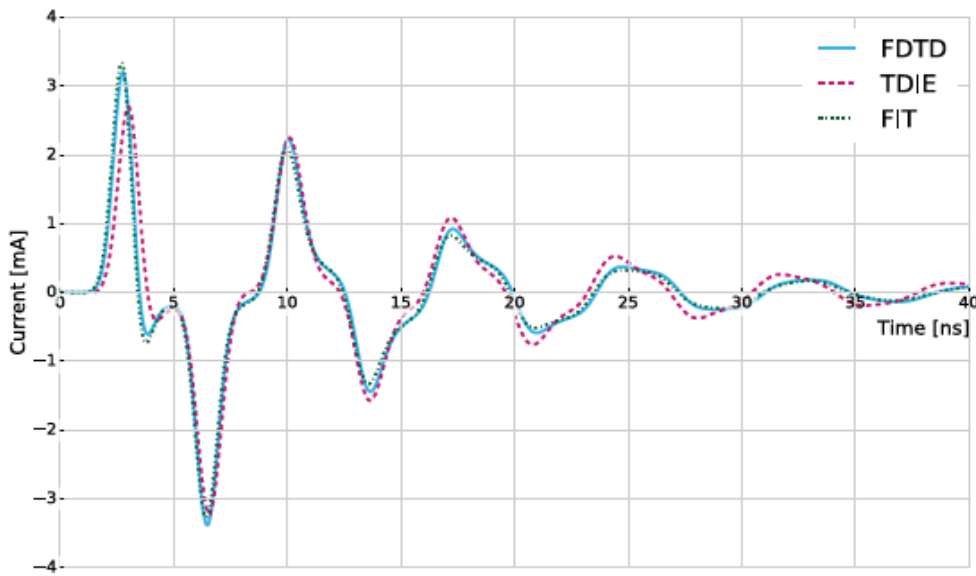
Fig. 21– Same as in Fig. 13, with a lossy half-space (ε_r=10; σ =10 mS/m).
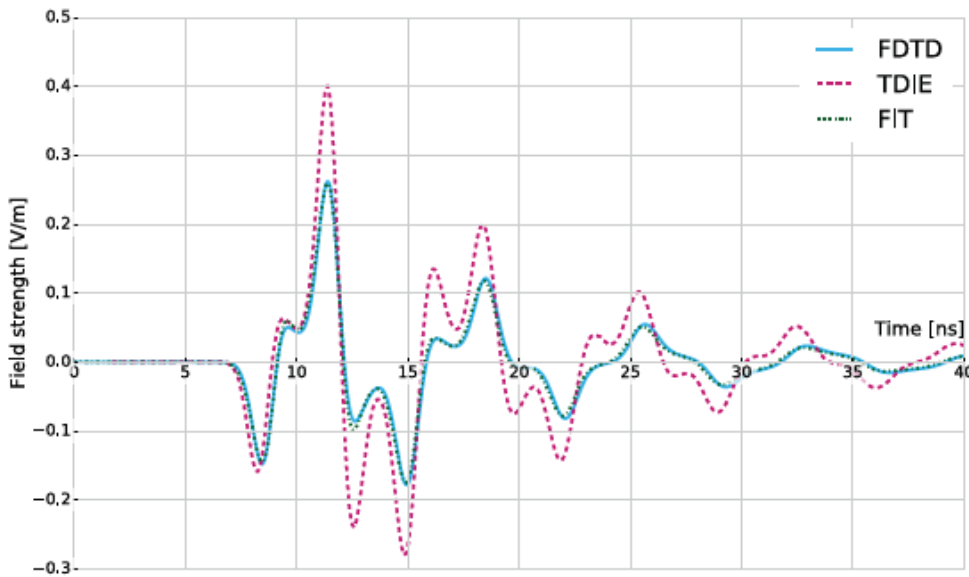
Fig.22 – Same as in Fig. 14, with a lossy half-space (ε_r=10; σ =1 mS/m).
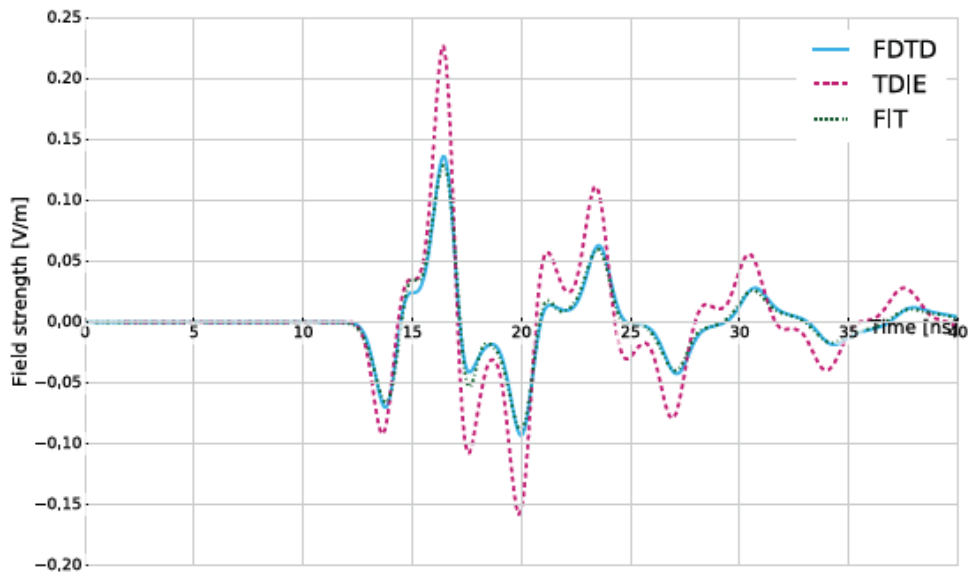
Fig. 23– Same as in Fig. 22, with d=1.0 m.
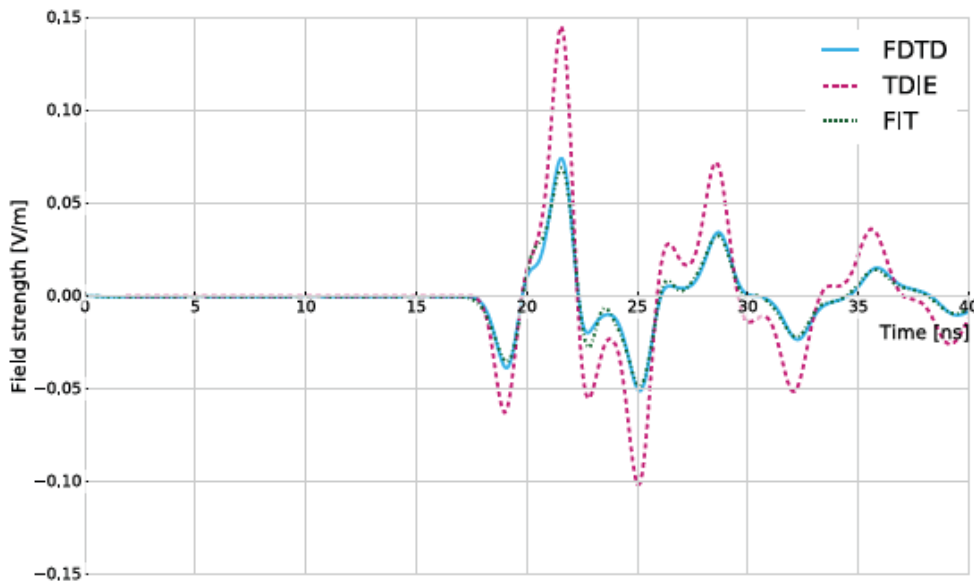
Fig. 24 – Same as in Fig. 22, with d=1.5 m.
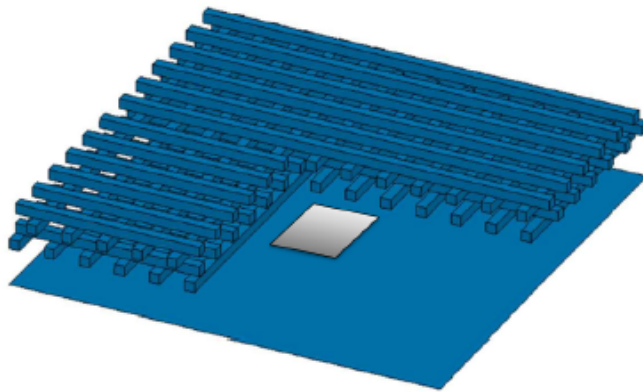
Fig. 25– A woodpile-covered antenna.
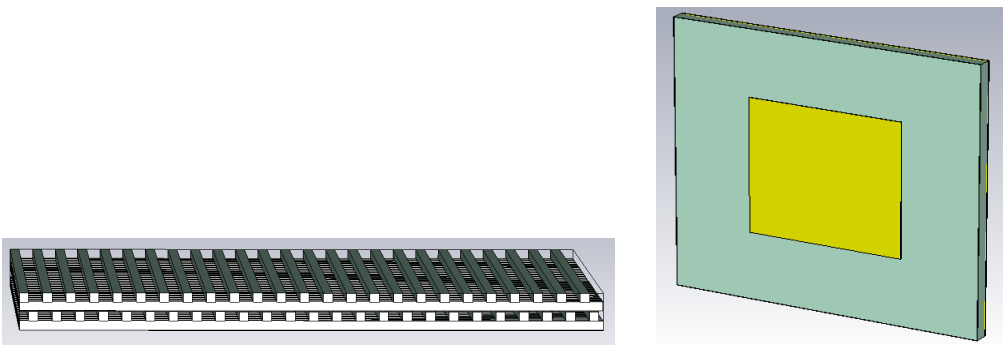
Fig. 26 – Woodpile electromagnetic band-gap material.

In CST microwave studio there is a macro function, which allows to easily include biological media or entire human-body models in the scenarios; the human-body models belong to the so-called "CST Voxel Family" of CST models. This is a set of seven human model voxel data sets created from seven persons of different gender, age and stature. Table I and Figure 27 give an overview of the seven models. The properties of the biological media

were recalculated, during this STSM, by using the 4-Cole-Cole formulation at a given frequency. The formula and parameters that we used are available in [5]. More time is needed to bring forward this activity and obtain results.

4. FUTURE COLLABORATION WITH THE HOST INSTITUTION

We plan to bring forward activities presented in Sections 3.3 & 3.4.

TABLE I – HUMAN MODELS IMPLEMENTED IN CST STUDIO SUITE

Model	Age/Sex	Size/cm	Mass/kg	Resolution / mm
Baby	8-week female	57	4.2	0.85 × 0.85 × 4.0
Child	7y female	115	21.7	1.54 × 1.54 × 8.0
Donna	40y female	176	79	1.875 × 1.875 × 10
Emma	26y female	170	81	0.98 × 0.98 × 10
Gustav	38y male	176	69	2.08 × 2.08 × 8.0
Laura	43y female	163	51	1.875 × 1.875 × 5.0
Katja	43y pregnant, 24w	163	62	1.775 × 1.775 × 4.84
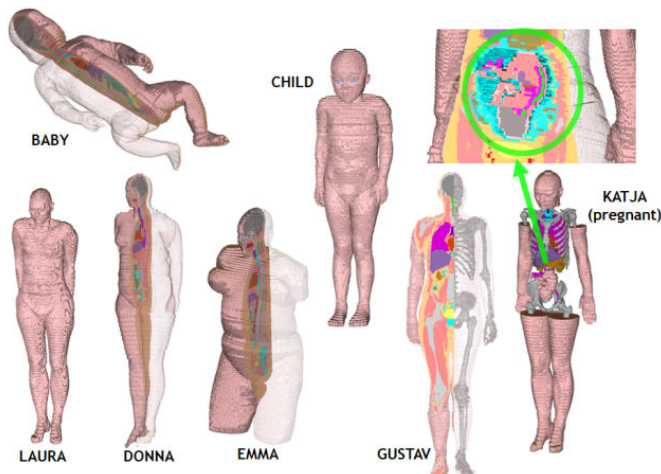
Fig. 27 – CST Voxel Family.

5. FORESEEN PUBLICATIONS/ARTICLES RESULTING FROM THE STSM

An open-access paper was published on a peer-reviewed international journal, which included some of the results presented in Sections 1 & 2, please see Ref. [6].

The results of the STSM were also presented during the international conference GPR 2016 (see [2]).

We consider the data obtained for the dipole are especially interesting, because for such scenario it is possible to carry out a comparison between several different techniques.

ACKNOWLEDGEMENT

REFERENCES

[1] C. Warren, L. Pajewski, A. Ventura, A. Giannopoulos, "An Evaluation of Finite-Difference and Finite-Integration Time-Domain Modelling Tools for Ground Penetrating Radar Antennas," 2016 IEEE European Conference on Antennas and Propagation (EuCAP), 11-15 April 2016, Davos, Switzerland.

[2] C. Warren, L. Pajewski, D. Poljak, A. Ventura, A. Giannopoulos, S. Sesnic, "A comparison of Finite-Difference, Finite-Integration and Integral-Equation methods in the Time Domain for modelling Ground Penetrating Radar antennas," pp. 1-6, Proc. 16th International Conference on Ground Penetrating Radar (GPR 2016), Hong Kong, 13-16 June 2016.

[3] L. Pajewski, F. Frezza, M. Marciniak, E. Piuzzi, G. Rossi, "Experimental Analysis of a Directive Antenna with a 3D-EBG Superstrate," Journal of Telecommunications and Information Technology, 2017.

[4] F. Frezza, L. Pajewski, E. Piuzzi, C. Ponti, G. Schettini, "Radiation-Enhancement Properties of an X-Band Woodpile EBG and Its Application to a Planar Antenna," International Journal of Antennas and Propagation, vol. 2014, Article ID 729187, 15 pages, 2014.

[5] *http://niremf.ifac.cnr.it/docs/DIELECTRIC/AppendixC.html:* dielectric properties of body tissues at RF and microwave frequencies.

[6] C. Warren, S. Sesnic, A. Ventura, L. Pajewski, D. Poljak, and A. Giannopoulos, "Comparison of time-domain finite-difference, finite-integration, and integral-equation methods for dipole radiation in half-space environments," Progress In Electromagnetics Research M, Vol. 57, 175-183, 2017. doi:10.2528/PIERM17021602.

STSM 11

GPR APPLICATIONS IN CIVIL ENGINEERING: COLLABORATING WITH A COMPANY AND PREPARING MATERIAL FOR THE EDUCATION PACK

Visiting Scientist: Viviana Sossa, Polytechnic University of Catalonia, Barcelona, Spain (vivi.sossa.ar@gmail.com)

Host Scientist: Sonia Santos Assunçao, Murphy Surveys, Dublin, Ireland (sonicsantos03@gmail.com)

STSM Dates: 25 April – 29 April 2016

1. PURPOSE OF THE STSM

This STSM was proposed in order to introduce the visiting scientist to the environment of GPR private end-users and see how a company carries out GPR surveys. The STSM had two main objectives:

1) To develop the module of the Education Pack devoted to the use of GPR in archaeology.

2) To accompany the company crew in civil-engineering surveys, as well as in the subsequent processing of collected data.

2. DESCRIPTION OF THE WORK CARRIED OUT DURING THE STSM

DAY 1

During the first day, the visiting scientist visited the company installations, met the company members and was informed about the company activities. During the morning, the visiting and host scientist also developed a plan of activities. Moreover, they performed some simple experiments with the equipment of the

company, with the purpose of introducing the visiting scientist to the equipment and methodologies employed by the company.

In the afternoon, the visiting scientist reviewed, under the supervision of the host scientist, some projects undertaken by the company in the past. These were related to the assessment of a bridge and to the detection of rebar in reinforced concrete slabs.

DAY 2

A new project was carried out, concerned with pipe detection by GPR. Data acquisition was planned and done. A 500 MHz shielded antenna was used. The first step was the supervision of maps showing the presumed location of some pipes. This allowed to select the most appropriate antenna and the position of GPR profiles to be acquired (see Figure 1). The objective of the company was to determine the real depth and position of the pipes. The survey consisted in acquiring some isolated profiles, covering the entire surface and trying to intersect the pipes.
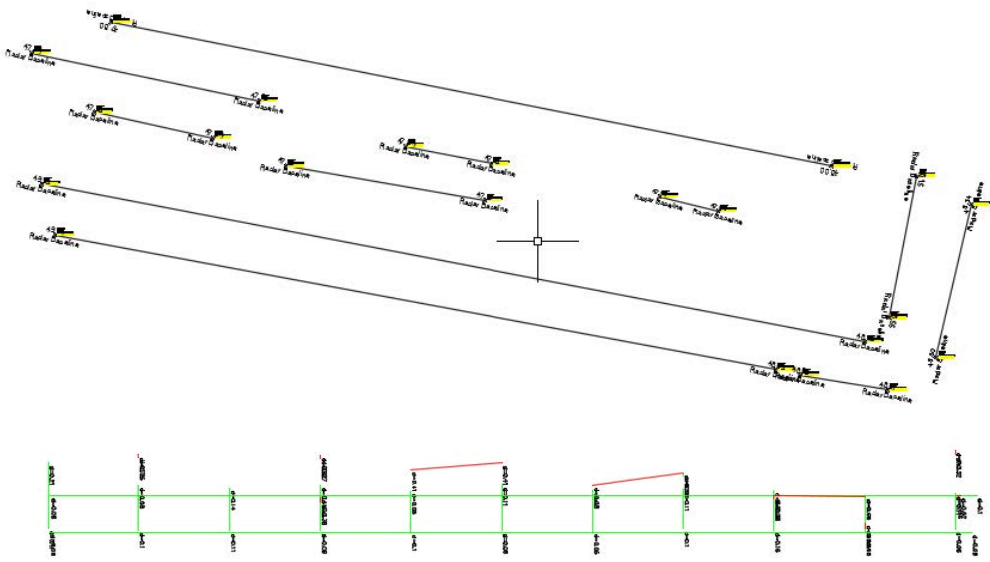
Fig. 2 – Information about the survey (AutoCad file).

During data acquisition, the position of the antenna was recorded by GPS. This method allowed a quick survey and enough accuracy in the location of the different profiles. The intersection of each profile with the pipes were marked in-situ on the terrain.

During the afternoon, we focused on data interpretation. Therefore, we exported all data and looked for signatures of pipes. The purpose of this activity was to determine whether the position estimated on field needed to be corrected. The conclusion was that the results in field were accurate enough for the company purposes.

A possible recommendation for this type of survey (location of buried pipes or other utilities) is to combine GPR with other methodologies allowing a more accurate geo-referencing of the location of the profiles. GPS is a proper methodology but some difficulties arise in cities, among buildings, and in forests, because the signal may be weak or absent in some areas.

DAY 3

During the third day of the STSM a more complicated project was carried out, concerned with the use of GPR on reinforced concrete. This time, data were acquired in a mesh of profiles because in this case the company wanted a three dimensional analysis of the structure. In addition, the topography of the slab was not completely flat. Therefore, it was necessary to determine the height of the different points with respect to a reference level. The survey consisted of 242 radar lines, covering the entire surface. The distance between adjacent lines was half meter. The location of the antenna was defined with an odometer because the study was inside a building and the GPS had not enough coverage. After the data acquisition, it was necessary to do some processing:

1) The first sequence of processing was applied to each A-scan. It included zero time correction, automatic gain application, Gaussian filter application, dynamic correction and application of band pass filters to remove most of the noise.

2) The second sequence of processing was applied to each B-scan. It included migration and background removal. Also, we transformed the amplitudes into the square amplitudes.

3) The third sequence of processing consisted in interpolating the various processed B-scans, in order to obtain a 3D image.

4) An additional processing to obtain 3D images of the rebar and ducts was done by identifying anomalies in each B-scan. These anomalies were marked with points of different colours, and the images were connected one to the other with AutoCad. This procedure allowed, in some cases, to draw the different bodies embedded in concrete. However, in some other cases, due to the bad conditions of the material, it was very difficult to correlate the different anomalies to targets. Figure 2 shows some examples: here we were picking the anomalies that could be associated to the same kind of bodies, in different radargrams.
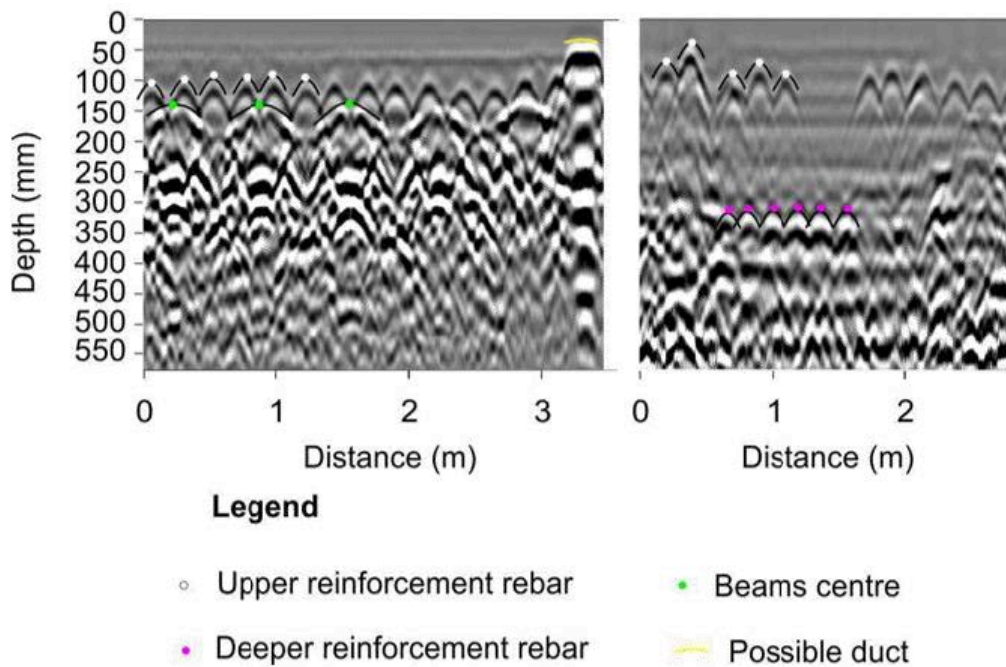
Fig. 2 – Identification of targets in the B-scans.

The result of the project, showing the bodies in the slab, is shown in Figure 3. The average depth of the objects was about 45 cm.
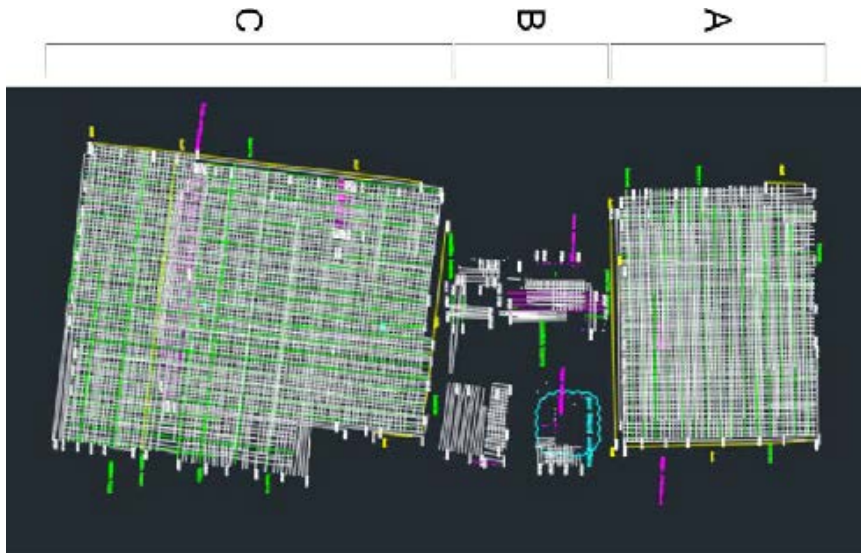
Fig. 3 – Final result in AutoCad, showing the different targets that produce the anomalies recorded in the B-scans. Three zones were distinguish.

After the processing described above, we began to centralise the geographic information and database management systems. We used the software Surfer 8 that was used to represent the 3D features in the ground. Figure 4 shows some different stages during the use of the software.

DAY 4

In the morning, we processed again the data collected during the first project (detection of pipes), but in this case we used the software GPRSlice. The first step was to convert raw files into GPRSlice files. Figures 5 to 10 show the stages of the processing sequence. Figure 5 shows different filters applied to each A-scan and B-scan. One of those filters was migration. Figure 6 shows the definition of pixel maps using gridding. In this study we applied the

inverse-distance gridding method, which is a weighted interpolation where the influence of each point declines with the distance to the selected node.

In the afternoon we worked on a new project, focused on the use of GPR in a building. It was necessary to assess the floor in order to detect elements below tiles and other constructive elements. A shielded antenna was used and a survey wheel.

DAY 5

In the morning, we worked at the presentation of the results collected during the previous days.
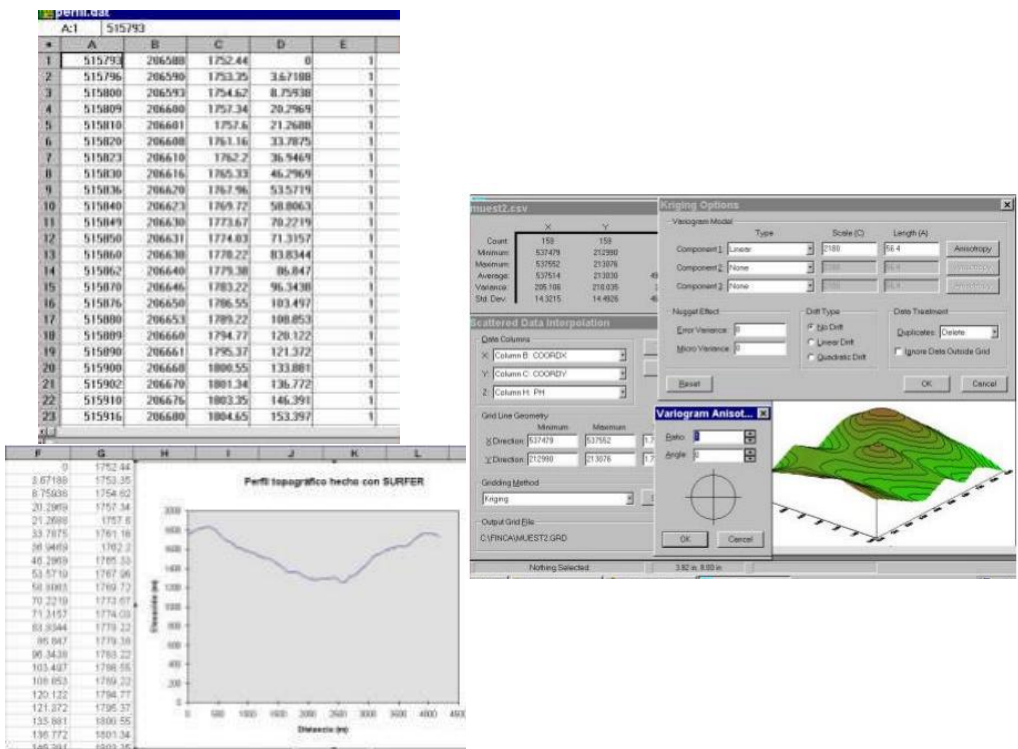
Fig. 4 – Representing the topography and the surface with the software Surfer.

Fig. 5 – Processing the radargrams with the GPR Slice software.

Fig. 6 – Inverse distance power gridding parameters.
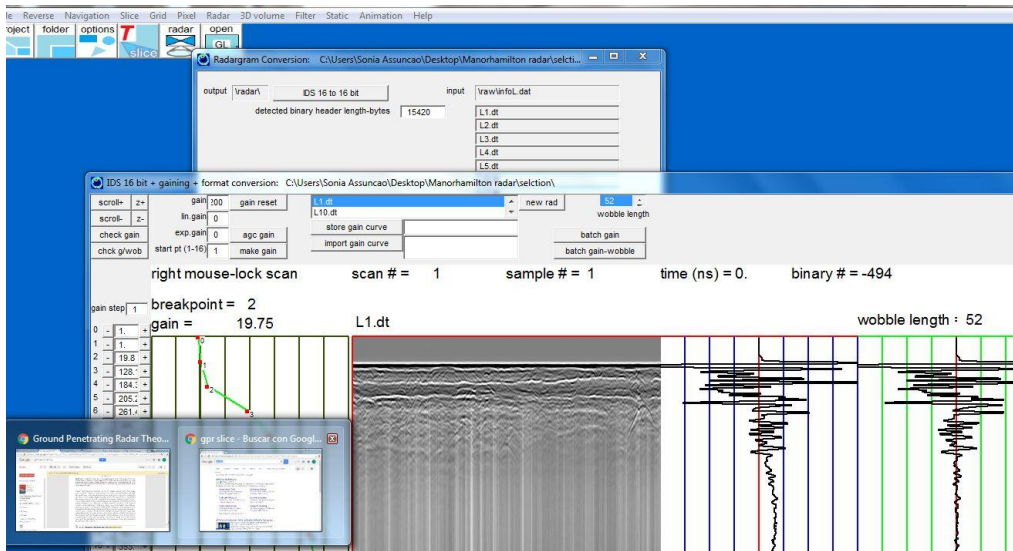
Fig. 7 – Conversion of data and gain application.
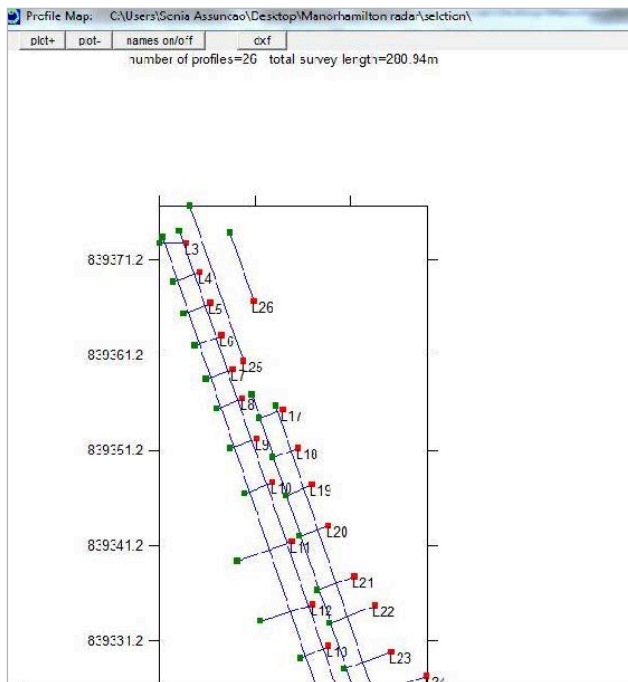
Fig. 8 – Defining the grid of profiles.
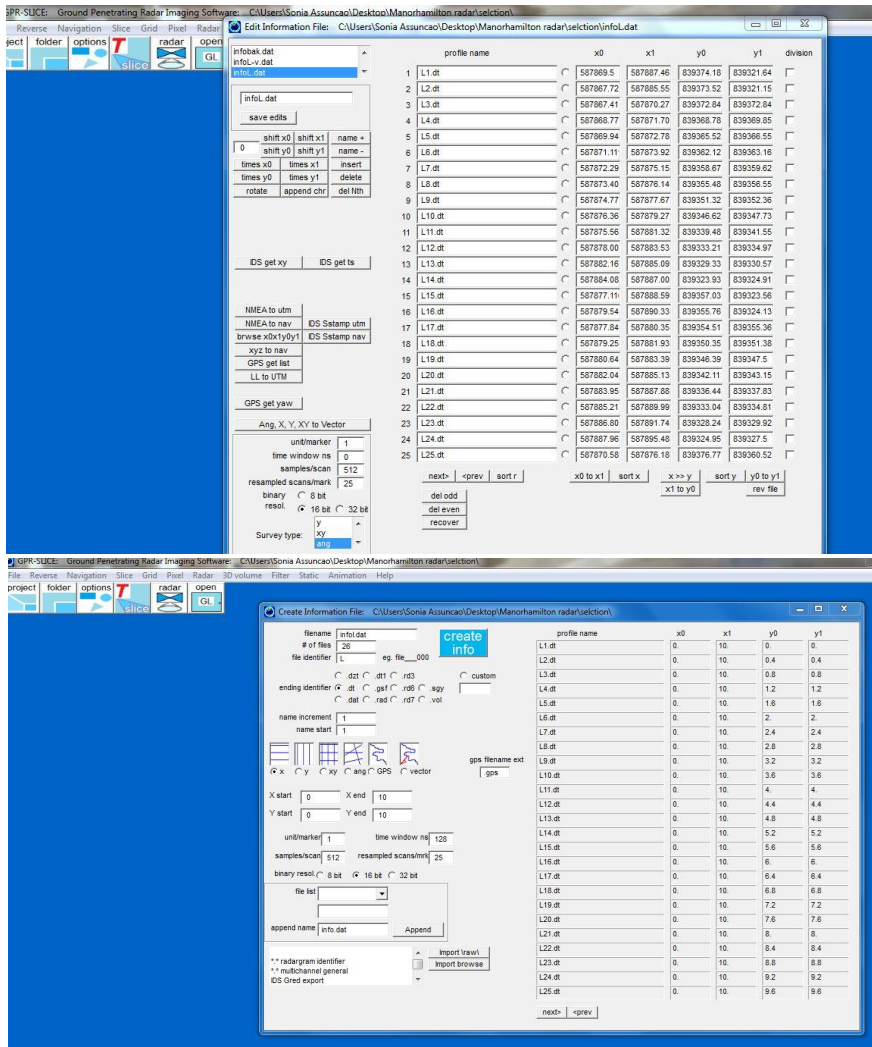
Fig. 9 – Association of the information about the profiles
to the different files.

In the case of the detection of pipes, a complete plan showing the location of the different bodies was realised. Some discontinuities appeared in some regions (see red circles in Figure 11). A possible explanation is that a change in soil water content

occurred (denoting leaks). Higher water content produces higher energy dissipation, hence lower amplitudes of reflected waves.

In the case of the building assessment, the results were elaborated and presented as shown in Figure 12.

During the afternoon, we finally focused on the module of the Education Pack devoted to presenting the use of GPR in archaeology. This work started during the STSM and will be finalised in remote collaboration.

3. DESCRIPTION OF THE MAIN RESULTS OBTAINED DURING THE STSM AND FUTURE COLLABORATION WITH THE HOST INSTITUTION

Mainly, the STSM was useful to see how a private company carries out GPR surveys, from planning to data acquisition, to interpretation and presentation of results.
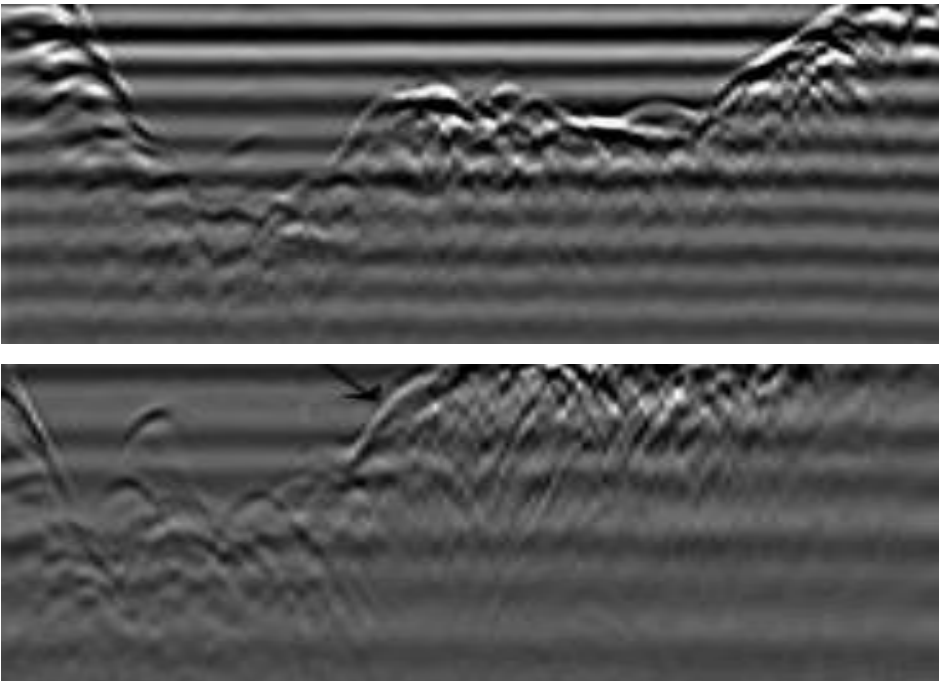
Fig. 10 – Example of topographic corrections, based on the surfer files. After the corrections, some zones were better distinguished and the location of pipes highlighted (see the arrow).

5. FORESEEN PUBLICATIONS/ARTICLES RESULTING FROM THE STSM

Some of the results were presented during the EGU GA 2017.

ACKNOWLEDGEMENT

The visiting and host scientists would like to thank COST for funding COST Action TU1208 and this STSM.
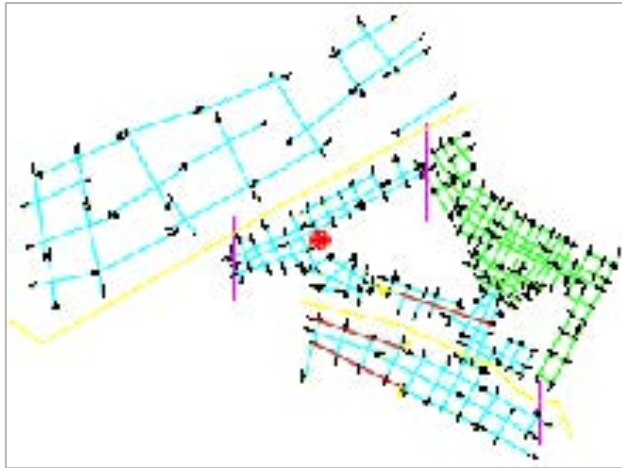
Fig. 11 – Final interpretation of the location of pipes.
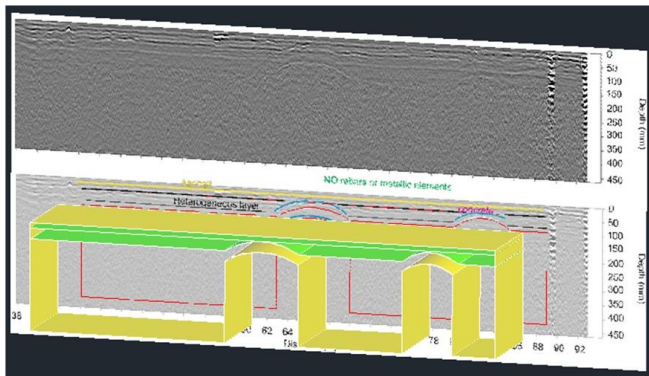
Fig. 12 – Interpretation of the building structures and representation of the anomalies in the radar data, associated to these structures.

189

STSM 12

COUPLED WKB APPROACH APPLIED TO GROUND PENETRATING RADAR

Visiting Scientist: Alexei Popov, Pushkov Institute of Terrestrial Magnetism, Ionosphere and Radio Wave Propagation Moscow, Troitsk, Russia (popov@izmiran.ru)

Host Scientist: Marian Marciniak, National Institute of Telecommunications, Warsaw, Poland (m.marciniak@itl.waw.pl)

STSM Dates: 24 April – 30 April 2016

1. PURPOSE OF THE STSM

This work was a continuation of the previous STSM TU1208-26813 carried out by Igor Prokopovich at the National Institute of Telecommunications, Warsaw, under supervision of Prof. Marian Marciniak. The main goal of both missions was the development of an efficient semi-analytical simulation technique for the problems of subsurface electromagnetic probing with ground penetrating radar (GPR). Although accurate numerical algorithms exist, as well as computer codes modelling electromagnetic wave emission and propagation in non-uniform subsurface medium, analytical approaches can provide better physical insight and dramatic acceleration of quantitative estimates.

Our work is based on the rectification of the classical WKB (Wentzel-Kramers-Brillouin) approximation proposed by Bremmer and Brekhovskikh in the 50-ies of the last century. It consists in the iterative solution of coupled ordinary differential equations of WKB type (the method is indeed denominate also "coupled-wave method" or "two-way WKB") [1-2]. This approach accounts for the backscattered signals and provides a good accuracy in a wide frequency range [2]. The possibility of applying coupled-wave theory to GPR by solving a one-dimensional inverse problem was studied

in [3]. It was shown that the time-domain counterpart of Bremmer-Brekhovskikh method allows accurately reconstructing the parameters of subsurface transition layers, starting from the waveform of the return radar pulse generated by the permittivity gradients.

Our work was aimed at a further development of Bremmer-Brekhovskikh approximation applied to GPR problems. As the one-dimensional probing scheme considered in [3] was oversimplified, we have developed a more realistic model: ultra-wide band electromagnetic probing of a horizontally layered half-space by a GPR with separated dipole antennas lying at the ground-air interface. The use of Fourier-Laplace transform reduces the problem to an ordinary differential equation, which is solved approximately by Bremmer-Brekhovskikh method.

The backward integral transform yields an approximate representation of the time-domain Green function – subsurface medium response to an elementary current jump in the GPR transmitter antenna. General equations of the coupled-WKB approximation were derived during the first STSM by Igor Prokopovich. The work performed during this second STSM was aimed at the numerical implementation, verification and practical application of this prospective semi-analytical method.

2. DESCRIPTION OF THE WORK CARRIED OUT DURING THE STSM AND MAIN RESULTS

The scientific report prepared after this STSM was further developed and enriched in the subsequent months, in cooperation with the Action Chair and the STSM Manager. Further simulations were performed, the method was compared with the finite-difference time-domain technique and applied to two practical case studies. The resulting work was then published as a joint open access paper, on the MDPI peer-reviewed journal *Remote Sensing* [4]. The interested Reader is invited to download [4] where the work carried out during the STSM and the main results achieved are described in detail.

3. FUTURE COLLABORATION WITH THE HOST INSTITUTION

Possible topics of further collaborations are: extension of the theory to three dimensions and to the case of smoothly varying layered media with slow permittivity dependence along both the x and y axes. The STSM has strengthened the existing links between guest and host institutions. STSM is an excellent networking tool offered offered by COST Actions.

4. FORESEEN PUBLICATIONS/ARTICLES RESULTING FROM THE STSM

The STSM results were published in [4].

ACKNOWLEDGEMENT

REFERENCES

[1] H. Bremmer, "Propagation of Electromagnetic Waves," in: Handbuch der Physik, Ed.S. Flugge, pp. 423-639. Springer, 1958.
[2] M. Brekhovskikh, "Waves in Stratified Media" (in Russian), USSR Academy of Sciences, Moscow, 1957; Waves in Layered Media. Academic Press, 1980.
[3] V.A. Vinogradov, V.V. Kopeikin, and A. Popov, "An Approximate Solution of 1D Inverse Problem," in Proc. 10th Internat. Conf. on GPR, Delft, Netherlands, 2004.
[4] I. Prokopovich, A. Popov, L. Pajewski, and M. Marciniak, "Application of Coupled-Wave Wentzel-Kramers-Brillouin Approximation to Ground Penetrating Radar," Remote Sensing vol. 10(1), 22, pp. 1-20, 2018, doi: 10.3390/rs10010022

TABLE OF CONTENTS

193

194